TU Delft

Delft University of Technology

Plug-and-Play Optical Waveguide Sensor Systems for Chemical and Biomedical Sensing

Xin, Yu

DOI
10.4233/uuid:53b30dab-04d8-4904-9e08-4d7d2a2997d2

Publication date
2018

Document Version
Final published version

Citation (APA)
Xin, Y. (2018). *Plug-and-Play Optical Waveguide Sensor Systems for Chemical and Biomedical Sensing*. [Dissertation (TU Delft), Delft University of Technology]. https://doi.org/10.4233/uuid:53b30dab-04d8-4904-9e08-4d7d2a2997d2

Important note
To cite this publication, please use the final published version (if applicable).
Please check the document version above.

Copyright
Other than for strictly personal use, it is not permitted to download, forward or distribute the text or part of it, without the consent of the author(s) and/or copyright holder(s), unless the work is under an open content license such as Creative Commons.

Takedown policy
Please contact us and provide details if you believe this document breaches copyrights.
We will remove access to the work immediately and investigate your claim.

This work is downloaded from Delft University of Technology.
For technical reasons the number of authors shown on this cover page is limited to a maximum of 10.

Plug-and-Play Optical Waveguide Sensor Systems for Chemical and Biomedical Sensing

Plug-and-Play Optical Waveguide Sensor Systems for Chemical and Biomedical Sensing

Proefschrift

ter verkrijging van de graad van doctor
aan de Technische Universiteit Delft,
op gezag van de Rector Magnificus prof. dr. ir. T.H.J.J. van der Hagen,
voorzitter van het College voor Promoties,
in het openbaar te verdedigen op dinsdag 19 juni 2018 om 15:00 uur

door

Yu XIN

Master of Mechanical Engineering,
National University of Defense Technology, Changsha, Hunan, China.
geboren te Henan, China.

Dit proefschrift is goedgekeurd door de

promotor: Prof. dr. P.J. French

Samenstelling promotiecommissie:

Rector Magnificus	voorzitter
Prof. dr. P.J. French	Technische Universiteit Delft, promotor
Onafhankelijke leden:	
Prof. dr. ir. P.M. Sarro	Technische Universiteit Delft
Prof. dr. G.Q. Zhang	Technische Universiteit Delft
Prof. dr. J. Dankelman	Technische Universiteit Delft
Prof. dr. E.J.R. Sudhölter	Technische Universiteit Delft
Prof. dr. X.Z. Wu	National University of Defense Technology, China
Overige leden:	
Dr. G. Pandraud,	Technische Universiteit Delft

This project was financially sponsored by China Scholarship Council. National University of Defense Technology also supported the research since 2017.

Keywords: optical waveguide, evanescent wave, sensing, plug-and-play

Printed by: Ipskamp Printing, The Netherlands.

Front & Back: Inspired by paintings from Vincent van Gogh and combined with the library and EWI building of TU Delft.

Copyright © 2018 by Yu Xin

ISBN 978-94-6186-936-4

An electronic version of this dissertation is available at
http://repository.tudelft.nl/.

Contents

Summary

Outbreaks of bacteria have caused many problems over the last few years and are a major public health concern. Bacteria are now affecting our lives in many ways to a more severe extent, from contaminated food in markets to polluted water. There are some devices available which detect bacteria, however, all of them can only be used in the lab condition and are very expensive. This research is aimed at the development of a biomedical sensor which is capable of monitoring bacteria, especially focusing on diagnosing colorectal anastomotic leakage (AL) in patients at an early stage by detecting the existence of *E. coli* in the drain fluid. The occurrence of AL in patients after colon surgery is high and is cause for concern as it can lead to severe consequences, such as morbidity or even mortality. Therefore, there is a vital need for an efficient, on-line bedside tool to monitor the bacteria in the leakage: a diagnostic on-line device that is accurate, cost-effective, and ideally operates in an easy plug-and-play fashion which is beneficial for practical application.

In this thesis, optical waveguide sensors based on MEMS fabrication have been researched for their beneficial fast-response, high-sensitivity, and miniaturization capabilities while being free from electric/electromagnetic influence. Devices based on a label-free optical waveguide are proposed to fulfill the requirements. The basic working principle is evanescent wave sensing. When light propagates in the waveguide, it will generate evanescent waves on the core-cladding interface, which is used for sensing. The waveguide surface area is sensitive to the attached targets on the surface or changes in the refractive index in the cladding and results in optical absorption or phase changes, which can be detected to monitor the targets.

This research focuses on the structure design, material selection, and fabrication optimization of the optical sensing system. The system is label-free and based on the evanescent sensing principle. By comparing different waveguide structures and material properties, two waveguide sensing systems are proposed: a SiC waveguide sensing system and an SU-8 waveguide sensing system.

The SiC waveguide sensing system is robust due to the excellent chemical resistance and mechanical stability of SiC. It has the potential to be developed into a highly sensitive waveguide system by optimizing the design, such as making it freestanding to increase the sensing area and available evanescent wave. SiC has some alternative processing methods which are beneficial to the design flexibility.

For the SU-8 waveguide system, a new waveguide structure is proposed in this thesis. The waveguide is designed vertically with a large height-width ratio in such a way that evanescent wave is distributed in both left and right sides of the waveguide cladding for sensing. This structure is demonstrated to be effective and more efficient in sensing than horizontal waveguides. As a photosensitive polymer, it has the intrinsic advantages of easy fabrication and fast prototyping by photolithography, with a guaranteed surface quality.

Alignment tolerance is an important aspect in our plug-and-play system, for which most optical waveguide systems are restricted. These systems demand precise and time-consuming adjustments before usage. Tapered couplers are added to the waveguide system to increase the coupling efficiency and alignment tolerance of the systems to relieve the problem. They are designed to meet the sensing requirements and to be integrated with the current MEMS fabrication technology at the same time.

Various methods for fabricating different types of waveguides have also been investigated. In the SiC waveguide design and fabrication, the LPCVD and PECVD deposition techniques are combined to achieve a thin, uniform layer for the waveguide sensing structure and a thick layer for the taper part. A novel transfer method is proposed to fabricate the 3D taper designed for the SiC waveguide, which is able to obtain a slope of 2 degrees in SiC. For the SU-8 waveguide fabrication, E-beam lithography is applied to obtain delicate structures with high resolution. It is a fast and simple one-step lithography process without dry etching. This contributes to a better sidewall surface used for sensing.

The performance of the proposed waveguide systems has been tested chemically and biomedically. Measurements demonstrate that the waveguide systems are qualified for chemical elements and bacteria sensing. In addition to the common properties that optical sensors exhibit, which are integration and high sensitivity, our sensing system has the advantages of on-line detection, cost effectiveness, and plug-and-play operation, which are competitive features that can ultimately be implemented in the development of a bedside handheld device. Multiple waveguide lines can be added to diagnose different bacteria simultaneously.

Samenvatting

Bacterie-uitbraken in de gezondheidszorg hebben de laatste jaren voor een groot aantal problemen gezorgd. In grotere mate beïnvloeden bacteriën nu vele aspecten van ons leven, van besmet voedsel op de markt tot vervuild water. Er bestaat een aantal apparaten om bacteriën te detecteren, echter zijn ze allemaal bedoeld voor gebruik in laboratoria en erg duur. Dit onderzoek is gericht op het ontwikkelen van een biomedische sensor die bacteriën kan detecteren, waarbij gefocust wordt op vroege diagnose van naadlekkage in de dikke darm door de aanwezigheid van *E. coli* te detecteren in de drain-vloeistof. Bij patiënten die darmchirurgie hebben ondergaan is de kans op naadlekkage groot, wat kan leiden tot ernstige ziekte of sterfte. Het ontbreken van een on-line en efficiënt hulpmiddel, dat de bacteriën in de drain-vloeistof in de gaten kan houden, maakt het belangrijk om naar een oplossing te zoeken: een diagnose-hulpmiddel dat on-line, accuraat en betaalbaar is en, idealiter, op een gemakkelijke plug-and-play wijze te gebruiken is.

In deze thesis worden sensoren met optische golfgeleiders onderzocht, gebaseerd op MEMS fabricagetechnieken, vanwege hun voordelen: snelle reactietijd, hoge dichtheid, miniaturisatie mogelijkheden en omdat ze geen last hebben van elektrische en elektromagnetische invloeden. Om aan de vereisten te voldoen worden systemen gebaseerd op labelvrije optische golfgeleiders voorgesteld. Het werkingsprincipe is gebaseerd op het detecteren van uitdovende golven. Wanneer licht in de golfgeleider propageert zal het op het grensvlak tussen de kern en mantel uitdovende golven genereren, die gebruikt kunnen worden voor de detectie. Het oppervlakte van de golfgeleider is gevoelig voor de aan het oppervlak gehechte bacteriën of voor veranderingen in de brekingsindex van de mantel waardoor er optische absorptie of faseveranderingen plaats vinden. Die veranderingen kunnen worden gedetecteerd om de aanwezigheid van een bacterie te controleren.

Dit onderzoek richt zich op het ontwerpen van de structuur, de materiaalkeuze en optimalisatie van het fabricageproces van het optische meetsysteem. Het vergelijken van verschillende golfgeleider-structuren en materiaaleigenschappen heeft tot twee voorstellen voor meetsystemen geleid: een SiC-golfgeleider systeem en een SU-8-golfgeleider systeem.

Het SiC meetsysteem is robuust door de uitstekende chemische weerstand en mechanische stabiliteit van SiC. Door het verder te optimaliseren heeft het de potentie om ontwikkeld te worden tot een zeer gevoelig golfgeleider systeem, door het bijvoorbeeld vrijstaand te maken om het detectie-oppervlak en daarmee de beschikbare uitdovende golven te vergroten. Alternatieve verwerkingsmethodes van het SiC kunnen ook voordelig zijn voor de flexibiliteit van het ontwerp.

Voor het SU-8 golfgeleider systeem wordt in deze thesis een nieuwe structuur voorgesteld. De golfgeleider wordt verticaal ontworpen met een grote hoogte-breedte verhouding, op zo' n manier dat uitdovende golven zowel over de rechter

als linker kant van de golfgeleider-mantel verspreid zijn. Het is aangetoond dat de structuur effectief is en efficiënter werkt dan horizontale golfgeleiders. Als lichtgevoelige polymeer heeft SU-8 de intrinsieke voordelen van gemakkelijke fabricage, snelle prototypes en fotolithografie met een gegarandeerde oppervlakte kwaliteit.

Uitlijningstoleranties vormen een belangrijk aspect in ons plug-and-play systeem, waar de meeste andere optische golfgeleider-systemen gelimiteerd zijn. Ze vergen een precieze en tijdrovende afstelling voordat ze gebruikt kunnen worden. Tapse koppelingen zijn toegevoegd aan het golfgeleider-systeem om de koppelingsefficiënte en uitlijningstoleranties van het systeem te vergroten. Ze zijn ontwerpen om aan de meetvereisten te voldoen en tegelijkertijd om geïntegreerd te kunnen worden met de huidige MEMS-fabricage technologie.

Voor het maken van golfgeleiders zijn verschillende fabricagemethodes onderzocht. In het ontwerp van de SiC golfgeleider worden LPCVD en PECVD depositie gecombineerd om de uniforme dunne laag van het golfgeleider-meetsysteem te verkrijgen in combinatie met de dikke laag voor het tapse gedeelte. Een nieuwe overdrachtsmethode wordt voorgesteld voor het fabriceren van de ontworpen 3D-tapse koppeling, waarmee een hoek van 2 graden in SiC behaald kan worden. Voor SU-8 fabricage wordt E-beam lithografie toegepast om fijne structuren met een hoge resolutie te verkrijgen. Dit is een snel en simpel één-staps lithografieproces zonder droogetsen, wat bijdraagt aan een oppervlak van de zijwanden dat beter geschikt is voor de detectie.

De prestaties van het voorgestelde golfgeleider-systeem zijn chemisch en biomedisch getest. Metingen tonen aan dat de golfgeleider-systemen geschikt zijn voor het meten van chemische elementen en bacteriën. Naast de algemene eigenschappen die geïntegreerde en gevoelig optische sensoren vertonen, heeft ons meetsysteem het voordeel van on-line detectie, kosten-efficiëntie en een plug-and-play werking, wat het concurrerend maakt voor de ontwikkeling tot een draagbaar systeem. Meerdere golfgeleider-kanalen kunnen worden toegevoegd om verschillende bacteriën tegelijk te kunnen detecteren.

1

Introduction

1

This chapter will introduce the background of the research in this thesis. It will also describe the motivation and current method used to solve the imminent problems. Afterwards, our approach will be briefly explained and the thesis outline will be outlined at the end.

1.1. Background

With the increase bacteria hazards in environment, food system, and health care, safety has attracted much attention and been brought to the forefront. Biosensors are one safety measure that can detect, monitor and analyze a target substance (i.e. chemical or biological species, or microorganism), and convert it into an electrical or optical signal [1]. This process normally includes a source, analytical targets, sensor, and signal detectors. There are various ways to transform the response of targets to the stimulating source into detectable signals. Based on the mechanism, biosensors can be categorized as being electronic, mechanical, optical, thermometric, piezoelectric, etc. They should be able to provide fast, accurate, sensitive, and cost-effective analysis [2]. An ideal biosensor is easily operated by a non-skilled person and miniaturized down to a handheld device. Biosensors based on optical waveguides stand out and have been widely explored as well-established technologies for their advantage over other sensors. They are free from electric shock and electromagnetic influence and also have higher sensitivity and miniaturization capability. On-line detection is also extremely important for biosensors. There are also different detection methods: labelled and label-free detection. Labelled detection utilizes fluorescence for detecting marked targets. Although this method is sensitive, the time-consuming labelling procedure might interfere with the biotargets. On the contrary, label-free detection which is based on absorption, refractive change, and alternatively Raman spectroscopic detection, does not change the targets [3]. Raman spectroscopic uses Raman light scattered by the targets for sensing, but it needs extra instrumentation and is quite expensive. The major advantage of absorption-based sensors is that they are simple, easy to use and cost-effective [1]. The basic working principle of label-free detection is evanescent wave sensing. When light propagates in the waveguide, it generates evanescent waves on the core-cladding interface, which are used for sensing. The nearby surface area is sensitive to the attached targets, or the refractive index change, which will result in optical absorption or phase change that can be monitored to detect targets.

There are numerous optical biomedical or chemical waveguide sensors, from labelled [4, 5] to label-free [6–10]. Many optical waveguide sensors are fabricated with conventional silicon-based materials such as silicon dioxide, silicon carbide, silicon nitride, etc. These are robust, stable, and standard materials for sensors. A waveguide with TiO_2 core and SiN substrate has been put forward in [11, 12]. It was fabricated by dry etching, while the freestanding membrane was released by KOH back etching. Measurements showed the sensitivity to be 1dB/% when tested with the drain fluid from real patients. The schematic of the waveguide system is shown in Fig. 1.1. In 2015, an optical ultrasound sensor was proposed and demonstrated with potential applications in the medical field such as medical

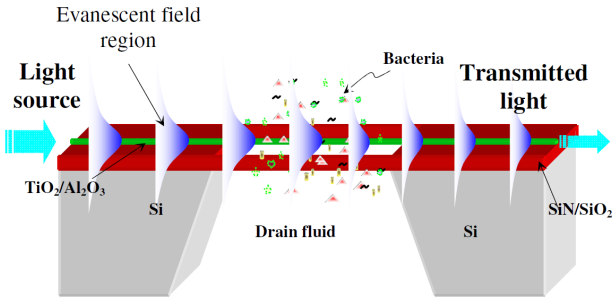

Figure 1.1: Schematic of the biomedical sensing waveguide system

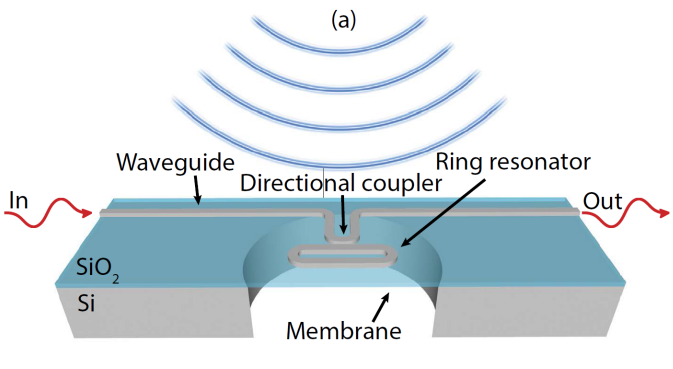

Figure 1.2: Sketch of the OMUS

ultrasound imaging and non-destructive testing (see Fig. 1.2). The basic idea is to measure the strain caused by the acoustic pressure with a membrane based ring resonator. The induced strain will cause a resonant shift in the ring resonator that is measured by a photodiode. The sensing structure contains a silicon ring resonator and a SiO_2 membrane underneath. The membrane was formed using backside etching with SF6 which can stop well on SiO_2. The measured sensitivity of the sensor is 2.1mV/Pa for pressure up to 150Pa in a linear range [13].

Dry etching is usually needed in the fabrication of conventional optical waveguides but the induced surface roughness will result in extra loss. Later, polymers such as PDMS and SU-8 were introduced which brought much attention to this field because of their suitable optical properties, mechanical stability, as well as their feasibility in fabrication [14–18]. Freestanding polymer waveguides with closed cavities were shown in [19], where photolithography and imprinting were used to transfer patterns from photoresist to PDMS and then to UV resin. An SU-8 polymer integrated optic microsystem was designed in [20] which has the advantage of easier fabrication than other conventional materials, and can be applied in microfluidic networks. An optical cantilever made of SU-8 was presented in [21] which utilized displacement of the cantilever for homocysteine detection. The minimum detected concentration was 10μm and the minimum displacement and the surface stress were 5nm and 1mN/m, respectively. It was reported to be the first polymer cantilever that could operate in the fluid. These outcomes have demonstrated the promising application of polymer waveguides in sensing.

The current developing trend is to make the optical waveguide sensing system more integrated, sensitive, reliable and easy to handle. In [22], an array of waveguide micro-cantilevers for biosensing was made that was also based on the the stress-induced deformation caused by adsorption or heating-up from chemical reactions. The cantilevers were made with standard MEMS technologies including deposition, DRIE etching, and TMAH etching. It is designed to have an array of 20 waveguide cantilever channels, which allows for a higher integration level. In order to improve the sensitivity, a freestanding waveguide was proposed. In this way, evanescent waves will generate on both surfaces, which could both be used as active sensing areas.

Despite the tremendous amount of research in optical biosensors and chemical sensors, some performance features of these sensors, such as stability, sensitivity, and easy operation, still need to be improved for final application in the biochemical field.

1.2. Motivation and aim

Outbreaks of bacteria in the healthcare sector have caused many problems over the last few years. Bacteria are now affecting our lives in many ways to a more severe extent, from contaminated food in the markets to polluted water. It is dangerous when hazardous bacteria get into the food or water chain. Furthermore, it can also be fatal in hospitals. As patients' immune systems are already compromised, if they are not monitored well or treated in time, the original or induced bacteria could result in serious consequences. One scenario that has raised our interest is

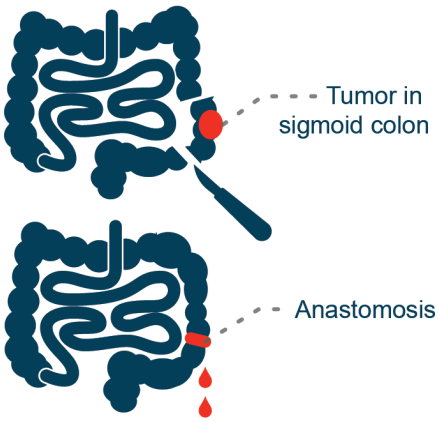

Figure 1.3: Colon surgery

the leakage that occurs after colon surgery. Patients who suffer from colon cancer require a surgery to cut off part of the colon and then reconnect the remaining two ends. This reconnection is called anastomosis. Leakage can happen after anastomosis as shown in Fig. 1.3, which is called anastomosis leakage (AL). This occurs in 3-13% of patients and can cause severe complications or even death. It is among the most dreaded complications after colorectal surgery [23], yet over the last decade, AL has not decreased [24–26]. It is most likely to happen to patients who are vulnerable after the surgery. Nevertheless, it can also happen to patients with no obvious risk [27]. If the leakage occurs, patients require another surgery immediately. Therefore, after the surgery, it is important to monitor the condition of the patients to see whether they need another operation or not. Currently, there are two methods hospital used to detect anastomosis after colon surgeries. The first method follows two steps. The first involves observation: if certain symptoms (e.g. fever) appear after the surgery, these may indicate a leakage. What follows is a CT scan to check whether there are holes around the anastomosis location. However, CT scans are not always accurate, because sometimes the hole is too small to be detected even when the leakage occurs. The other method to detect anastomosis leakage is PCR (Polymerase Chain Reaction) which is faster and more accurate. However, this method is too expensive to be frequently used to monitor patients after surgery. In addition, the currently used methods applied after symptom has appeared will take up to 7-11 days [27], but such a delay could be fatal for the patients who have anastomosis. The fact that there is a high occurence possibility of AL which can lead to life-threatening results such as morbidity and even mortality makes solving the problem imperative. Moreover, the lack of efficient, timely methods to monitor the leakage makes it important to look for a reliable device to solve this. It is important for hospitals to detect anostomosis early and accurately to save lives.

In this thesis, we are aimed at making a plug-and-play biomedical sensor which is capable of detecting AL in patients at an early stage. Proper bio-indicator(s) will be chosen and the corresponding sensor will be designed and tested. To develop a device for AL detections, some important criteria need to be fulfilled.

- **Real-time**: Real-time detection is crucial in AL detection since time is extremely important. A delay in detection can result in a missed opportunity for a corrective operation to save a patient's life.
- **Accurate**: Accuracy is a basic feature of biomedical devices that is of the same importance: whether the leakage happens or not. Only after AL has been accurately detected, can decisions be made on whether the patient needs another operation or not.
- **Low cost**: Cost is a limiting factor in the application of a new technology. A low-cost device will always be beneficial to the patients and enable widespread application of the medical device.

Apart from that, there are other properties that can expend the application of the device: easy operation and integration. These result in a plug-and-play sensing system which contains the following merits:

- **Easy operation**: No expert knowledge is needed to operate this device and people can use the device bedside. The device should be robust enough to tolerate non-expert handling.
- **Integration**: All the elements needed for the device should be integrated on a chip, which shares the same idea as a lab-on-chip device. By miniaturization, it can be made into a handheld device.

1.3. Approach

As we are targeting the fabrication of a sensor to detect AL, the first to be considered are the sensing parameters, which are the reliable biomedical indicators which can be used to determine the occurrence of AL. After that, the construction of the system is taken into account.

1.3.1. Biomedical indicators

Once leakage occurs, the bacteria, which should only remain in the colon, leaks out into the abdominal cavity of the patient. Detecting these bacteria can therefore be an effective indicator of a leakage. Among all bacteria, we need to determine which are reliable indicators. There are several bacteria which can act as indicators such as *E. coli* and *E. faecalis*. They both have positive indication on AL. Previous research shows that *E. faecalis* may grow faster [28], but it is not always present when there is leakage. However, *E. coli* is always present when leakage happens, thus making it a reliable indicator. *E. coli* may also occur because of the incomplete flushing of the wound after surgery when there is no leakage. However, in that case, the concentration of *E. coli* in the drain fluid will decrease gradually after

the surgery. By detecting the existence of *E. coli* and monitoring the change in concentration of it in the drain fluid of patients, the occurrence of leakage can be determined.

1.3.2. Methods

Our research is to develop a thin-film optical waveguide-based biosensor. Here, we are particularly interested in the detection of the bacteria *E. coli*. Evanescent waveguides are proposed as a method to detect *E. coli* in the drain fluid. The system will consist of two waveguide branches: one for detection and another for reference. The detection waveguide surface will be functionalized with antibodies which are specific *E. coli* from the drain fluid. Light is channeled into the waveguide and when it propagates to the sensing region, the evanescent waves on the surfaces can be used to sense the bacteria captured by the antibodies on the surfaces. The more *E. coli* that are present, the more that will be captured on the surface and the more light that will be absorbed by them. By comparing the output light from the two branches, concentration of *E. coli* can be acknowledged.

1.4. Thesis organization

This thesis focuses on developing an optical waveguide to be used in bio-chemical sensing. Specifically, we are aimed at detecting bacteria involved in AL after colorectal surgery. This thesis includes the introduction of optical waveguides, their basic principled and related MEMS fabrication techniques, as well as the design, simulation, and fabrication process of the designed waveguide systems. After the fabrication, this thesis also presents the various chemical and biomedical sensing measurements of the waveguides in our research. The remaining part of this thesis is organized as follows:

- Chapter 2: Micromachined optical waveguides for sensing.

  This chapter introduces the basic optical waveguide theories, structures, related MEMS fabrication technologies, and the applications of these waveguide sensors in the chemical and biomedical fields.

- Chapter 3: Waveguide structures, materials, and taper design consideration.

  This chapter focuses on the waveguide structure design and the material choices made. Simulations are made to compare different structures. Tapers are also introduced into the system to increase the operation feasibility.

- Chapter 4: Design and fabrication of SiC waveguide.

  This chapter investigates SiC as the core material of evanescent waveguides. Simulations are carried out to aid in designing the structures. LPCVD and PECVD deposition methods are combined in fabricating the waveguide. 3D tapered couplers are designed for this SiC waveguide to reduce the coupling loss and misalignment effect. A novel method for fabricating the 3D taper is also presented and demonstrated. This SiC waveguide has the potential to be designed as a freestanding structure to increase the sensitivity.

- Chapter 5: Design and fabrication of vertical SU-8 waveguide.

  This chapter introduces a vertical SU-8 wave-guide for evanescent biomedical sensing. It illustrates the design, simulations, and fabrication of the waveguide. Moreover, this vertical structure is compared with traditional ones by simulations to prove its advantage in sensitivity. A horizontal taper is added to the waveguide to help develop a plug-and-play system.

- Chapter 6: Waveguide sensing measurement.

  In this chapter, experiments are carried out to test the optical properties and sensing characteristics of the system. Biomedical tests are also put forward and demonstrated.

- Chapter 7: Conclusions and future development.

  This chapter concludes the work in this thesis and puts forward the development potential of the waveguide sensing system.

References

[1] P. N. Patel, V. Mishra, and a. S. Mandloi, *Optical Biosensors : Fundamentals & Trends,* Journal of Engineering Research and Studies **I**, 15 (2010).

[2] M. C. Estevez, M. Alvarez, and L. M. Lechuga, *Integrated optical devices for lab-on-a-chip biosensing applications,* Laser & Photonics Reviews **6**, 463 (2012).

[3] X. Fan, I. M. White, S. I. Shopova, H. Zhu, J. D. Suter, and Y. Sun, *Sensitive optical biosensors for unlabeled targets: A review,* Analytica Chimica Acta **620**, 8 (2008).

[4] D. V. Lim, *Detection of microorganisms and toxins with evanescent wave fiber-optic biosensors,* Proceedings of the IEEE **91**, 902 (2003).

[5] G. P. Anderson, J. P. Golden, and F. S. Ligler, *A fiber optic biosensor: Combination tapered fibers designed for improved signal acquisition,* Biosensors and Bioelectronics **8**, 249 (1993).

[6] S. Lee, S. C. Eom, J. S. Chang, C. Huh, G. Y. Sung, and J. H. Shin, *Label-free optical biosensing using a horizontal air-slot SiNx microdisk resonator.* Optics express **18**, 20638 (2010).

[7] K. Schmitt, B. Schirmer, and A. Brandenburg, *Label-free detection of biomolecules by waveguide interferometry,* Proceedings of SPIE **5855**, 459 (2005).

[8] H. K. Hunt and A. M. Armani, *Label-free biological and chemical sensors.* Nanoscale **2**, 1544 (2010).

[9] T. Claes, J. G. Molera, K. De Vos, E. Schacht, R. Baets, and P. Bienstman, *Label-free biosensing with a slot-waveguide-based ring resonator in silicon on insulator,* IEEE Photonics Journal **1**, 197 (2009).

[10] C. F. Carlborg, K. B. Gylfason, a. Kaźmierczak, F. Dortu, M. J. Bañuls Polo, a. Maquieira Catala, G. M. Kresbach, H. Sohlström, T. Moh, L. Vivien, J. Popplewell, G. Ronan, C. a. Barrios, G. Stemme, and W. van der Wijngaart, *A packaged optical slot-waveguide ring resonator sensor array for multiplex label-free assays in labs-on-chips.* Lab on a chip **10**, 281 (2010).

[11] A. Purniawan, G. Pandraud, K. Vakalopoulos, P. French, and P. Sarro, *Surface functionalisation of tio 2 evanescent waveguide sensor for e. coli monitoring,* in *Optical Sensing and Detection II*, Vol. 8439 (International Society for Optics and Photonics, 2012) p. 843926.

[12] Y. Xin, A. Purniawan, L. Pakula, G. Pandraud, and P. J. French, *Simulation of Bio-medical Waveguide in Mechanical and Optical Fields,* COMSOL (2014).

[13] S. M. Leinders, W. J. Westerveld, J. Pozo, P. L. M. J. V. Neer, B. Snyder, and P. O. Brien, *A sensitive optical micro-machined ultrasound sensor (OMUS) based on a silicon photonic ring resonator on an acoustical membrane,* Nature Publishing Group , 1 (2015).

[14] A. Prabhakar and S. Mukherji, *Microfabricated polymer chip with integrated U-bend waveguides for evanescent field absorption based detection,* Lab on a Chip **10**, 748 (2010).

[15] N. Pelletier, B. Bêche, E. Gaviot, L. Camberlein, N. Grossard, F. Polet, and J. Zyss, *Single-mode rib optical waveguides on SOG/SU-8 polymer and integrated Mach-Zehnder for designing thermal sensors,* IEEE Sensors Journal **6**, 565 (2006).

[16] T. C. Sum, A. A. Bettiol, J. A. Van Kan, F. Watt, E. Y. B. Pun, and K. K. Tung, *Proton beam writing of low-loss polymer optical waveguides,* Applied Physics Letters **83**, 1707 (2003).

[17] S. W. Kwon, W. S. Yang, H. M. Lee, W. K. Kim, G. S. Son, D. H. Yoon, S. D. Lee, and H. Y. Lee, *The fabrication of polymer-based evanescent optical waveguide for biosensing,* Applied Surface Science **255**, 5466 (2009).

[18] M. Wang, J. Hiltunen, C. Liedert, L. Hakalahti, and R. Myllylä, *An integrated young interferometer based on UV-imprinted polymer waveguides for label-free biosensing applications,* Journal of the European Optical Society **7** (2012), 10.2971/jeos.2012.12019.

[19] R. Horváth, H. C. Pedersen, N. Skivesen, D. Selmeczi, and N. B. Larsen, *Optical waveguide sensor for on-line monitoring of bacteria.* Optics letters **28**, 1233 (2003).

[20] R. Müller, D. Cristea, M. Kusko, P. Obreja, D. Esinenco, V. Damian, and P. C. Logofatu, *SU8 polymer materials used in integrated optic microsystems,* OPTOELECTRONICS AND ADVANCED MATERIALS-RAPID COMMUNICATIONS **4**, 228 (2010).

[21] S. T. Koev, R. Fernandes, W. E. Bentley, and R. Ghodssi, *A cantilever sensor with an integrated optical readout for detection of enzymatically produced homocysteine,* IEEE Transactions on Biomedical Circuits and Systems **3**, 415 (2009).

[22] K. Zinoviev, J. A. Plaza, V. Cadarso, C. Dominguez, and L. M. Lechuga, *Optical biosensor based on arrays of waveguide microcantilevers,* **6477**, 64771A (2007).

[23] N. Hyman, T. L. Manchester, T. Osler, B. Burns, and P. a. Cataldo, *Anastomotic leaks after intestinal anastomosis: it's later than you think.* Annals of surgery **245**, 254 (2007).

[24] Z. Wu, D. Freek, and J. Lange, *Do normal clinical signs and laboratory tests exclude anastomotic leakage?* Journal of the American College of Surgeons **219**, 164 (2014).

[25] A. Alves, Y. Panis, M. Pocard, J.-M. Regimbeau, and P. Valleur, *Management of anastomotic leakage after nondiverted large bowel resection,* Journal of the American College of Surgeons **189**, 554 (1999).

[26] C. Platell, N. Barwood, G. Dorfmann, and G. Makin, *The incidence of anastomotic leaks in patients undergoing colorectal surgery,* Colorectal Disease **9**, 71 (2007).

[27] P. Matthiessen, I. Strand, K. Jansson, C. Törnquist, M. Andersson, J. Rutegård, and L. Norgren, *Is early detection of anastomotic leakage possible by intraperitoneal microdialysis and intraperitoneal cytokines after anterior resection of the rectum for cancer?* Diseases of the Colon and Rectum **50**, 1918 (2007).

[28] N. Komen, J. Slieker, P. Willemsen, G. Mannaerts, P. Pattyn, T. Karsten, H. De Wilt, E. Van Der Harst, W. Van Leeuwen, C. Decaestecker, H. Jeekel, and J. F. Lange, *Polymerase chain reaction for Enterococcus faecalis in drain fluid: The first screening test for symptomatic colorectal anastomotic leakage. The Appeal-study: Analysis of Parameters Predictive for Evident Anastomotic Leakage,* International Journal of Colorectal Disease **29**, 15 (2014).

2

Micromachined Optical Waveguide for Sensing

This chapter focuses on micromachined optical waveguide sensors. It introduces the basic optical waveguide theories, commonly used materials, and structures. The related MEMS fabrication technology will also be described and the application of micromachined optical waveguide sensors will be presented.

2

2.1. Introduction

Dielectric guides originated from the work for one century ago since the work of Hondros and Debye on dielectric rods in 1910 [1], and after that optical waveguides was introduced and have been studied with interest since 1960s [2]. The period of 1962 to about 1968 saw the emergence of thin-film phenomena study and in 1965, photolithographic techniques were combined to construct the thin-film or other planar waveguides that eventually developed into integrated optics [3].

An optical waveguide is defined as "a dielectric structure that transports energy at wavelength in the infrared or visible portions of the electromagnetic spectrum" [4]. In these structures, optical energy is constrained by total internal reflection from the dielectric interfaces. The working principle can be described by using the simple slab waveguide as shown in Fig. 2.1. The basic structure consists of 3 layers. The core layer has the refractive index of n_1, the layer below (substrate) has the refractive index of n_2, and the medium above (cladding) is with the refractive index of n_3. When $n_1 > n_2, n_1 > n_3$, light would be reflected at the interface and guided in the waveguide. When the incident angle is greater than critical angle, the total internal reflection occurs at the interface. However, there will be a certain amount of wave penetrate into the cladding medium, which is called evanescent wave.

$$\sin \theta_c = \frac{n_2}{n_1} \tag{2.1}$$

The bigger the difference is between n_1 and n_2, the better confinement of light will be in the waveguide. The evanescent electric field intensity $I(z)$ decays exponentially with perpendicular distance z from the interface.

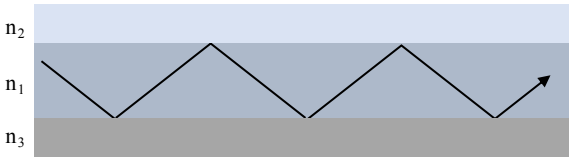

Figure 2.1: Basic structure of dielectric waveguide

The evanescent wave has already been widely researched especially in sensing [5–8] as it is sensitive to the refractive index change near the interface and the optical energy will be absorbed by the surroundings. In this way, if the surface is functionalised by a layer of, for example, antibodies, the specified bacteria will be absorbed on the surface when bacteria in the detected target applied to the waveguide. It can also be used in coupling [9].

2.2. Waveguide materials

There are many materials for fabricating optical waveguides, from silicon and its compounds such as SiO_2, SiC, SiN, SiON to polymers as PDMS, SU-8, etc. As introduced in the previous section, for the optical waveguide design, the key properties of materials of optical waveguides lie in the refractive index, optical transparent range, optical loss, fabrication feasibility, and mechanical property when necessary. This section will introduce materials related to these aspects.

The first thing that needs to be considered is the function of the waveguide, then goes to which wavelength is going to be used: the absorption should be low at that wavelength. Whether it is used for communication or sensing, it is mechanical-optical or electrical-optical determines the choice of materials.

2.2.1. Material properties

Optical properties

An electromagnetic wave can be described in different ways: by energy (eV), by wavelength (λ), by frequency (Hz). They might be used in different papers. To make it clear, the relationships between the three different units are given by:

$$E = hc/\lambda \tag{2.2}$$

$$v = c/\lambda \tag{2.3}$$

where h is a constant equals to 6.63×10^{-34}J·s. In this chapter, we are using wavelength to introduce waveguides.

Refractive index When a waveguide is designed, the refractive index contrast is a dominate factor. If the waveguide is used to transmit optical energy, high contrast will lead to a better confinement of light. If the waveguide is used for sensing, especially evanescent sensing, it is essential to keep a certain amount of light outside the waveguide core, which is often called the evanescent wave tail. Then it is wise to choose a moderate refractive index difference [10].

Loss The optical loss is an important characteristic for optical waveguides. There are three different types of losses: scattering, absorption, and radiation. In the perspective of materials, the main losses type are scattering and absorption, where the first loss predominates in glass or dielectric waveguides and the second one counts in semiconductors and other crystalline materials [11]. Here we are not going to specify the loss type but show the losses in general. For semiconductor materials, there would be the transparent range for materials which is useful in choosing the light source.

Transparent range This factor determines the light used in the waveguide. which means the optical range where there is low absorption rate. Choosing the proper wavelength according to materials can reduce unnecessary optical loss.

Mechanical properties

When fabricating waveguides with mechanical structures, where mechanical structure is a part of the sensing system, then mechanical properties need to be considered. When depositing layers of different materials at different temperatures, stress induced by thermal difference might lead to cracks in the layer. This should be avoided by designing the fabrication process properly. If there are freestanding structures in the system, the structure should maintain stable after release and remain robust afterwards for the following test. In this chapter, two of the mechanical properties which dominate in fabrication: Young's modulus (E) and thermal expansion coefficient (α) will be presented. The thermal expansion coefficient is related to the induced thermal stress during fabrication, while Young's modulus can give an idea of the extent that this stress deforms the structure.

Fabrication feasibility

The fabrication feasibility and the adhesive of material to the substrate is also a key factor for optical waveguides. The fabrication needs to be repeatable and stable. Fabrication techniques and the process sequence are the crucial factors when designing a waveguide.

2.2.2. Typical optical waveguide materials

There are various waveguides and a growing number of materials can be used in the waveguide fabrication. Since silicon is the basic, silicon and its compounds will be firstly introduced.

Silicon Silicon is an important material for optical MEMS for its good micromachining property and widespread application in MEMS. Silicon itself fits for optical MEMS for its optical properties and it is easy to be integrated with other materials by deposition, oxidation, etc. Silicon is transparent to infrared light with wavelength above 1.1μm and has a high refractive index of around 3.5. Young's modulus of crystal silicon depends on the crystal orientation which was shown in [12]. The band gap increases from 1.1eV in crystalline silicon to 1.7eV in amorphous silicon and the absorption coefficient of a-Si is much higher than that of crystalline silicon.

Porous silicon Porous silicon is a nanoscale composite material with an effective refractive index between that of air and silicon, that can easily be fabricated in multilayer structures [13]. Fabrication details can be found in [14–16] by electrochemical etching in HF. The refractive index depends on the porosity of the silicon wafer [16] and it can have a porous layer of refractive index from silicon substrate (3.4) to air (1.0). Porous silicon is an attractive material for biosensing. Waveguides made from porous silicon have been used to detect the presence of liquids [17]. The theoretical and experimental demonstrations of porous silicon waveguide biosensors with superior sensitivity to surface plasma resonator (SPR) sensors have been reported [18, 19].

SiO_2 It is usually combined with silicon to fabricate SOI waveguides or used as an isolation layer between the waveguide and silicon substrate to prevent optical leakage into the substrate. The advantage of silicon dioxide is its perfect match of the refractive index to fibre. There are various ways to fabricate SiO_2, thermal oxidation, APCVD, PECVD, TEOS, and LPCVD. The refractive index of SiO_2 ranges from 1.44 to 1.47 due to different fabrication methods.

SiC There exist single crystal, poly, and amorphous SiC, however, the micromachined SiC mentioned here are commonly used poly SiC and amorphous SiC. There are several ways to grow silicon carbide including APCVD, LPCVD, PECVD, and so on. APCVD and LPCVD are usually used to deposit poly-SiC at high temperature, above 800°C, whereas Sputtering and PECVD are employed to form amorphous SiC at low temperature, below 700°C.

SiN Silicon nitride can be deposited by APCVD, LPCVD, and PECVD, although the first of these is now rarely used [20]. The optical band gap could be reproducibly varied by changing the disilane flow rate during the film growth. Increasing the disilane flow rate will increase the silicon content (or Si to N ratio) in the films, thereby decreasing the optical band gap [21].

SiON Silicon oxynitride or SiON recently has been widely used in optics. SiON shows excellent optical properties, such as low absorption losses in the visible and near infrared wavelength range. Moreover, the refractive index of SiON thin films can be easily adjusted over a large range, i.e., between 1.45 (SiO_2) and 2.0 (Si_3N_4) which makes this material very attractive [13]. Low-index PECVD SiON loss can be reduced to less than 0.2dB/cm at 1550nm wavelength after the thermal treatment to reduce the hydrogen content.

TiO_2 TiO_2 is a promising material in optical MEMS systems for its high refractive index and high optical transmittance [22]. TiO_2 can be prepared by several ways such as CVD, pulsed laser deposition, reactive sputtering, sol-gel deposition [23], etc. Recently, there has been an increasing in the interest of the research in ALD which can also been used in fabricating TiO_2. In the MEMS application, ALD is a good way for depositing TiO_2 layer. It is a technique to form the layer by sequential surface reaction steps, atom layer by atom layer by which the layer thickness can be in good control. ALD can also be used to tune mechanical properties of TiO_2 enabling a wide use in the mechanical field [24]. Furthermore, TiO_2 is bio-compatible which makes it potential in biomedical field.

GaAs/AlGaAs Gallium arsenide/aluminium gallium arsenide (GaAs/AlGaAs) rib waveguides are useful for many optical and electro-optical devices such as switches, modulators, and filters [25]. Many of these devices are required to be single mode. The GaAs material has the advantage of exhibiting very low absorption across the whole mid-infrared to a wavelength of 16μm where the first multiphonon absorption

features are present. Low loss waveguides can be epitaxially grown utilizing the relatively large refractive index step between AlxGa1-xAs and GaAs materials [26, 27]. The GaAs waveguides are usually fabricated by MBE(molecular beam epitaxy) [25, 26, 28] and MOCVD [27].

InP Indium phosphide (InP) is attractive for optical communications due to its suitability as a substrate material for active optical devices made of indium gallium arsenide phosphide (InGaAsP) [29] operating at the λ=1550nm wavelength. The InP layers can be grown with a metal organic vapor phase epitaxy process (MOVPE) or low pressure metal-organic vapor phase epitaxy (LP-MOVPE), then processed with CH_4:RIE etching into ridge waveguide amplifiers with various widths (2 to 7μm) [30].

SU-8 SU-8 is a negative-toned, chemically amplified resist that has been extensively applied in MEMS applications [31]. Since the epoxy-based SU-8 resist has good optical transparency, it has been used as the waveguide material in various integrated optical systems [32–34]. It can be mass-produced via polymer molding or the so-called UV-LIGA process [35]. The previous work done within the area clearly showed the high interest and suitability of SU-8 for integrated optical components [36, 37]. The refractive index of SU-8 is highly dependent on the processing temperature and the exposure dosage, so the core and cladding of the waveguide can all be fabricated from SU-8 with different treatment [38].

PDMS Polydimethylsiloxane (PDMS) is an optical material with excellent optical and elastic properties. In the visible range of spectrum, PDMS shows high transparency and it is well formable by imprinting techniques [39]. In the field of PDMS optical waveguides there are two approaches reported: the first one where the index contrast between the core and cladding is generated by curing the same material at different temperatures [40] resulting in intrinsic temperature instabilities and the second one which is followed by the authors [41] and comprises two distinct materials for the core and cladding. The typical fabrication method is to first fabricate patterned channel and then fill the channel with a higher-index material such as PDMS cured at different temperatures [40] or UV curable resin [42].

Glass Ion exchange in glass is a well-established method for fabrication of passive and active integrated photonic devices. The fabrication of optical waveguides in glass by ion exchange was first achieved in 1972 using a melt containing thallium ions [43]. The creation of integrated optical devices in glass offers several obvious benefits over other technologies. Intrinsic absorption is very low in the near infrared region of the spectrum [44]. Coupling losses to the optical fibre are minimised due to the similarity in refractive index. In addition, glasses are amorphous, meaning that they exhibit no intrinsic material birefringence, unlike crystalline semiconductors. In addition to ion exchange, other processes exist through which glass waveguides have been fabricated. Most of them involve the flame hydrolysis deposition (FHD), chemical vapor deposition (CVD) and solgel processing [45].

Ta_2O_5 Tantalum pentoxide (Ta_2O_5) is a promising material for both linear and nonlinear integrated optical devices due to its high refractive index, low broadband absorption (0.3-10μm) [46], high nonlinear refractive index $n_2 = 7.23 \pm 0.36 \times 10^{-19}$m^2/W [47], large third order nonlinear susceptibility ($chi^{(3)}$ or "Chi 3") [48], and high optical damage threshold [49]. Ta_2O_5 waveguides were found to be stable for high power applications with no significant absorption peaks over a large range of wavelengths (600-1700nm) [50]. Ta_2O_5 waveguides provide high intensity in the evanescent field, which is useful for bio-sensing and efficient optical propelling of micro-particles [51]. The Ta_2O_5 can be deposited by chemical solution deposition, magnetron sputter deposition, and RF sputtering deposition; the etching methods including reactive ion etching, ion-beam milling, and inductively coupled plasma [50, 52–54]. Ta_2O_5 is becoming a welcomed material due to its high refractive index and it can be applied to make sensor based on evanescent wave sensing, particular in bio-chemical field. Schmitt et al. concluded label-free biosensor based on Ta_2O_5 such as grating couplers, interferometric sensors, and fluorescence system [20]. The refractive index of the Ta_2O_5 films is $n = 2.1 \pm 0.02$ at $\lambda = 633$nm. Experiments showed that up to a strain of 45%, which corresponds to a constant elastic modulus of 1.76MPa for Sylgard 184 and 1.54MPa for RTV 615. Afterwards, the value of Sylgard 184 is increasing up to 13.9MPa at 97% strain. The curve for RTV 615 increases only up to 7.5MPa at 92% strain, before is decreases again to 2.16MPa at 115% strain.

$LiNbO_3$ Lithium niobate ($LiNbO_3$) has become a very attractive material for integrated optical applications because of its excellent electro-optical, acousto-optical, and nonlinear optical properties [55]. The $LiNbO_3$ crystal waveguides can be fabricated by means of proton exchange (PE) [56], double proton exchange process (Double Exchange, DE) [57], titanium in-diffusion [58]. Recent developments have led to the fabrication of ridge waveguides that provides more flexibility and more stable behavior even under high average optical power [59–61]. Lithium Niobate ($LiNbO_3$) waveguides are already widely used in many functional electro-optic and acoustooptic waveguide devices.

ZnO Zinc oxide ZnO is a semiconductor material with a wide broad-band gap of 3.4eV. It displays attractive properties permitting to apply it in sensor techniques as well as in systems of integrated optics. Data quoted in literature indicates that it is transparent in a visible range. It is characterized by a high value of the refractive index (n $\approx$ 2) [62], which is a favourable feature of the waveguide in systems of integrated optics [63]. The ZnO layers can be fabricated by spin coating [64], magnetron sputtering [65], reactive cathode sputtering [63], and so on.

2.3. The classification of optical waveguide

Optical waveguide can be categorized by different criteria. It can be categorized into 3 types according to the geometry of the cross section, which are planar waveguide (slab waveguide), circular waveguide (such as optical fibre), and non-planar

Table 2.1: Properties of typical optical waveguide materials

Materials	Fabrication	Optical Property		Mechanical property		Reference
		Refractive index	Transparent range[μm]	E	Thermal expansion coefficient ($\times 10^{-6}\mathrm{K}^{-1}$)	
Crystal Silicon	Crystal growth	3.5@1.3μm	>1.1μm	130-168.9 GPa	2.626	[12, 13, 66]
Porous silicon	Electro-chemical etching	1.3@85%porosity 1.5@70%porosity 2.7@25%porosity 3.4@0%porosity				[13–16]
SiO_2	Oxidation, PECVD, LPCVD, APCVD	1.445@1.3μm	0.12-4.5μm	76.5GPa-91GPa	0.35	[67, 68]
SiC	LPCVD, PECVD	2.2-2.9	>0.5μm	127-206 GPa, 88-694 Gpa	4.2	[69–75]
SiN	PECVD, LPCVD, APCVP	2-2.4@635nm	>600nm (a-Si 0.54 N 0.46: H)	230-360GPa, 170GPa		[68, 76, 77]
TiO_2	ALD Sol-gel Sputtering	2.45@1.3 μm 2.304-2.499@633nm	>0.4μm	133Mpa-684Mpa		[22, 78]
SiON	LPCVD, PECVD, Sputtering E-beam evaporation	1.45-2.0		65-153	-1.27-2.28	[79]
GaAs	molecular beam epi-taxy(MBE), MOCVD	3.3-3.6@1.77μm-886nm	1.0-22μm	85.3 GPa	4.56	[26–28, 79, 80]
InP	LP-MOVPE, MOVPE	3.17@1550nm		60.9GPa	6.03	[30, 79, 81, 82]
SU-8	Coating, UV-LIGA	1.569@632.8nm, 1.575@1550nm, 1.574@1310nm	800nm-1600nm	1.5-3.1 GPa	102.0 ±5.1	[74, 83, 84]
PDMS	Curing, UV-Curing	1.41-1.43	>400nm	1.7-13.9MPa	310	[85, 86]
Glass	ion ex-change, FHD, CVD	1.4-1.6		7.4-17.2 GPa	55-860	

Table 2.2: Properties of typical optical waveguide materials (cont.)

Ta_2O_5	ICP, magnetron sputtering deposition, chemical solution deposition ion-beam milling	2.1@1070nm 2-2.5@1064nm	0.3-10μm	132-177 GPa	3.9 ±0.1	[20, 87]
$LiNbO_3$	PE, DE, titanium indiffusion	2.2@633nm	0.2-1.2μm	170 GPa	14.8	[88, 89]
ZnO	spin coated, magnetron sputtering, reactive cathode sputtering	$n \approx 2$	visible range	30 to 250 GPa	Depend on the temperature	

waveguide, also defined as rectangular waveguide. The planar waveguide is the simplest waveguide. It is only finite in one direction and infinite in the other two which is the ideal structure and good for mode analysis [90]. The circular waveguide is normally used for telecommunications. Its big advantage over the non-planar waveguide (rectangular waveguide) is low cost for long communications. But this type of waveguide is not the focus here. The last one is the non-planar waveguide which is the most frequently used type in integrated optics. For the non-planar optical waveguide, it can be classified into ridge waveguide, rib waveguide, strip loaded waveguide, embedded waveguide, immersed waveguide, bulge waveguide, metal waveguide, and buffered metal waveguide as shown in Fig. 2.2 [91]. The basic principle of the waveguides is the same. The difference lies in the structure and the optical confinement. Light is confined in the core material which has the highest refractive index. Ridge and rib waveguides are similar, ridge waveguide can be considered as the total etch away of the core material besides the core and this would increase the confinement of light in the core. These two waveguide structures have a high requirement on the surface smoothness. For the strip-loaded waveguide, the strip on the top has a lower refractive index than the core material beneath, light would confined in the core material under the strip. For the embedded waveguide, electro-optic material can be used for the core to be connected to the external field [91]. Only one side is exposed to the cladding. The immersed waveguide is totally buried in the cladding and it is simple for symmetry. Bulge waveguide is almost the same with rib waveguide apart from the rib profile. Metal waveguide can be put together with buffered metal waveguide, the light is confined in the core material without metal cladding on it. The difference is that there is a dielectric layer between metal and thin film to light loss in the metal layer. The structure is chosen mainly depending on the application. However, there are also other kinds of waveguides that confines light in the low refractive index area of the waveguide. It was first put forward by Duguay in 1986 [92]. There are two

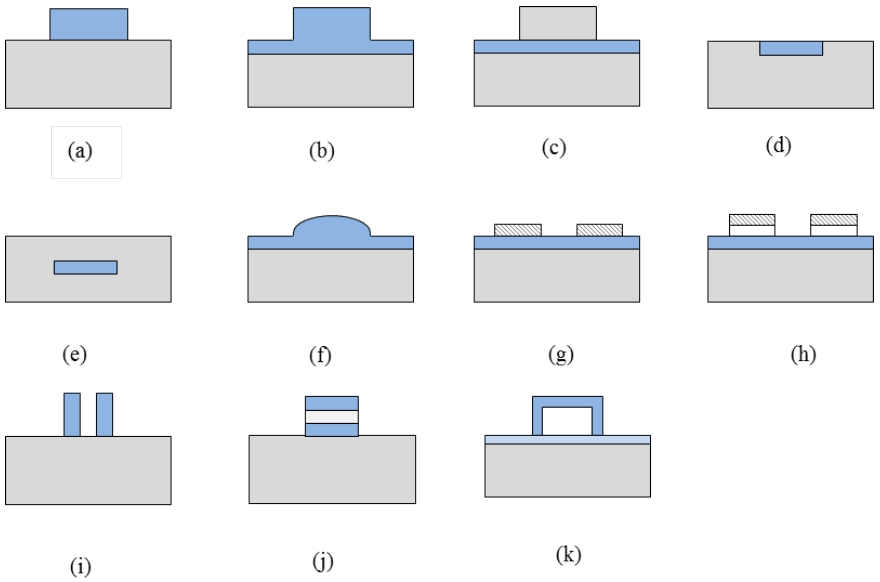

Figure 2.2: Various types of waveguides: (a) ridge waveguide; (b) rib waveguide; (c) strip-loaded waveguide; (d) embedded waveguide; (e) immersed waveguide; (f) bulge waveguide; (g) metal waveguide; and (h) buffered metal waveguide (i) vertical slot waveguide (j) horizontal slot waveguide (k) hollow waveguide [91]

common structures: slot waveguides and hollow waveguides, shown in Fig. 2.2 (i) (j) (k) separately. Fig. 2.2 (i) (j) are the basic structures for horizontal and vertical slot waveguides. Slot waveguides strongly confine light in a subwavelength-scale low refractive index region by total internal reflection. For hollow waveguides, they also have a lower refractive core than cladding. In this situation, there will be no total internal reflection but leaky waves in the waveguide. The above describes some basic structure of optical waveguide, there are various devices built based on this, such as Mach-Zehnder interferometer, directional coupler, micro-ring resonator, etc. [93].

Classified by mode, waveguides have multimode waveguides and single mode waveguides. A waveguide that can only support one mode for a given polarization is referred to as a single-mode waveguide. If the waveguide can support a number of modes, it is referred to as a multimode waveguide. Whether a waveguide is single or multimode depends not only on the geometry and media of which it is constructed but also on the wavelength of the electromagnetic wave (light) it supports. A multimode waveguide provides bigger cross-section area for light collecting and transmission, and it is also easier to coupler light into the waveguide. However, in sensing aspect, especially evanescent wave sensing, single mode waveguide is applied for it carries more power in the evanescent waves [51, 94, 95].

According to the role of the waveguides in the sensor, they can be classified into intrinsic and extrinsic waveguides [96]. Fluitman also defined a third type

called active waveguides in 1986 which includes an additional optical modulator [97]. Defined by function, waveguides can be used in sensing (temperature sensor, pressure sensor, gas sensor, fluid sensor, displacement sensor, etc.), Mach-Zehnder modulator, directional coupler, optical scanner [98], optical switches [99] and so on.

Now optical waveguides are more integrated into an optical system which includes optical sources, optical waveguides/sensors, modulators, and detectors. "Integrated optics" was first put forward by Miller in 1969 [100]. It has the idea of integrating circuits and detectors on the same chip with optical waveguides. Integrated optics make the optical system smaller, less power consuming, and more efficient. Later, the combination of micromachining and optics contribute more benefits and made the optical system even more integrated. It is smaller, lighter, faster, and more rugged compared to macroscale optical mechanical devices. It allows movable micromechanical structure to be integrated monolithically with microoptical elements which cannot be achieved by conventional fabrication methods [101]. Furthermore, mass fabrication can reduce the production cost. The MEMS application in optical is called microoptoelectromechanical systems (MOEMS) or microoptomechanical systems (MOMS).

There are some review papers about optical waveguides and their applications already. In early times, Tien wrote a review about integrated optics and new phenomena in optical waveguides about the state of art at that time and optics in thin films and couplers [102]. To the latest one by Chollet about the integration of MEMS actuators and optical waveguides [103], it focused on the waveguide which was driven by MEMS actuators. In between, there are many review papers about different kinds of waveguide structures (hollow waveguides [104]), of different materials (such as ion-exchanged glass waveguide [105], polymer based optical waveguide) or different applications (like chemical analysis [96], biosensors [106–108], optical waveguide switching [109]), etc.

2.4. MEMS fabrication technology

Microfabrication is the process of fabricating miniature structures of micrometre scales and smaller. Micromachining refers to the fabrication of micromechanical structures with the aid of etching techniques to remove part of the substrate or thin film [110]. Microfabrication technologies originated from the microelectronics industry, and the devices are usually made on silicon wafers even though glass, plastics, and many other substrate are in use as well. It mainly includes surface micromachining, bulk micromachining, and EPI micromachining. Micromachining is used to fabricate MEMS devices for a long time since 1962 when Honeywell fabricated a sensor by wet etching in silicon [111]. Later in 1982, Petersen presented optical MEMS in his paper [66] for the first time, also called "micro-opto-electromechanical system" (MOEMS) which integrated optical functions into the mechanical and electrical parts in one device [12]. The introduction of micromachining into the optical waveguide fabrication produced more possibility for this field. Optical components are usually strict in the surface roughness which can be minimized by micromachining fabrication. By doping different elements or using different fab-

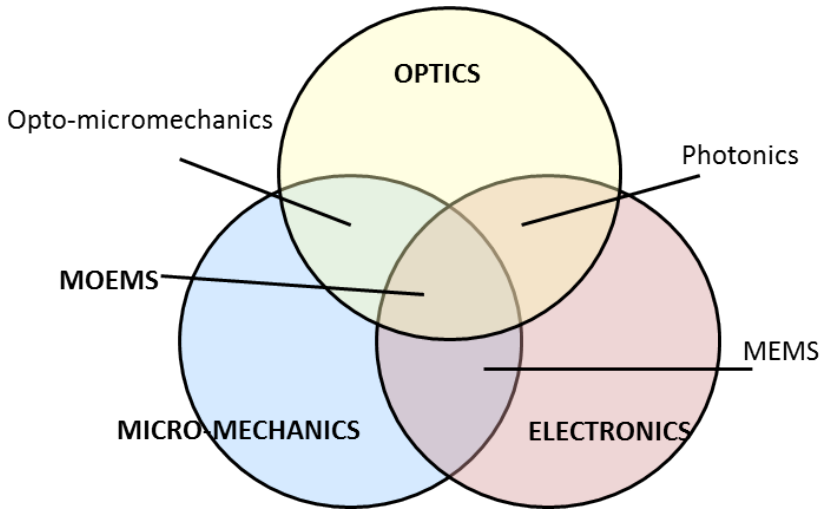

Figure 2.3: MEMS: convergence technology zone of micromechanics and electronics. MOEMS: convergence technology zone of optics, micromechanics and electronics. [112]

rication parameters, the refractive index can be toned to a desired figure, which makes the design of waveguide more flexible. Freestanding or movable structures are possible due to micromachining technology. Also, micromachining makes the optical system more integrated which means power consumption less, size smaller, response faster. Fig. 2.3 shows the integration of optics, mechanics, electronics, and where the MOEMS lies and the relationship among different technologies.

2.4.1. Basic MEMS fabrication steps

Generally, basic microfabrication steps include lithography, oxidation and deposition, etching, doping. Each fabrication method will be introduced simply in the following parts.

Lithography: UV lithography, grey scale lithography, direct writing

Photolithography is a common method to transfer a designed pattern from a mask to photoresist. Photoresist is an organic layer sensitive to ultraviolet (UV) radiation. When it is exposed to UV radiation, it will cause chemical reaction. After development, the exposed area will stay for negative photoresist and will be get rid of for positive photoresist [113].

To achieve 3-D lithography for 3D fabrication, grayscale lithography was used. The grayscale mask is partially transparent and under exposure, photoresist will only be partially removed. In this way, 3D structure with variable heights will be obtained in the photoresist, as shown in Fig. 2.4. The left one is the normal photolithography and the right one is the greyscale lithography [114].

The direct writing technique is a maskless lithography process which includes electron beam lithography, laser beam direct writing, and proton beam writing. It patterns the photoresist by using a focused beam. The biggest advantage for this

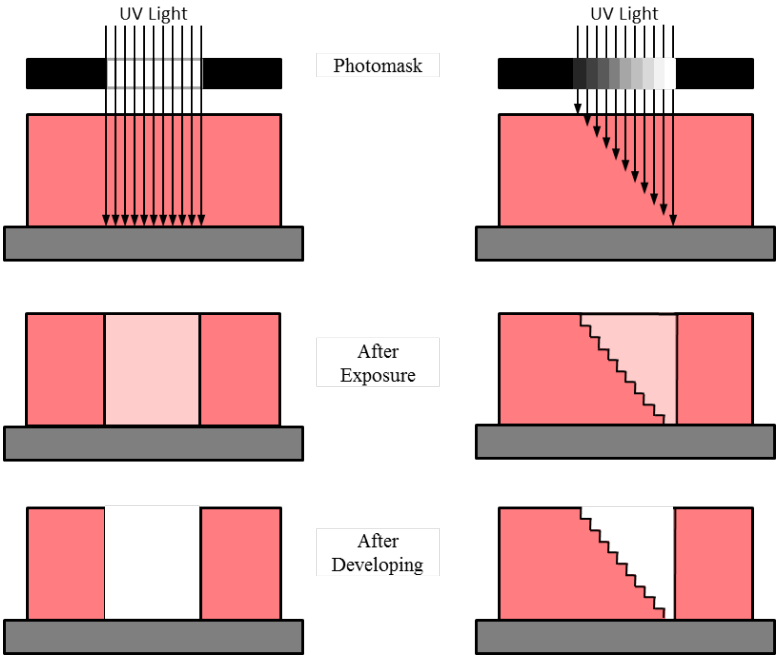

Figure 2.4: The comparison of normal lithography and grayscale lithography

method is maskless which makes it is feasible for fabricating waveguides with arbitrary structures. And it has high fabrication precision and is suitable for making delicate designed and size sensitive structures. However, it also has the disadvantage of low output compared with conventional fabrication.

Additive techniques
Adding a thin layer of target material to a substrate is an important technique in MEMS fabrication. It includes the chemical reaction with current substrate such as oxidation, deposition techniques which has physical vapour deposition (PVD) and chemical vapour deposition (CVD) and doping which is adding impurities to a material [2].

Oxidation Oxidation is adding a layer of SiO_2 to the silicon substrate. There are wet oxidation and dry oxidation. The chemical reaction is different as the following equation shows, the quality of dry oxide layer is higher than wet, but the reaction rate is lower:

$$\text{Dry oxidation:} \quad \mathrm{Si} + \mathrm{O_2} \rightarrow \mathrm{SiO_2} \tag{2.4}$$

$$\text{Wet oxidation:} \quad \mathrm{Si} + 2\mathrm{H_2O} \rightarrow \mathrm{SiO_2} + 2\mathrm{H_2} \tag{2.5}$$

Deposition The MEMS deposition methods can be categorized into two groups which are with chemical reaction and with physical reaction. CVD and electrodepos-

tion belong to chemical deposition, which exploit chemical reactions in gas and/or liquid compositions or with the substrate materials to create solid materials. PVD is a physical process which mainly contains evaporation and sputtering. Atomic layer deposition (ALD) is a technique capable of depositing a variety of thin film materials from the vapor phase with a precise thickness control and good surface quality [115].

Doping Doping is to introduce atoms to replace the atoms of the lattice atoms in order to change the electrical or optical property of the material. There are several doping methods such as diffused dopant, ion exchange, and ion implantation. Diffused dopant is usually conducted in a furnace at 700°C to 1000°C in the presence of the dopant atom source which can be in a condition of gas, liquid, or solid film. Ion exchange is a local substitution of relatively mobile ions (typically Na+) originally in glass by other ions with different size and polarizability, a change of refractive index in selected regions is achieved, allowing patterning of waveguiding regions into planar substrates. It is common to be used for fabricating glass waveguides [116, 117]. Ion implantation is a high-energy process that is often used in the semiconductor industry and is becoming more and more common in IO as well [118]. In this process, a beam of atoms is ionized, accelerated to kinetic energies up to several MeV, and aimed at a suitable material target.

Etching: wet etching and dry etching
Etching is useful in creating structures such as trenches and cavities, also for the releasing of membrane, cantilevers, or free hanging masses [113]. Etching can be divided into wet etching and dry etching. Wet etching is the process that etch the material with the aid of chemical solutions, while dry etching is to remove materials with reactive ions or a vapour phase etchant. These two method will be discussed more specifically in the micromachining technology.

2.4.2. Micromachining technology

The micromachining technology can be divided into bulk micromachining, surface micromachining, and epi-micromachining.

Bulk micromachining
Bulk micromachining covers all techniques that remove significant amounts of the substrate (bulk) material to create the desired micromachined structure, which can be performed with wet or dry etches.

Wet etching Wet etching is a material removal process that uses chemical solutions or etchants to remove materials from a wafer. The specific patterns are defined by lithography using masks to transfer onto the wafer. The wet etch process can be described by three basic steps. (1) Diffusion of the liquid etchant to the structure that is to be removed. (2) The reaction between the liquid etchant and the material being etched away. (3) Diffusion of the byproducts in the reaction from the reacted surface [1].

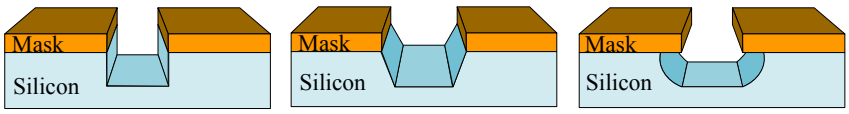

Figure 2.5: The etched structure of different etching: Completely anisotropic (left); Partially anisotropic (middle); Isotropic etching of silicon (right)

When a material is attacked by a liquid or vapour etchant, it is removed isotropically (uniformly in all directions) or anisotropic etching (uniformity in vertical direction). The difference between isotropic etching and anisotropic etching is shown in Fig. 2.5. The left and the middle figures show the etched structures of anisotropic etching and the right figure shows the result of isotropic etching.

Wet anisotropic etching of the silicon substrate is the more mature technology and the most widely used process for the fabrication of mechanical microstructures for commercially available micro-sensors. The important agents used for anisotropic wet etching are potassium hydroxide (KOH) [3, 119], Ethylenediamine pyrocatechol (EDP) [6, 7], and tetra methyl ammonium hydroxide (TMAH) [8, 9].

For isotropic wet etching, the most common etchant solvent for silicon is "HNA", a mixture of hydrofluoric acid (HF), nitric acid (HNO), and acetic acid (CHCOOH) [10]. The concentrations of each etchant determines the etch rate. Silicon dioxide or silicon nitride is usually used as a masking material against HNA.

The presence of light has a strong impact on the isotropy of the porous silicon formation process, both in HF or AFEM solutions. By properly using this effect, both isotropic and anisotropic modes of the porous silicon formation can be achieved in a single etch step. This approach results in high-aspect-ratio microstructures, made in a single-step electrochemical etching, using only one mask [11–13]. The electrochemical etching setup is shown in Fig. 2.6 [66]. A capacitor based on an electrochemically etched macroporous silicon substrate is reported in [120].

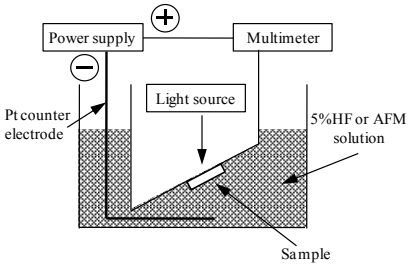

(a) schematic drawing of the electrochemical etching setup

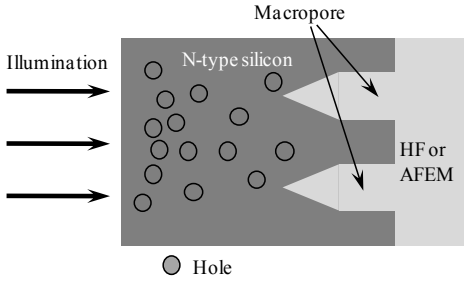

(b) the macro pores formation mechanism

Figure 2.6: The electrochemical etching setup [66]

Dry etching Dry etching is one of the most widely used processes in semiconductor manufacturing. In dry etching, plasma or etchant gasses remove the substrate

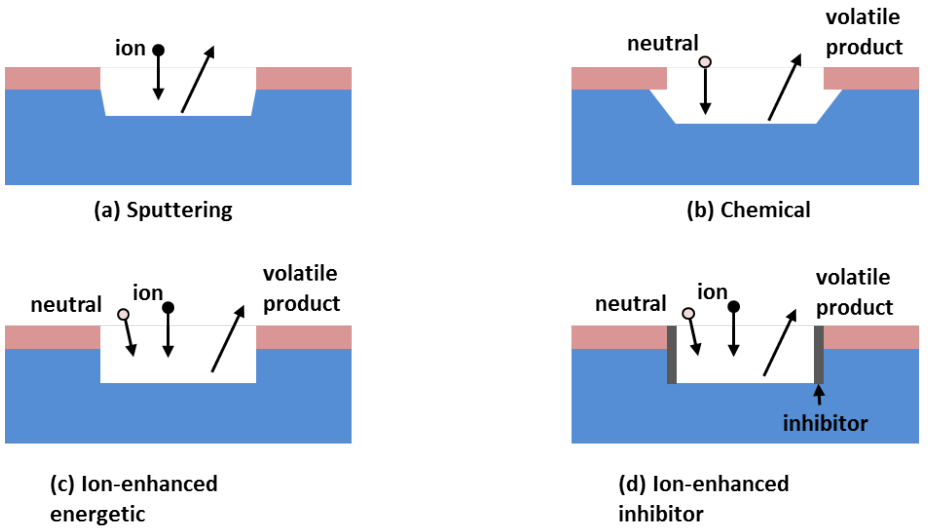

Figure 2.7: The four dry etching mechanisms

material. The reaction that takes place can be done utilising high kinetic energy of particle beams, chemical reaction, or a combination of both. Dry etching provides the ability to control sidewall anisotropic etching through plasma-generated non-reactive and reactive ions. There are several different kinds of dry etching, such as plasma etching, gas etching, physical dry etching, chemical dry etching. Dry etching can be used to etch silicon to depths ranging from submicrometer to 10 μm, giving either isotropic or anisotropic profiles. A new variant of dry etching is deep-reactive-ion etching (DRIE) [66]. This technique has the capability to make very deep and narrow structures in silicon [14].

In general, we may divide dry etching mechanisms into the four basic phenomenological categories shown in Fig. 2.7, sputtering, chemical etching, ion-enhanced energetic mechanisms, and ion-enhanced inhibitor processes.

Surface micromachining

Surface micromachining basically involves depositing thin films on the wafer surface and selectively removing one or some of these layers to leave free-standing structures. Most common depositing methods are chemical vapour deposition (CVD), electrodeposition, epitaxy, thermal oxidation (for sacrificial layers), and physical vapour deposition (PVD).

The basic principle of surface micromachining is shown in Fig. 2.8: (a) Deposition of sacrificial layer; (b) patterning of the sacrificial layer; (c) depositing structural layer; (d) removal of sacrificial layer; (e) drying.

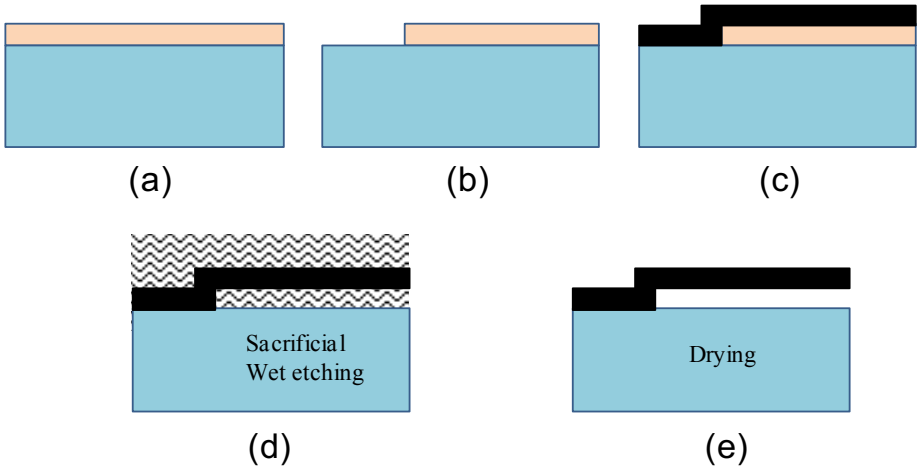

Figure 2.8: Basic process of surface micromachining

Epi-micromachining

Epi-micromachining is a group of micromachining technologies that use the epitaxial layer, or a similar thickness of the upper part of the substrate, as the mechanical layer and use a buried layer, or simply the substrate, as the sacrificial layer. Surface and bulk micromachining both have advantages and disadvantages, Epi-micromachining tries to take the advantages from both sides while minimizing the disadvantages.

Fig. 2.9 shows the basic epi-micromachining process. As with bulk micromachining this is essentially a post-processing step. After the completion of a bipolar process (Fig. 2.9a) an opening is made through the epi to the sacrificial layer (Fig. 2.9b). Finally, as with surface micromachining, the sacrificial layer is removed.

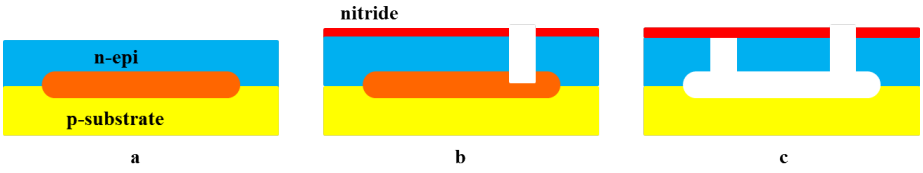

Figure 2.9: Epi-micromachining process

2.5. Micromachined optical waveguides

The former sections introduced the basic MEMS technology steps. In this section, we mainly focus on micromachined optical waveguides with freestanding, movable structures such as cantilevers, bridges, membranes, etc.

2.5.1. Micromachined waveguide structures and fabrication

Micromachined optical waveguides, including cantilever waveguide, membrane waveguide, bridge waveguide, or other types of waveguides, are quite common in optical sensing such as mechanical sensing and biomedical sensing. The main feature of micromachined waveguides lie in the mechanical structure and it plays a role in the waveguide system.

The main fabrication process contains the general fabrication of waveguide and the release of the structure which can be achieved by wet etching or dry etching [99] to detach the waveguide from the substrate. The general fabrication can be expressed by an example of a freestanding waveguide in Fig. 2.10 where the waveguide is fabricated by RIE and freestanding structure is released by wet etching. The freestanding structure is made to increase the sensing area and sensitivity.

2.5.2. Micromachined waveguide development and applications

An early freestanding waveguide can be traced back to 1992 researched in Delft University of Technology as shown in Fig. 2.11. The fabrication process includes sputtering, photolithography, and isotropic wet etching. This waveguide was mainly for acoustic signal sensing and can also be used to sense vibration, acceleration, scanning force microscope, and surface profile with an estimated sensitivity of 0.1$\mathring{A}$ displacement and 10^{-10}N force [122].

In the same year, Vadekar also proposed an integrated silicon micromechanical interferometer as a pressure sensor. It used phase change caused by pressure induced beam deflection for sensing. The calculated sensitivity is $1.29\times10^{-14}P$ (P is the applied pressure here). One year later, Wagner proposed a Mach-Zenhner interferometer based sensor similar optical pressure sensor with a different core material which is SiON. They were both released by KOH etching. In 1994, De Brabander combined the optical ring resonator with diaphragm for pressure sensing. A linear response to pressure is observed for the TM mode with a sensitivity of 0.0094 rad/kPa. Fisher presented a pressure sensor with strip-loaded Mach-Zehner interferometer located on the sensing membrane and TM was proved to be more sensitive than TE mode. Then in 1995, Eng made silicon on insulator cantilever waveguide with less than 1.8dB/cm propagation loss at 1.3μm wavelength (shown in Fig. 2.12a). This waveguide system was fabricated using surface micromachining by etching away the sacrificial layer under the waveguide. The optical loss of the cantilever waveguide was measured to be less than 2dB/cm [125]. In 1998, Burcham fabricated channel waveguide with air-silicon-air and SiO_2-silicon-SiO_2 structure with losses of 0.57-0.80dB/cm and 1.12-1.52dB/cm, respectively. The advantage lied in the integration with silicon platform for an optimal alignment for maximizing coupling [126]. The system is shown in Fig. 2.12b. In 1999, Ollier developed an optical vibrometer to allow monitoring rotating machine in harsh electromagnetic environments, shown in Fig. 2.12c. The measured frequency range is from 30 to 2000Hz with a linearity better than ±5% [127]. In 2000, Pandraud proposed a new way to fabricate freestanding structure in <111> silicon wafers rather than SOI which will reduce the cost significant if applied to the integrated optical system. The

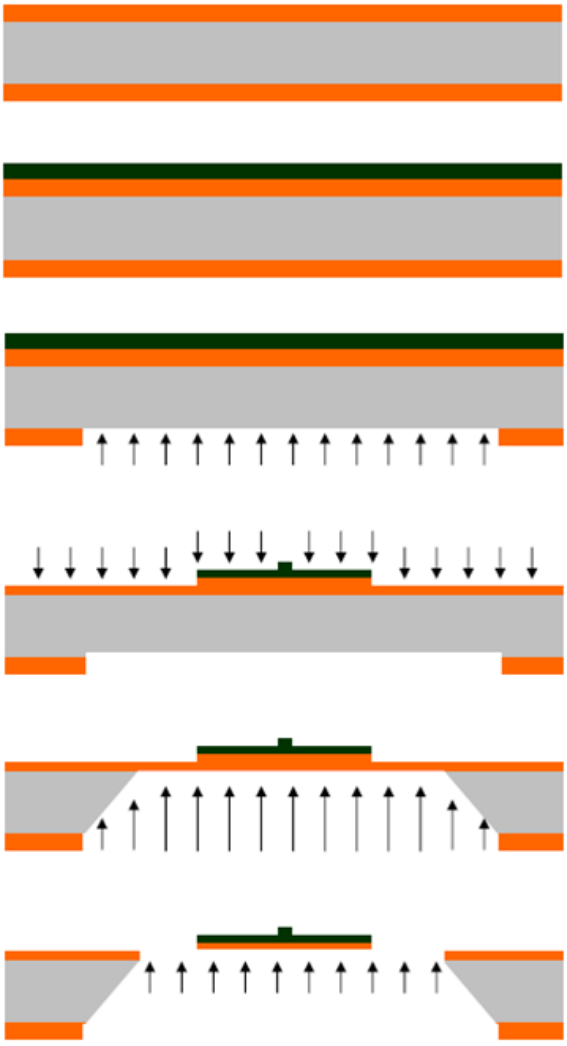

Figure 2.10: Fabrication flowchart of the freestanding waveguide [121]

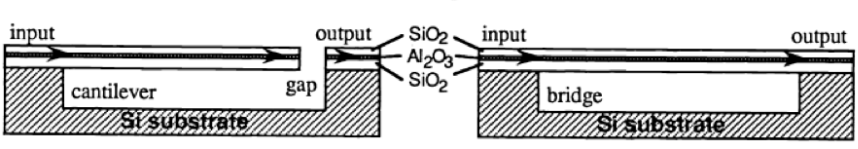

Figure 2.11: Freestanding cantilever waveguide and bridge waveguide

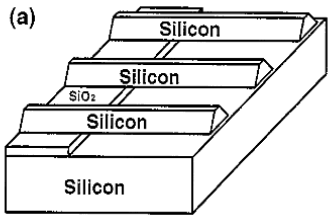

(a) Surface-micromachined epitaxial silicon cantilevers as movable optical waveguides on the silicon-on-insulator substrate [123]

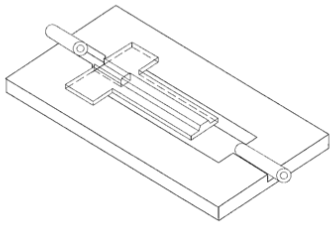

(b) Example of a MEMS platform supporting fibers and a freestanding waveguide designed by Burcham

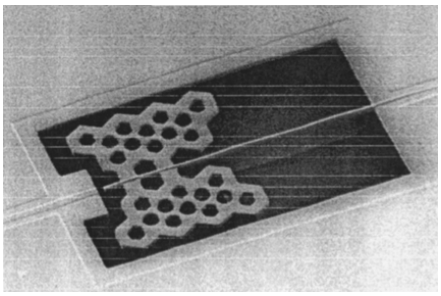

(c) SEM view of the sensitive part of the sensor [99]

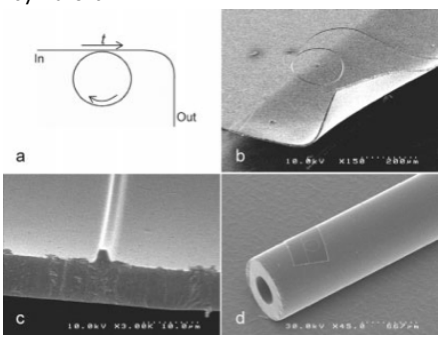

(d) Freestanding all polymer ring resonator [124]

Figure 2.12: Typical waveguide structures

low surface roughness made it promising for evanescent sensing [128]. Then optical mechanical waveguides began to be used in optical-mechanical switches/logic gates [99, 129–131], optical scanners [98], or micro-vibration sensors. Recently, polymers are increasingly widely used in fabricating optical waveguides and they were also made into freestanding mechanical structures [124, 132, 133]. Lee in 2000 proposed and demonstrated a low-power consumption thermos-optic variable optical attenuator using micromachined membrane-type waveguide made of a fluorinated polyimide, with the power consumption 25mW at 1500nm. Later in 2003, Horvath presented a new methodology to fabricate all-polymer freestanding waveguide, which has a reverse symmetry structure to increase the penetration depth of evanescent wave. UV curable resin was the waveguide material and PDMS was acting as supporting and transporting structures. This fabrication method is attractive to microfluidic and packaging. In [124], freestanding all polymer integrated optical ring resonator was fabricated using SU-8 as core and UV15 as the substrate which can be seen in Fig. 2.12d. The core waveguide structure was made by E-beam lithography and then the whole device was peeled off. Then the whole device can be transferred to various substrate because of its flexibility. Yang in 2007 proposed a direct-write process to produce freestanding silicon waveguides

by scanning focused beam over silicon substrate and then developed by electrochemical etching. The propagation loss is rather high for preliminary structures for 13.4dB/cm and 14.6dB/cm for TE and TM separately.

To date, optical mechanical waveguides already have various applications in many aspects such as optical communication including optical switches/logic gate and optical attenuators, pressure sensor, optical scanner, optical vibration sensor, biomedical, and chemical sensor due to their following advantages.

1. If the waveguide is released, then there will be less leakage into the substrate.

2. More properties of the waveguide can be used for sensing, such as mechanical, thermal, and so on, which will broaden the application of waveguides.

3. Very thin layers can be fabricated which will enhance the sensitivity of the whole system. And for sensing, the released surface can also be used to increase the sensing areas.

The examples above are only few typical ones picked from the numerous waveguides. For different applications, different structures and materials are needed based on practical considerations.

2.6. Conclusions

This chapter introduced optical waveguide from its basic principle, materials, fabrication, and also applications. Materials of the waveguides were expanded from traditional silicon materials to polymers such as PMMA, SU-8, PDMS because the proper refractive index and as well as the low-cost, simple fabrication method.

Micromachined optical waveguide shows great advantages for its ability to be integrated with mechanical structures and electrical structures. The fact that it can be fabricated with standard MEMS technology making it compact and precise. The surface functionalization and the integration with optical microfluidic system enable the promising development for the lab-on-chip system, especially for biomedical sensing.

The current trend of optical waveguide systems is the integration of the system, which is to integrate waveguide sensing structure with optical source and detector in one chip/platform. In this way, a compact system with whole function can be achieved in a single chip. Flexible or stretchable waveguide is another trend especially in wearable photonic devices and curved surface or some bending optical system. In the development of polymer waveguides, there are more and more opportunity in making flexible/stretchable optical waveguides or optical systems. Besides the promising sides of the optical waveguide systems, there are still a lot to do such as improving the sensitivity and also the detection limit of the waveguides. There has been a lot of research in optical waveguide system, however, few can meet the medical diagnose requirements. So in the future, efforts should be paid more on the sensitivity and detect limit, also the stability and reliability of the whole system before its application in biomedical field.

References

[1] P. Hondros, D., Debye, *Elektromagnetische Wellen an dielektrischen Drähten,* Ann. Phys. **337**, 465 (1910).

[2] T. M. Adams and R. A. Layton, *Introductory MEMS* (Springer US, Boston, MA, 2010).

[3] T. Tamir and E. Garmire, *Berlin: Springer-Verlag*, Vol. 2 (1979) arXiv:arXiv:1011.1669v3 .

[4] A. W. Snyder and J. Love, *Optical waveguide theory* (Springer Science & Business Media, 2012).

[5] H. Schmidt, D. Yin, J. P. Barber, and A. R. Hawkins, *Hollow-core waveguides and 2-D waveguide arrays for integrated optics of gases and liquids,* IEEE Journal on Selected Topics in Quantum Electronics **11**, 519 (2005).

[6] V. Brioude and O. Parriaux, *Normalised analysis for the design of evanescent-wave sensors and its use for tolerance evaluation,* Optical And Quantum Electronics **32**, 899 (2000).

[7] Y. Xin, A. Purniawan, L. Pakula, G. Pandraud, and P. J. French, *Simulation of Bio-medical Waveguide in Mechanical and Optical Fields,* COMSOL (2014).

[8] C. R. Taitt, G. P. Anderson, and F. S. Ligler, *Evanescent wave fluorescence biosensors,* Biosensors and Bioelectronics **20**, 2470 (2005).

[9] M. W. Pruessner, K. Amarnath, M. Datta, D. P. Kelly, S. Kanakaraju, P. T. Ho, and R. Ghodssi, *InP-based optical waveguide MEMS switches with evanescent coupling mechanism,* Journal of Microelectromechanical Systems **14**, 1070 (2005).

[10] A. Melloni, R. Costa, G. Cusmai, and F. Morichetti, *The role of index contrast in dielectric optical waveguides,* International Journal of Materials and Product Technology **34**, 421 (2009).

[11] R. G. Hunsperger, *Integrated optics*, Vol. 4 (Springer, 1995).

[12] M. Hoffmann and E. Voges, *Bulk silicon micromachining for mems in optical communication systems,* Journal of Micromechanics and Microengineering **12**, 349 (2002).

[13] X. C. Tong, *Advanced materials for integrated optical waveguides* (Springer, 2016).

[14] H. Ohji, P. T. J. Gennissen, P. J. French, and K. Tsutsumi, *Fabrication of a beam-mass structure using single-step electrochemical etching for micro structures (SEEMS),* Journal of Micromechanics and Microengineering **10**, 440 (2000).

[15] H. Ohji, S. Izuo, P. J. French, and K. Tsutsumi, *Macroporous-based micromachining on full wafers,* Sensors and Actuators, A: Physical **92**, 384 (2001).

[16] W. Theiss, *Optical properties of porous silicon,* Surface Science Reports **29**, 91 (1997).

[17] H. F. Arrand, T. M. Benson, P. Sewell, A. Loni, R. J. Bozeat, R. Arens-Fischer, M. Krüger, M. Thönissen, and H. Lüth, *The application of porous silicon to optical waveguiding technology,* IEEE Journal on Selected Topics in Quantum Electronics **4**, 975 (1998).

[18] J. J. Saarinen, S. M. Weiss, P. M. Fauchet, and J. Sipe, *Optical sensor based on resonant porous silicon structures,* Optics Express **13**, 3754 (2005).

[19] G. Rong, A. Najmaie, J. E. Sipe, and S. M. Weiss, *Nanoscale porous silicon waveguide for label-free DNA sensing,* Biosensors and Bioelectronics **23**, 1572 (2008).

[20] K. Schmitt, K. Oehse, G. Sulz, and C. Hoffmann, *Evanescent field sensors based on tantalum pentoxide waveguides–a review,* Sensors **8**, 711 (2008).

[21] S. V. Deshpande, E. Gulari, S. W. Brown, and S. C. Rand, *Optical properties of silicon nitride films deposited by hot filament chemical vapor deposition,* Journal of Applied Physics **77**, 6534 (1995).

[22] Y. Huang, G. Pandraud, and P. M. Sarro, *Characterization of low temperature deposited atomic layer deposition TiO2 for MEMS applications,* Journal of Vacuum Science & Technology A: Vacuum, Surfaces, and Films **31**, 01A148 (2013).

[23] B.-H. Moon, Y.-M. Sung, and C.-H. Han, *Titanium oxide films prepared by sputtering, sol gel and dip coating methods for photovoltaic application,* Energy procedia **34**, 589 (2013).

[24] Y. Huang, G. Pandraud, and P. M. Sarro, *Reflectance-based two-dimensional TiO_2 photonic crystal liquid sensors,* Optics Letters **37**, 3162 (2012).

[25] A. Ferguson, A. Kuver, J. Heaton, Y. Zhou, C. Snowden, and S. Iezekiel, *Low-loss, single-mode gaas/algaas waveguides with large core thickness,* IEE Proceedings-Optoelectronics **153**, 51 (2006).

[26] C. Charlton, M. Giovannini, J. Faist, and B. Mizaikoff, *Fabrication and characterization of molecular beam epitaxy grown thin-film GaAs waveguides for mid-infrared evanescent field chemical sensing,* Analytical Chemistry **78**, 4224 (2006).

[27] H. Inoue, K. Hiruma, K. Ishida, T. Asai, and H. Matsumura, *Low loss gaas optical waveguides,* IEEE Transactions on Electron Devices **32**, 2662 (1985).

[28] Z. Zheng, A. M. Weiner, J. H. Marsh, and M. M. Karkhanehchi, *Ultrafast optical thresholding based on two-photon absorption GaAs waveguide photodetectors,* IEEE Photonics Technology Letters **9**, 493 (1997).

[29] S. Adachi, *Physical properties of III-V semiconductor compounds* (John Wiley & Sons, 1992).

[30] W. Van Parys, M. Vanwolleghem, D. Van Thourhout, R. Baets, J. Decobert, B. Dagens, B. Thedrez, R. Wrix-Speetjens, and L. Lagae, *Inp-based monolithically integrated optical waveguide isolator with 32 db/cm isolation,* in *Lasers and Electro-Optics Society, 2004. LEOS 2004. The 17th Annual Meeting of the IEEE*, Vol. 1 (IEEE, 2004) pp. 386–387.

[31] K. Lee, N. LaBianca, S. Rishton, S. Zolgharnain, J. Gelorme, J. Shaw, and T.-P. Chang, *Micromachining applications of a high resolution ultrathick photoresist,* Journal of Vacuum Science & Technology B: Microelectronics and Nanometer Structures Processing, Measurement, and Phenomena **13**, 3012 (1995).

[32] B. Bêche, N. Pelletier, E. Gaviot, and J. Zyss, *Single-mode te00–tm00 optical waveguides on su-8 polymer,* Optics Communications **230**, 91 (2004).

[33] S. Balslev, B. Bilenberg, O. Geschke, A. M. Jorgensen, A. Kristensen, J. P. Kutter, K. B. Mogensen, and D. Snakenborg, *Fully integrated optical system for lab-on-a-chip applications,* in *Micro Electro Mechanical Systems, 2004. 17th IEEE International Conference on.(MEMS)* (IEEE, 2004) pp. 89–92.

[34] N. Pelletier, B. Bêche, N. Tahani, J. Zyss, L. Camberlein, and E. Gaviot, *Su-8 waveguiding interferometric micro-sensor for gage pressure measurement,* Sensors and Actuators A: Physical **135**, 179 (2007).

[35] B. Y. Shew, Y. C. Cheng, and Y. H. Tsai, *Monolithic SU-8 micro-interferometer for biochemical detections,* Sensors and Actuators, A: Physical **141**, 299 (2008).

[36] D. A. Chang-Yen and B. K. Gale, *An integrated optical oxygen sensor fabricated using rapid-prototyping techniques,* Lab on a Chip **3**, 297 (2003).

[37] J. Hsieh, C.-J. Weng, H.-L. Yin, H.-H. Lin, and H.-Y. Chou, *Realization and characterization of su-8 micro cylindrical lenses for in-plane micro optical systems,* Microsystem technologies **11**, 429 (2005).

[38] M. Nordström, D. a. Zauner, A. Boisen, and J. Hübner, *Single-mode waveguides with SU-8 polymer core and cladding for MOEMS applications,* Journal of Lightwave Technology **25**, 1284 (2007).

[39] P. Gaso, D. Pudiš, I. Martincek, and D. Jandura, *Fabrication of optical waveguide structures based on pdms using photoresist fibers,* in *19th Polish-Slovak-Czech Optical Conference on Wave and Quantum Aspects of Contemporary*

Optics, Vol. 9441 (International Society for Optics and Photonics, 2014) p. 944118.

[40] D. A. Chang-Yen, R. K. Eich, and B. K. Gale, *A monolithic PDMS waveguide system fabricated using soft-lithography techniques,* Journal of Lightwave Technology **23**, 2088 (2005).

[41] A. Neyer, S. Kopetz, E. Rabe, W. Kang, and S. Tombrink, *Electrical-optical circuit board using polysiloxane optical waveguide layer,* in *Electronic Components and Technology Conference, 2005. Proceedings. 55th* (IEEE, 2005) pp. 246–250.

[42] H. Hosseinkhannazer, L. Kostiuk, and J. McMullin, *Two-species microparticle detection in optofluidic biochips with polymeric waveguides,* in *Photonics North 2008*, Vol. 7099 (International Society for Optics and Photonics, 2008) p. 70990H.

[43] T. Izawa and H. Nakagome, *Optical waveguide formed by electrically induced migration of ions in glass plates,* Applied Physics Letters **21**, 584 (1972).

[44] S. Honkanen, B. R. West, S. Yliniemi, P. Madasamy, M. Morrell, J. Auxier, A. Schülzgen, N. Peyghambarian, J. Carriere, J. Frantz, R. Kostuk, J. Castro, and D. Geraghty, *Recent advances in ion exchanged glass waveguides and devices,* Physics and Chemistry of Glasses: European Journal of Glass Science and Technology Part B **47**, 110 (2006).

[45] M. Bertolotti, A. N. Chester, and S. Martellucci, *Advances in integrated optics* (Springer Science & Business Media, 2012).

[46] P. Dobal, R. Katiyar, Y. Jiang, R. Guo, and A. Bhalla, *Raman scattering study of a phase transition in tantalum pentoxide,* Journal of Raman Spectroscopy **31**, 1061 (2000).

[47] C.-Y. Tai, J. S. Wilkinson, N. M. Perney, M. C. Netti, F. Cattaneo, C. E. Finlayson, and J. J. Baumberg, *Determination of nonlinear refractive index in a ta 2 o 5 rib waveguide using self-phase modulation,* Optics express **12**, 5110 (2004).

[48] C. Chen, X. Sun, D. Zhang, Z. Shan, S. Y. Shin, and D. Zhang, *Dye-doped polymeric planar waveguide devices based on a thermal UV-bleaching technique,* Optics and Laser Technology **41**, 495 (2009).

[49] J. Jasapara, A. Nampoothiri, W. Rudolph, D. Ristau, and K. Starke, *Femtosecond laser pulse induced breakdown in dielectric thin films,* Physical Review B **63**, 045117 (2001).

[50] B. S. Ahluwalia, O. G. Helleso, A. Z. Subramanian, N. M. Perney, N. P. Sessions, and J. S. Wilkinson, *Fabrication and optimization of Tantalum Pentoxide waveguides for optical micro-propulsion,* Proc. of SPIE **7604**, 1 (2010).

[51] G. L. Duveneck, A. P. Abel, M. A. Bopp, G. M. Kresbach, and M. Ehrat, *Planar waveguides for ultra-high sensitivity of the analysis of nucleic acids,* Analytica Chimica Acta **469**, 49 (2002).

[52] M. F. A. Muttalib, R. Y. Chen, S. J. Pearce, and M. D. B. Charlton, *Anisotropic Ta2O5 waveguide etching using inductively coupled plasma etching,* Journal of Vacuum Science & Technology A: Vacuum, Surfaces, and Films **32**, 041304 (2014).

[53] A. Subramanian, C. J. Oton, R. Greef, and J. S. Wilkinson, *Er: Ta2o5 waveguide optimization & spectroscopy,* (2008).

[54] G. Li, T. Maruyama, and K. Iiyama, *Low-propagation-loss Ta2O5 optical waveguides on silica substrate,* Japanese Journal of Applied Physics **53** (2014), 10.7567/JJAP.53.04EG12.

[55] K. Gallo, J. Prawiharjo, N. Broderick, and D. J. Richardson, *Proton-exchanged linbo/sub 3/waveguides for photonic applications,* in *Transparent Optical Networks, 2004. Proceedings of 2004 6th International Conference on*, Vol. 1 (IEEE, 2004) pp. 277–281.

[56] J. L. Jackel, C. Rice, and J. Veselka, *Proton exchange for high-index waveguides in linbo3,* Applied Physics Letters **41**, 607 (1982).

[57] M. J. Li, M. P. de Micheli, D. B. Ostrowsky, and M. Papuchon, *High index low loss LiNbO3 waveguides,* Optics Communications **62**, 17 (1987).

[58] D. Hofmann, G. Schreiber, C. Hasse, H. Hermann, R. Ricken, and W. Sohler, *Continuous wave midinfrared optical parametric oscillators with periodically poled ti: Linbo3 channel waveguides,* Opt. Lett **24**, 696 (1999).

[59] O. Tadanaga, T. Yanagawa, Y. Nishida, H. Miyazawa, K. Magari, M. Asobe, and H. Suzuki, *Efficient 3-μ m difference frequency generation using direct-bonded quasi-phase-matched linbo 3 ridge waveguides,* Applied physics letters **88**, 061101 (2006).

[60] R. Kou, S. Kurimura, K. Kikuchi, A. Terasaki, H. Nakajima, K. Kondou, and J. Ichikawa, *High-gain, wide-dynamic-range parametric interaction in mg-doped linbo 3 quasi-phase-matched adhered ridge waveguide,* Optics Express **19**, 11867 (2011).

[61] S. Kurimura, Y. Kato, M. Maruyama, Y. Usui, and H. Nakajima, *Quasi-phase-matched adhered ridge waveguide in li nb o 3,* Applied physics letters **89**, 191123 (2006).

[62] P. Struk, T. Pustelny, K. Gut, K. Golaszewska, E. Kaminska, M. Ekielski, I. Pasternak, E. Lusakowska, and a. Piotrowska, *Planar optical waveguides based on thin ZnO layers,* Acta Physica Polonica-Series A General Physics **116**, 414 (2009).

[63] P. Struk, T. Pustelny, K. Golaszewska, M. a. Borysiewicz, E. Kami??ska, T. Wojciechowski, and A. Piotrowska, *ZnO - Wide bandgap semiconductor and possibilities of its application in optical waveguide structures,* Metrology and Measurement Systems **21**, 401 (2014).

[64] R. E. Mohan, P. Neha, T. Shalu, K. Darshana, and K. Sreelatha, *Fabrication of zno and doped zno waveguides deposited by spin coating,* in *IOP Conference Series: Materials Science and Engineering*, Vol. 73 (IOP Publishing, 2015) p. 012003.

[65] M. S. Wu, A. Azuma, T. Shiosaki, and A. Kawabata, *Low-loss zno optical waveguides for saw-ao applications,* IEEE transactions on ultrasonics, ferroelectrics, and frequency control **36**, 442 (1989).

[66] K. E. Petersen, *Silicon As a Mechanical Material.* Proceedings of the IEEE **70**, 420 (1982).

[67] M. Kawachi, *Silica waveguides on silicon and their application to integrated-optic components,* Optical and Quantum Electronics **22**, 391 (1990).

[68] M. Henini, *Microelectronics Journal*, Vol. 31 (2000) p. 219.

[69] A. Stoffel, A. Kovács, W. Kronast, and B. Müller, *LPCVD against PECVD for micromechanical applications,* Journal of Micromechanics and Microengineering **6**, 1 (1999).

[70] G. Pandraud, H. Pham, P. French, and P. Sarro, *Polarization-insensitive pecvd sic waveguides for sensor platform,* Optical Materials **28**, 380 (2006).

[71] G. Pandraud, H. T. M. Pham, L. S. Pakula, P. M. Sarro, and P. J. French, *Polarization-insensitive pecvd sic waveguides for photonic sensing,* in *17th International Conference on Optical Fibre Sensors*, Vol. 5855 (International Society for Optics and Photonics, 2005) pp. 836–840.

[72] L. Liu, W. Tang, B. Zheng, and H. Zhang, *Fabrication and characterization of SiC thin films,* 2011 6th IEEE International Conference on Nano/Micro Engineered and Molecular Systems , 146 (2011).

[73] H. T. M. Pham, C. R. de Boer, L. Pakula, and P. M. Sarro, *Influence of Deposition Parameters and Temperature on Stress and Strain of In Situ Doped PECVD Silicon Carbide,* Materials Science Forum **389-393**, 759 (2002).

[74] M. Gad-el Hak, *The MEMS handbook* (CRC press, 2001).

[75] M. Mehregany, C. a. Zorman, N. Rajan, and C. H. Wu, *Silicon carbide MEMS for harsh environments,* Proceedings of the IEEE **86**, 1594 (1998).

[76] P. French, P. Sarro, R. Mallée, E. Fakkeldij, and R. Wolffenbuttel, *Optimization of a low-stress silicon nitride process for surface-micromachining applications,* Sensors and Actuators A: Physical **58**, 149 (1997).

[77] W. C. Tan, S. Kobayashi, T. Aoki, R. E. Johanson, and S. Kasap, *Optical properties of amorphous silicon nitride thin-films prepared by vhf-pecvd using silane and nitrogen,* Journal of Materials Science: Materials in Electronics **20**, 15 (2009).

[78] A. Purniawan, G. Pandraud, P. French, and P. Sarro, *Tio 2 freestanding thin film as evanescent waveguide sensor for biomedical application,* in *Solid-State Sensors, Actuators and Microsystems Conference (TRANSDUCERS), 2011 16th International* (IEEE, 2011) pp. 2506–2509.

[79] I. R. McKerracher, L. Fu, H. H. Tan, and C. Jagadish, *Thermal expansion coefficients and composition of sputter-deposited silicon oxynitride thin films,* Journal of Physics D: Applied Physics **43**, 335104 (2010).

[80] D. T. F. Marple, *Refractive index of GaAs,* Journal of Applied Physics **35**, 1241 (1964).

[81] T. Brenner, M. Bachmann, and H. Melchior, *Vertically tapered InGaAsP/InP waveguides for highly efficient coupling to flat-end single-mode fibers,* Applied Physics Letters **65**, 798 (1994).

[82] E. Gini and H. Melchior, *Thermal dependence of the refractive index of InP measured with integrated optical demultiplexer,* Journal of Applied Physics **79**, 4335 (1996).

[83] T. C. Sum, A. A. Bettiol, J. A. Van Kan, F. Watt, E. Y. B. Pun, and K. K. Tung, *Proton beam writing of low-loss polymer optical waveguides,* Applied Physics Letters **83**, 1707 (2003).

[84] R. Feng and R. J. Farris, *Characterization of the Thermal and Elastic Constants for a Negative Photoresist : SU8 Coating,* Journal of Materials Science **7**, 423 (2002).

[85] S. Kopetz, D. Cai, E. Rabe, and A. Neyer, *PDMS-based optical waveguide layer for integration in electrical-optical circuit boards,* AEU - International Journal of Electronics and Communications **61**, 163 (2007).

[86] F. Schneider, J. Draheim, R. Kamberger, and U. Wallrabe, *Process and material properties of polydimethylsiloxane (PDMS) for Optical MEMS,* Sensors and Actuators A: Physical **151**, 95 (2009).

[87] M. R. Abernathy, J. Hough, I. W. Martin, S. Rowan, M. Oyen, C. Linn, and J. E. Faller, *Investigation of the Young's modulus and thermal expansion of amorphous titania-doped tantala films.* Applied optics **53**, 3196 (2014), arXiv:arXiv:1401.7061v1 .

[88] O. Heavens, *Integrated Optics,* Optica Acta: International Journal of Optics **20**, 915 (1973), arXiv:arXiv:1502.06504v1 .

[89] L. Y. Chen, W. S. Tsai, W. H. Hsu, K. Y. Chen, and W. S. Wang, *Fabrication and characterization of benzocyclobutene optical waveguides by UV pulsed-laser illumination,* IEEE Journal of Quantum Electronics **43**, 303 (2007).

[90] C. Pollock and M. Lipson, *Integrated Photonics* (Kluwer Academic Publisher, 2003).

[91] K. Iizuka, *Element of Photonics: For Fiber and Integrated Optics*, Vol. II (2002) pp. 670–672.

[92] M. A. Duguay, Y. Kokubun, T. L. Koch, and L. Pfeiffer, *Antiresonant reflecting optical waveguides in SiO2-Si multilayer structures,* Applied Physics Letters **49**, 13 (1986).

[93] F. Dell'Olio and V. M. Passaro, *Optical sensing by optimized silicon slot waveguides.* Optics express **15**, 4977 (2007).

[94] E. E. Carlyon, C. R. Lowe, D. Reid, and B. Ian, *A single mode fibre-optic evanescent wave biosensor,* Biosensors and Bioelectronics **7**, 141 (1992).

[95] Z. Hale, F. Payne, R. Marks, C. Lowe, and M. Levine, *The single mode tapered optical fibre loop immunosensor,* Biosensors and Bioelectronics **11**, 137 (1996).

[96] R. A. Potyrailo, S. E. Hobbs, and G. M. Hieftje, *Optical waveguide sensors in analytical chemistry: today's instrumentation, applications and trends for future development,* Fresenius' Journal of Analytical Chemistry **362**, 349 (1998).

[97] J. Fluitman and T. Popma, *Optical waveguide sensors,* Sensors and Actuators **10**, 25 (1986).

[98] W.-C. Wang, M. Fauver, J. N. Ho, E. J. Seibel, and P. G. Reinhall, *Micromachined optical waveguide cantilever as a resonant optical scanner,* Sensors and Actuators A: Physical **102**, 165 (2002).

[99] E. Ollier, *Optical MEMS devices based on moving waveguides,* IEEE Journal of Selected Topics in Quantum Electronics **8**, 155 (2002).

[100] S. E. Miller, *Integrated optics: An Introduction,* (1969).

[101] M. C. Wu, *Micromachining for optical and optoelectronic systems,* Proceedings of the IEEE **85**, 1833 (1997).

[102] P. K. Tien, *Integrated optics and new wave phenomena wave guides,* Reviews of Modern Physics **49**, 361 (1977).

[103] F. Chollet, *Devices based on co-integrated MEMS actuators and optical waveguide: A review,* Micromachines **7**, 1 (2016).

[104] J. A. Harrington, *A Review of IR Transmitting , Hollow Waveguides,* **217**, 211 (2000).

[105] B. R. West, *Ion-exchanged glass waveguide technology: a review,* Optical Engineering **50**, 071107 (2011).

[106] X. Fan, I. M. White, S. I. Shopova, H. Zhu, J. D. Suter, and Y. Sun, *Sensitive optical biosensors for unlabeled targets: A review,* Analytica Chimica Acta **620**, 8 (2008).

[107] P. Kozma, F. Kehl, E. Ehrentreich-förster, C. Stamm, and F. F. Bier, *Biosensors and Bioelectronics Integrated planar optical waveguide interferometer biosensors : A comparative review,* Biosensors and Bioelectronic **58**, 287 (2014).

[108] B. Kuswandi, Nuriman, J. Huskens, and W. Verboom, *Optical sensing systems for microfluidic devices: A review,* Analytica Chimica Acta **601**, 141 (2007).

[109] G. I. Stegeman and E. M. Wright, *All-optical waveguide switching,* Optical and Quantum Electronics **22**, 95 (1990).

[110] P. J. French and P. M. Sarro, *Micromachining Technology,* in *MEMS: DESIGN, ANALYSIS, AND ApPLICATIONS* (1984).

[111] O. N. Tufte, P. W. Chapman, and D. Long, *Silicon Diffused-Element Piezoresistive Diaphragms,* Journal of Applied Physics **33**, 3322 (1962).

[112] T. I. Bajenescu, C. Consulting, and L. Conversion, *Micro Electro-Optical-Mechanical Systems (MEOMS), Microelectromechanical Systems and Reliability : Challenging Issues,* , 1 (2009).

[113] H. V. Heeren and P. Salomon, *MEMS - Recent Developments, Future Directions,* Electronics Enabled Products : Technology Watch , 1 (2007).

[114] J. Melorose, R. Perroy, and S. Careas, *No Title No Title,* Statewide Agricultural Land Use Baseline 2015 **1** (2015), 10.1017/CBO9781107415324.004, arXiv:arXiv:1011.1669v3 .

[115] R. W. Johnson, A. Hultqvist, and S. F. Bent, *A brief review of atomic layer deposition: from fundamentals to applications,* Materials Today **17**, 236 (2014).

[116] A. Tervonen, B. R. West, and S. Honkanen, *Ion-exchanged glass waveguide technology: a review,* Optical Engineering **50**, 71107 (2011).

[117] A. Gabel, K. DeLong, C. Seaton, and G. Stegeman, *Efficient degenerate four-wave mixing in an ion-exchanged semiconductor-doped glass waveguide,* Applied physics letters **51**, 1682 (1987).

[118] G. C. Righini and A. Chiappini, *Glass optical waveguides: a review of fabrication techniques,* Optical Engineering **53**, 071819 (2014).

[119] K. Schmitt, B. Schirmer, and A. Brandenburg, *Label-free detection of biomolecules by waveguide interferometry,* Proceedings of SPIE **5855**, 459 (2005).

[120] V. Lehmann, W. Hönlein, H. Reisinger, A. Spitzer, H. Wendt, and J. Willer, *A novel capacitor technology based on porous silicon,* Thin Solid Films **276**, 138 (1996).

[121] A. Purniawan, *Evanescent Waveguide Sensors for Biomedical Applications*, Ph.D. thesis, TU Delft, Delft University of Technology (2014).

[122] S. Wu and H. J. Frankena, *Integrated optical sensors using micromechanical bridges and cantilevers,* **1793**, 1 (1992).

[123] T. T. Eng, S. S. Sin, S. C. Kan, and G. K. Wong, *Surface-micromachined movable soi optical waveguides,* in *Solid-State Sensors and Actuators, 1995 and Eurosensors IX.. Transducers' 95. The 8th International Conference on*, Vol. 1 (IEEE, 1995) pp. 348–350.

[124] Y. Huang, G. T. Paloczi, J. K. Poon, and A. Yariv, *Demonstration of flexible freestanding all-polymer integrated optical ring resonator devices,* Advanced Materials **16**, 44 (2004).

[125] T. T. Eng, S. C. Kan, and G. K. Wong, *Surface-micromachined epitaxial silicon cantilevers as movable optical waveguides on silicon-on-insulator substrates,* Sensors and Actuators A: Physical **49**, 109 (1995).

[126] K. E. Burcham and J. T. Boyd, *Freestanding, micromachined, multimode silicon optical waveguides at $\lambda = 1.3\ \mu m$ for microelectromechanical systems technology,* Applied optics **37**, 8397 (1998).

[127] E. Ollier, P. Philippe, C. Chabrol, and P. Mottier, *Micro-opto-mechanical vibration sensor integrated on silicon,* Journal of lightwave technology **17**, 26 (1999).

[128] G. Pandraud, G. Veldhuis, J. W. Berenschot, a. J. Nijdam, H. J. W. M. Hoekstra, O. Parriaux, and P. V. Lambeck, *Micromachining of high-contrast optical waveguides in 〈111〉 silicon wafers,* IEEE Photonics Technology Letters **12**, 308 (2000).

[129] G. P. Rehder, *Optical logic gates based on micro-electro-mechanical systems,* SPIE Newsroom , 10 (2007).

[130] P. Sun and R. M. Reano, *Submilliwatt thermo-optic switches using free- standing silicon-on-insulator strip waveguides,* **18**, 1315 (2010).

[131] Y. Akihama and K. Hane, *Single and multiple optical switches that use freestanding silicon nanowire waveguide couplers,* Light: Science & Applications **1**, e16 (2012).

[132] S. S. Lee, J. U. Bu, S. Y. Lee, K. C. Song, C. G. Park, and T. S. Kim, *Low-power consumption polymeric attenuator using a micromachined membrane-type waveguide,* IEEE Photonics Technology Letters **12**, 407 (2000).

[133] R. Horváth, H. C. Pedersen, N. Skivesen, D. Selmeczi, and N. B. Larsen, *Optical waveguide sensor for on-line monitoring of bacteria.* Optics letters **28**, 1233 (2003).

3

Waveguide Structures, Materials, and Coupler Design Considerations

Some basic knowledge of waveguides has already been generally introduced in Chapter 2, including waveguide structures, materials, and fabrication technology. In this chapter, a basic theoretical analysis of a waveguide will be introduced first. Then the design of a specific waveguide will also be studied. Structure is one important factor taken into consideration, while other properties, especially optical properties of the waveguide materials, are also very important. They must be combined with the optical source used and the applied condition. If the waveguide is used as a biomedical sensor, it should be chemically stable and biocompatible. On the other hand, if the waveguide is designed for an optical-mechanical sensor, mechanical stability matters. All these factors need to be taken into consideration for practical applications. In this chapter, three commonly used waveguide structures will be illustrated and compared, together with some potential waveguide materials. As an important component, coupler design will also be introduced.

3.1. Introduction: theoretical analysis of waveguides

Electromagnetic waves and their behavior must be considered, when analyzing photonic devices. When a waveguide is in a medium free of source, it fulfills the following simplified Maxwell equation:

$$\Delta \cdot D = 0 \tag{3.1}$$

$$\Delta \cdot B = 0 \tag{3.2}$$

$$\Delta \times E = -\frac{\partial B}{\partial t} \tag{3.3}$$

$$\Delta \times H = \frac{\partial D}{\partial t} \tag{3.4}$$

where E is the electric field (V/m), H is the magnetic field (A/m), D is electric flux density, and B is magnetic flux density.

3.1.1. Planar waveguide model

When light propagates in a dielectric waveguide, it will exist in some certain modes. A mode is transverse and its amplitude and polarization profiles remains constant along z direction.

The electric and magnetic fields of a propagating wave can be described as:

$$E_v(r,t) = E_v(x,y)\exp[j(kz \pm \omega t)] \tag{3.5}$$

$$H_v(r,t) = H_v(x,y)\exp[j(kz \pm \omega t)] \tag{3.6}$$

Where v is the mode index, E and H are the mode profiles, and k is the propagation constant in the direction of the wavefront. For planar waveguides, the mode profiles do not depend on the y coordinate, thus the equations can be rewritten as:

$$E_v(r,t) = E_v(x)\exp[j(kz \pm \omega t)] \tag{3.7}$$

$$H_v(r,t) = H_v(x)\exp[j(kz \pm \omega t)] \tag{3.8}$$

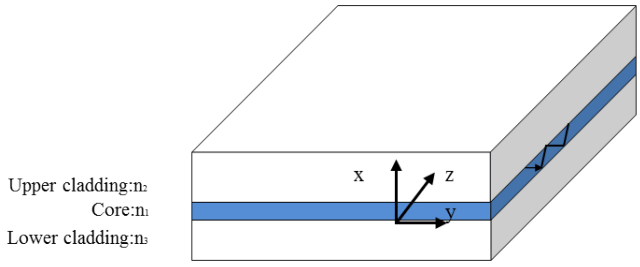

Figure 3.1: Basic structure of a planar waveguide

It illustrates a simple planar waveguide in Fig. 3.1, with a core refractive index of n_1, and upper cladding of n_2 and lower cladding of n_3. light propagates in z direction. Here $n_1 > n_2$, $n_1 > n_3$, and we assume that $n_3 > n_2$, which is the usual case for real application. For an optical waveguide with an angular frequency of ω and free space wavelength of λ, the propagation constants in three different media are defined as:

$$k_1 = n_1\omega/c,\ k_2 = n_2\omega/c,\ k_3 = n_3\omega/c, \tag{3.9}$$

where $k_1 > k_2 > k_3$.

The height of the waveguide is set to be h. As it is described in Chapter 2, light is confined by total internal reflection. There are two critical angles: one reflected at both the upper and lower interfaces.

$$\theta_{c2} = \sin^{-1}(n_2/n_1),\ \theta_{c3} = \sin^{-1}(n_3/n_1) \tag{3.10}$$

Here, $\theta_{c3} > \theta_{c2}$, because $n_3 > n_2$. When $\theta > \theta_{c3} > \theta_{c2}$, light will be totally reflected at the upper and lower interfaces and guided in the waveguide core (n_1), which will result in guided modes.

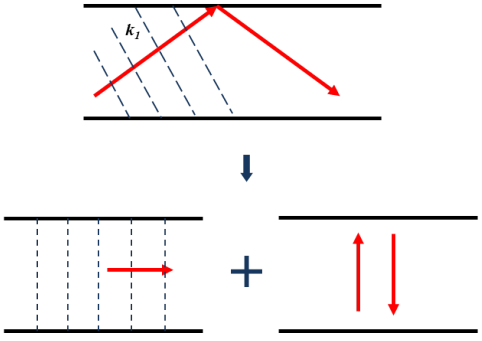

Figure 3.2: Decompose light propagation into y and z directions

In the waveguide core, light propagates along the zig-zag path with a wavevector of k_1. The zig-zag wave can also be regarded as two orthogonal components

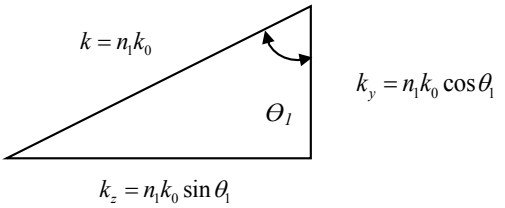

Figure 3.3: Decompose propagation constant into y and z components

travelling in the x and z directions, as shown in Fig. 3.2. Thus k_1 can be decomposed in the x and z directions into two components (shown in Fig. 3.3):

$$k_z = k_1 \sin\theta \tag{3.11}$$
$$k_x = k_1 \cos\theta \tag{3.12}$$

When a wave is reflected between two interfaces, it will interfere with itself and guided modes will form when the transverse condition is satisfied, which is:

$$2k_1 h \cos\theta_1 - \phi_u - \phi_l = 2m\pi \tag{3.13}$$

where ϕ_u and ϕ_l are the phase shifts on the reflection of the upper and lower interfaces, and m is an integer which can be 0, 1, 2, ... There will be a series of discrete solutions (angle θ) which means light can only propagate at some certain angles. Each solution is referred to as a mode [1].

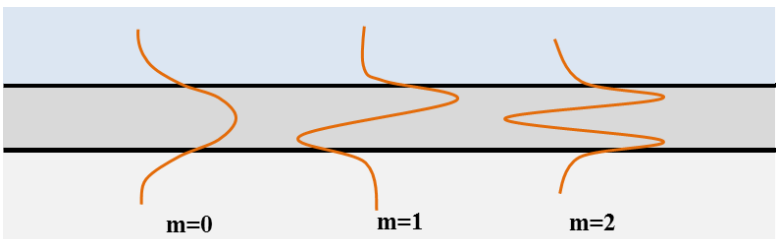

Figure 3.4: Fundamental mode and higher order mode profiles

The guided mode with $m = 0$ is called fundamental mode, while modes with $m = 1, 2, \ldots$ are referred to as higher-order modes (see Fig. 3.4).

3.1.2. Evanescent waveguide analysis

For the guided mode, there will be an evanescent field in the upper and lower claddings, which propagates only in the z direction and decays in x direction which is normal to the interface.

The propagation constant at the boundary on the n_1 side must match that with that of the n_2 side, for which is $k_1 = k_2$ must be satisfied. This condition is known

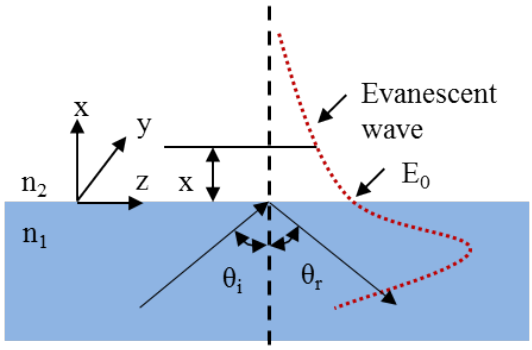

Figure 3.5: Evanescent wave profile on the interface of the waveguide

as the phase matching condition.

$$k_1 \sin\theta_1 = k_2 \sin\theta_2 \tag{3.14}$$

In the upper layer,

$$E_2 = E_0 \exp(\kappa x) \exp[j(k_{2z} z \pm \omega t)] \tag{3.15}$$

$$\kappa = k(n_1^2 \sin^2\theta_1 - n_2^2)^{1/2} \tag{3.16}$$

where E_0 is the electric field at the boundary: $\theta_i = \theta_r = \theta_1$. The interface between the cladding layer and core layer is set as the zero point of the x axis, as shown in Fig. 3.5. Regardless of the z direction absorption, at a certain cross section of waveguide, the evanescent wave can be rewritten as:

$$E_2(x) = E_0 \exp(-\kappa x) \tag{3.17}$$

These evanescent waves can be used for surface sensing or bulk sensing. When evanescent waves are applied in sensing, there are two detection methods: absorption measurements or fluorescence measurements. In this thesis, we focus on evanescent waveguides based on absorption measurements.

3.1.3. Confinement factors

For evanescent waveguides, not all of the optical energy is distributed in the waveguide core. It is therefore necessary to know the distribution of light in a waveguide. Understanding the amount of light distributed inside the optical waveguide core is useful, e.g., in telecommunication or other optical transmission devices. Additionally, knowing the percentage of light distributed in the cladding outside waveguide core is also necessary, especially in the sensing area. It is the evanescent wave that is used for sensing. The confinement factor (Γ_w) shown in the following equation is to quantify optical confinement, while the cladding filling factor (Γ_c) is to specify

the light distributed in the cladding/sensing area:

$$\Gamma_w = \frac{\iint_w |E(x,y)|^2 \, \mathrm{d}x \, \mathrm{d}y}{\iint_\infty |E(x,y)|^2 \, \mathrm{d}x \, \mathrm{d}y} \tag{3.18}$$

$$\Gamma_c = \frac{\iint_c |E(x,y)|^2 \, \mathrm{d}x \, \mathrm{d}y}{\iint_\infty |E(x,y)|^2 \, \mathrm{d}x \, \mathrm{d}y} \tag{3.19}$$

where $E(x,y)$ is the electric field vector, w is the core area and c is the cover medium area.

3.1.4. Waveguide sensitivity

Sensitivity is an important criterion for a waveguide sensing system. It is defined as the amount of change in sensor output resulting from a unit change on the sensor surface [2]. A unit of input can be the refractive index change in cladding, solution concentrations, absorbed bio-targets, etc. For evanescent wave sensing or slot sensing, sensitivity depends on the optical energy distribution in the cladding area which can interact with the targets in the cladding. Therefore, to achieve a waveguide with a higher sensitivity requires designing a structure that allows more optical energy to be distributed outside the waveguide core that reaches into the cladding. Thus the cladding filling factor in the cover medium or slot area, which is defined in Equation (3.18) and Equation (3.19) as a mathematical expression of the proportion of the optical energy distributed in the cladding or slot, can be used here as the criteria for designing waveguide [3]. This will be analyzed more specifically below.

3.2. Materials

Material selection is an important step in designing optical waveguides. As mentioned above, there are many materials that could be used as optical waveguides. When it comes to a specific waveguide, the choices must not only be based on optical properties, and sometimes mechanical properties, but they also depend on the fabrication techniques, surrounding set-ups (optical source), applications, and experimental conditions. The fabrication technique will determine the waveguide quality such as the surface roughness and homogeneity. The optical source decides the wavelength applied in the system and the chosen materials should be transparent or have a low absorption rate in this range. Moreover, the experimental condition or application may add more material requirements. All these factors above must be taken into account when designing waveguides.

For waveguide core materials, considering the robustness of the whole system, SiC is a proper material that has already generated considerable interest in MEMS device fabrication due to its excellent mechanical and electrical properties, and chemical resilience. It also has potential in optical waveguide fabrication. From an

optical point of view, it is transparent above 0.5μm wavelength. Thus wavelengths in the visible and the near infrared can be guided. SiC has a rather high refractive index generally ranging from 2.3 to 2.5 [4] or even higher than 2.5, making it a promising material in optics but also more preferable when fabricating bent and small radius waveguides [5]. Mechanically, SiC is robust and has a high Young's modulus making it stand out in the design of freestanding structures such as thin films or bridges. Chemically, it is highly stable even in harsh environments and it can be made into sensors in high temperature or fluctuating environments. Furthermore, SiC can be deposited on wafers using LPCVD, PECVD, and APCVD. By changing the processing conditions, such as temperature and gas ratio, a-SiC or poly-SiC with adjustable refractive indices and mechanical properties can be obtained, allowing for more flexibility in waveguide design. LPCVD shows good uniformity when depositing thin layers with a deposition rate of around 0.2nm/min, while PECVD SiC has a lower deposition temperature (200°C to 400°C) and a higher deposition rate ranging from 40nm/min to 100nm/min [6], which make it beneficial when thicker layer and lower temperature conditions need to be met. Considering the excellent properties of SiC, it is a potential waveguide core material in an evanescent sensing system.

TiO_2 is another potential suitable material that has some good properties for making into waveguides. TiO_2 can be deposited by Atomic Layer Deposition (ALD), which is a highly conformal coating method that can achieve high surface conformity. TiO_2 has a proper optical refractive index (2.45) which suits the optical waveguide core. It is also used in former waveguide designs which have already been illustrated in [7]. Therefore it also has potential for waveguide sensing applications.

Polymers are new emerging materials for MEMS applications and are commonly used in integrated optics due to their adjustable refractive indices, good mechanical properties, low cost, compatibility with semi-conductor technology, etc. [8]. Considering the simplicity and qualification of fabrication, SU-8 is a rather promising material to investigate. SU-8 is a photon-sensitive material that allows fabrication by photolithography which simplifies the fabrication process. By avoiding dry etching, the sidewall roughness is reduced and the scattering loss is lowered. SU-8, as an epoxy photoresist, can be fabricated by UV or E-beam lithography making it stand out with the advantage of allowing maskless processes, low-cost prototyping, and fast and sub-micron fabrication with high precision [9]. At the same time, SU-8 is a suitable material for optical waveguides in mechanical, optical, and bio-chemical perspectives. Mechanically, it is very stable after polymerization and hard baking, which is important for optical sensing [10–12]. Optically, it is transparent above 400nm, while the refractive of SU-8 is 1.57 at 1.3μm [5, 6], which meets the demands of waveguide core materials when SiO_2 is used as a substrate. Another important characteristic is that the surface of SU-8 has good biocompatibility and chemical resistance which play important roles in biomedical applications. Furthermore, the surface of SU-8 can be functionalized with antibodies [13], which broadens the application range of this material into biomedical sensors [10], medical diagnostic applications [14], etc. Considering the proper characteristics of SU-8,

it was chosen as one of the investigated waveguide materials.

For the sub-cladding material, currently, the most commonly used isolation layer to prevent light from leaking into the substrate is SiO_2, which is easily integrated with MEMS fabrication based on a silicon wafer. SiN is another good material which can work with SiC or TiO_2. It can be deposited with LPCVD and PECVD, with the gases NH_3 and DCS. It has an adjustable refractive index between 1.9 and 2.4 with different gas ratios. Also it has good mechanical stability and can be made into a low-stress film under certain deposition conditions [15, 16].

3.3. Waveguide Structures

Rib, ridge, and slot waveguides are some commonly used waveguides for biomedical or chemical sensing. The basic structures of these three types are shown in Fig. 3.6. For rib/ridge waveguides, light is confined in the high refractive index areas, while the wave used for sensing is the evanescent wave that penetrates into the cladding from the core. This means that the more the evanescent wave is distributed in the sensing area, the more sensitive the waveguide will be, which can be a guide for designing the waveguide structures. For slot waveguides, the evanescent wave is confined in the low refractive index area (the slot area), where light is used for sensing. In this situation, the optical energy distributed in the slot area determines the sensitivity of the waveguide. Different waveguides and the potential materials will be introduced and compared to obtain an optimal waveguide structure that fits our situation.

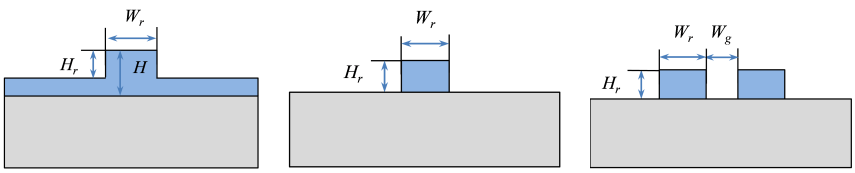

(a) Rib waveguide (b) Ridge waveguide (c) Slot waveguide

Figure 3.6: Different waveguide structures

After narrowing down the material range, in this section, simulations of different materials and structures are combined to find an optimal waveguide design.

For evanescent wave sensing or slot sensing, measurement sensitivity depends on optical distribution in the cladding area, thus the cladding filling factor or confinement factor in the cover medium is used here as the criterion. The confinement factor in the cover medium or in the gap of the slot waveguide has already been defined in Equation (3.18) and Equation (3.19), which they are rewritten here as:

$$\Gamma_c = \frac{\iint_c |E(x,y)|^2 \, \mathrm{d}x \, \mathrm{d}y}{\iint_\infty |E(x,y)|^2 \, \mathrm{d}x \, \mathrm{d}y} \tag{3.20}$$

$$\Gamma_G = \frac{\iint_G |E(x,y)|^2 \, \mathrm{d}x \, \mathrm{d}y}{\iint_\infty |E(x,y)|^2 \, \mathrm{d}x \, \mathrm{d}y} \tag{3.21}$$

Simulations were carried out for the cladding filling factor to compare the cladding filling factors of different structures with the same material setting. Here TiO_2 is taken as the waveguide core material with a refractive index of 2.45 and SiO_2 as the waveguide substrate cladding with a refractive index of 1.45.

3.3.1. Rib waveguide

For the rib waveguide, the influencing factors include rib width (W_r), rib height (H_r), and waveguide height (H). Simulations were also carried with different values for each parameter. The mode of rib waveguide is plotted in Fig. 3.7. The results are shown in Fig. 3.8. With the same waveguide and rib height, the cladding filling factor increases with the decrease in the rib width. The narrower the rib width is, the more influence the rib height will have on the cladding filling factor. Moreover, the total waveguide height also has an influence on the cladding filling factor. The increase in waveguide height will slightly decrease the cladding filling factor.

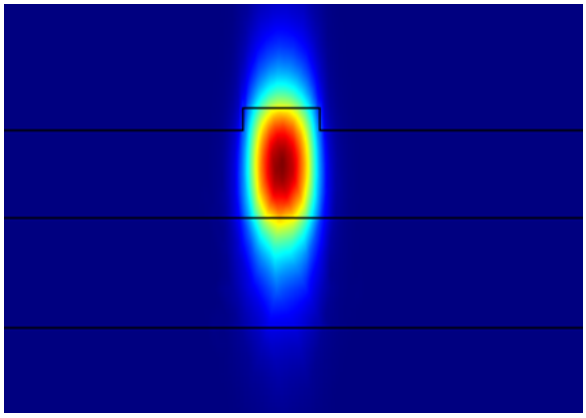

Figure 3.7: Rib waveguide mode simulation

3.3.2. Ridge waveguide

For the ridge waveguide, the parameters are more straightforward, which are ridge height (H_r) and width (W_r). Fig. 3.9 shows the mode distribution in a ridge waveguide. Simulations were carried out on the influence of the ridge height and width on the cladding filling factor. Results are shown in Fig. 3.10 for the cladding filling factors with different widths and heights. It is clearly seen in Fig. 3.10 that the thinner the waveguide is, the higher the CFF will be. What is more, ridge width has the same influence as the width of rib waveguide. With the increase of ridge width, the CFF will decrease.

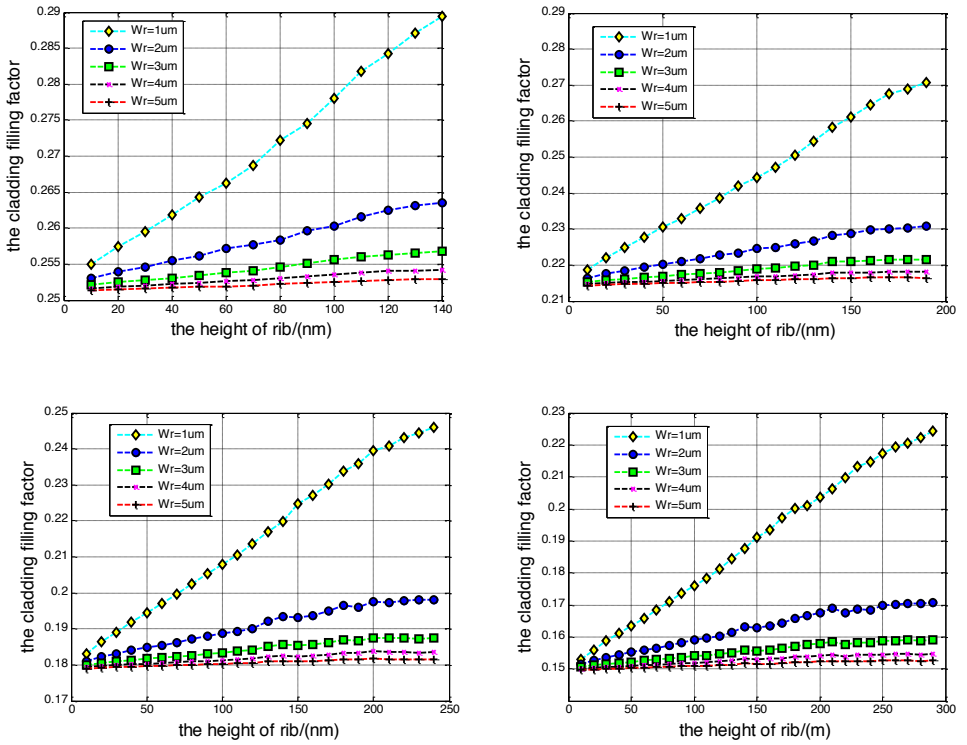

Figure 3.8: Cladding filling factors of rib waveguides with different waveguide heights: 150nm (top left), 200nm (top right), 250nm (bottom left), 300nm (bottom right). W_r is the waveguide rib width.

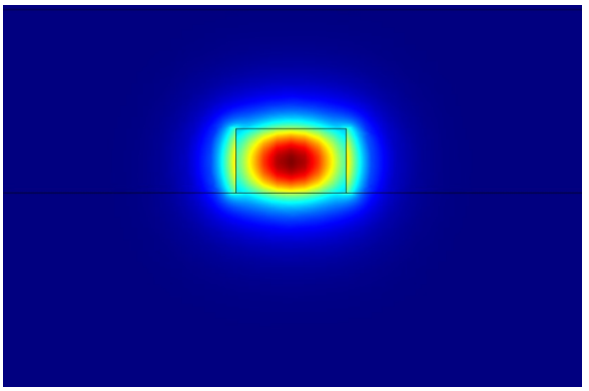

Figure 3.9: Ridge waveguide mode simulation

3.3.3. Slot waveguide

Slot waveguides contain two ridge waveguides that are located close to each other. Light is mainly confined in the gap (shown in Fig. 3.11), which is where most sensing

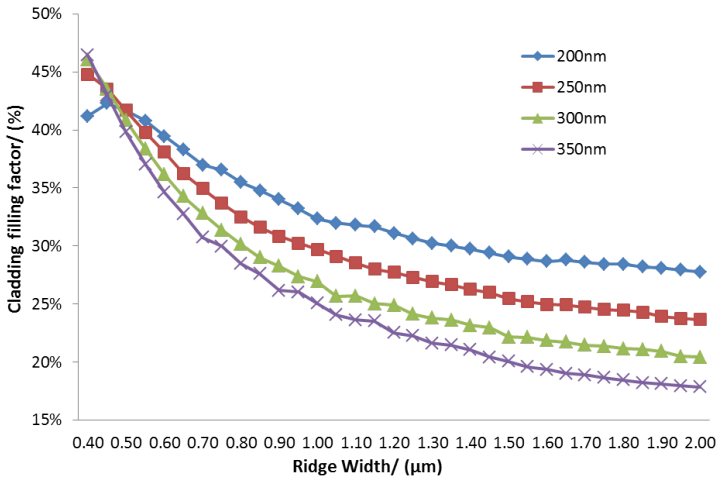

Figure 3.10: Cladding filling factors of ridge waveguide with different parameters. Different lines represent waveguides with different heights.

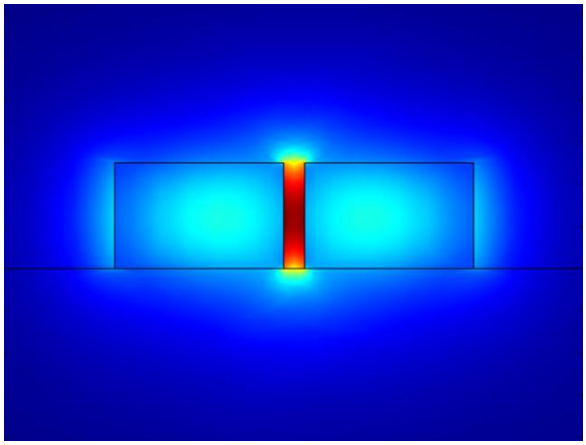

Figure 3.11: Slot waveguide mode simulation

is conducted. There are several parameters that will influence the cladding filling factors, which are slot width (W_g), ridge width (W_r), and height (H_r). To get an indication of how they influence the optical distribution of light, simulations were conducted in which the width of the waveguides and gap were changed, while the height of the waveguides was kept to be 250nm. The width of waveguide changed from 260nm to 450nm with a step of 10nm, while the gap width changed from 50nm to 210nm with a step of 10nm. The gap filling factor and cladding filling factor are shown in Fig. 3.12 and Fig. 3.13, respectively. When W_r =360nm, W_g =250nm, the gap filling factor reached the highest point, which is 8.62%, while the cladding filling factor is 44.3%. When W_r =260nm, W_g =50nm, the cladding filling factor

reached the highest point, which is 44.51%, while the gap filling factor is 4.99%. Actually, most of the sensing happens in the slot, where the optical distribution percentage is low. Furthermore, the slot is rather narrow whereas the requirement for fabrication is high, which is not optimal.

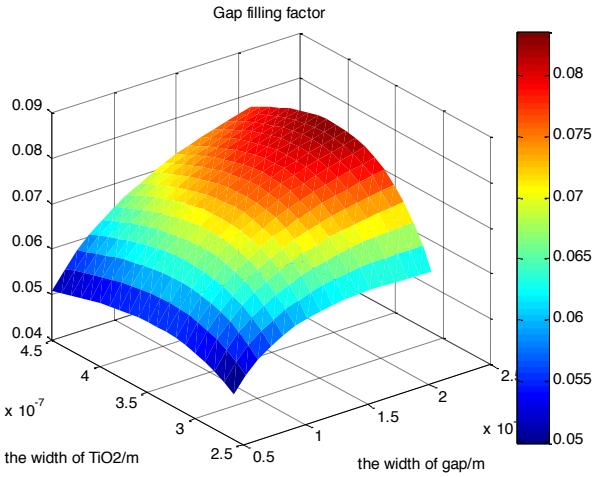

Figure 3.12: Cladding filling factor in the gap of the slot waveguides with different waveguide widths and gap widths

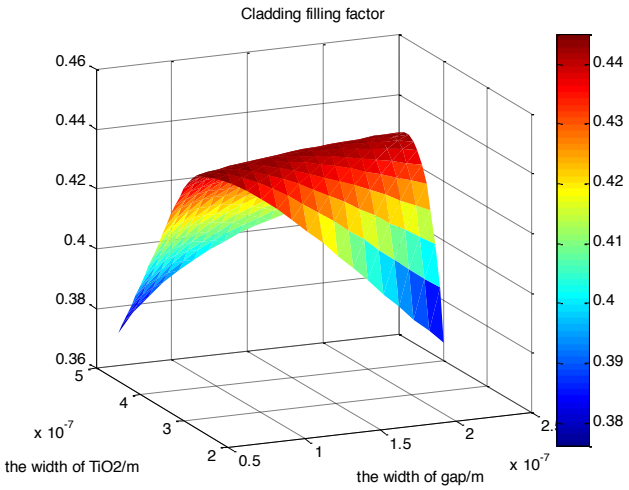

Figure 3.13: Cladding filling factor in the cladding of the slot waveguides with different waveguide widths and gap widths

According to the simulations here, slot waveguides have no obvious advantage

over rib or ridge waveguides. The structure is more complex than the other two waveguides and also requires more during fabrication. Ridge and rib waveguides can both reach a reasonable cladding filling factor value with a ridge waveguide, which presents an obvious advantage in the cladding filling factor. The structure of the ridge waveguide is simpler as only one etching is needed for fabrication, which is time-efficient and cost-effective. Considering the above factors, the ridge waveguide structure is preferable.

3.4. Waveguide design and simulations

Different structures have been analyzed and compared in the previous section. It has already been demonstrated that the ridge waveguide is an optimal structure for sensing. Different materials with the same structure were simulated to find a material that has more potential to create a higher-sensitivity waveguide system.

Simulations on the cladding filling factors were conducted. The variables in these simulations were the waveguide ridge width and height. The height of the waveguide was set at 200nm, 250nm, and 300nm for both SiC and TiO_2, while the width changed from 400nm to 2μm. The results are shown in Fig. 3.14. It can be determined from the data that the cladding filling factors between SiC and TiO_2 are quite close. The maximum cladding filling factor for SiC is slightly higher than TiO_2, but with an increasing in width, both are quite similar, with TiO_2 having a slightly higher cladding filling factor than SiC.

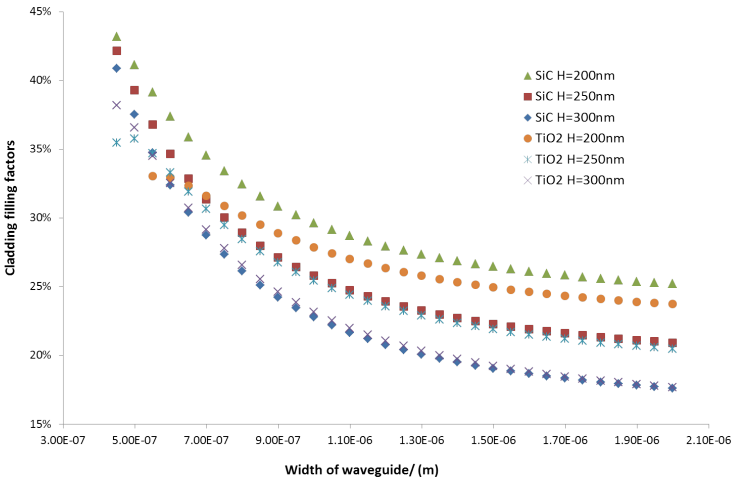

Figure 3.14: Simulations on cladding filling factor of SiC ridge and TiO_2 ridge with different waveguide parameters

Simulations of the changes in cladding filling factor with the cladding refractive index were conducted. Since the cladding filling factor is an index of the ratio of light distributed for sensing, it can indicate the sensitivity of the waveguide, thus

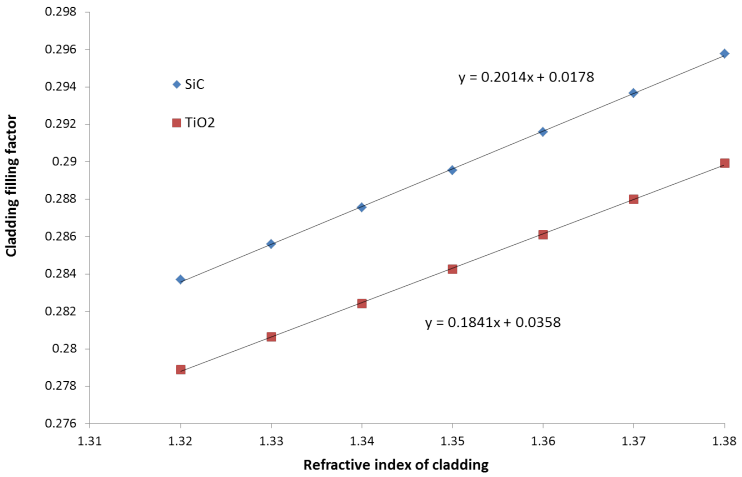

Figure 3.15: The change of cladding filling factor with cladding refractive index of SiC and TiO_2 ridge waveguide

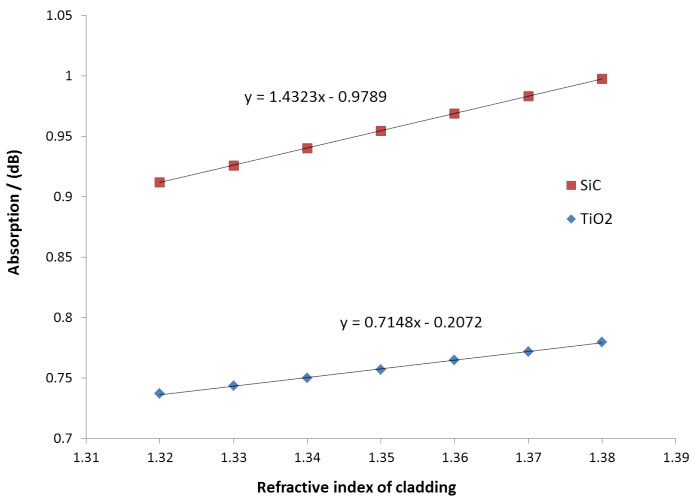

Figure 3.16: Absorption of the SiC and TiO_2 waveguides with the cladding of different refractive indices

the optical sensitivity of the waveguide here can be defined as:

$$S_{\mathrm{OPT}} = \frac{\Delta\Gamma}{\Delta n} \tag{3.22}$$

where Δn is the refractive index change, and $\Delta\Gamma$ is the change in the cladding filling factor. The simulations of the waveguide with $H_r = 200$nm and $W_r = 2\mu$m is shown in Fig. 3.15. The figure shows that $S_{\mathrm{OPT(SiC)}} = 0.20$ while $S_{\mathrm{OPT(TiO_2)}} = 0.18$. It also indicates that the SiC waveguide is more sensitive to the refractive index change under the same condition. A 3D model was built to further simulate the sensitivity of waveguides with different claddings of increasing refractive indices. The sensing path was set to 1cm. Results are shown in Fig. 3.16, which shows that the SiC waveguide has a sensitivity of 1.43dB per RI unit while the TiO_2 waveguide has a value of 0.71dB per RI unit. The trend of absorption is in proportion to that of the cladding filling factor, which demonstrates that the cladding filling factor is effective as an indicator of sensitivity.

Regarding the above simulations, SiC offers more benefits in the optical field. Additionally, SiC has good mechanical stability and chemical resistance, which can contribute to future developments such as making the waveguide system free-standing to further increase the sensing field and sensitivity of the system. For freestanding waveguide design, SiN is a suitable sub-cladding material as it has good mechanical stability and can be made stress-free by changing the process parameters.

Another promising material, SU-8, is a photosensitive polymer which has both a suitable optical property and stable mechanical property after being polymerized. Being a different material from the previously introduced dielectric materials, SU-8 has some intrinsic advantages such as being low cost, flexible, and easy fabrication. However, it is not as stable as the former materials. Using this material involves a different fabrication method and structure design, which will be introduced separately in Chapter 5.

3.5. Couplers

There is a lot of research being conducted on, and much interest in optical waveguides and optical devices, but an inherent problem for this is the low coupling efficiency between the optical source, such as optical fiber, and the optical waveguide. This issue can hinder the practical usage of optical devices if not solved. Moreover, getting light into these devices comes at a cost, which could outweigh the advantages/benefits of using them [17].

The low coupling efficiency of waveguides results from two factors. First, the difference in the refractive indices between fiber and optical waveguides creates an impedance mismatch, which reflects a large percentage of the incident light. Second, the core of a single-mode optical fiber is typically 9μm in diameter, while the dimensions of the optical waveguide devices are usually at the order of 1μm. Solutions to these problems, such as using an antireflection coating to solve the reflection problem and adding couplers to match modes, have been proposed. Another practical problem hindering the application is the alignment tolerance. Be-

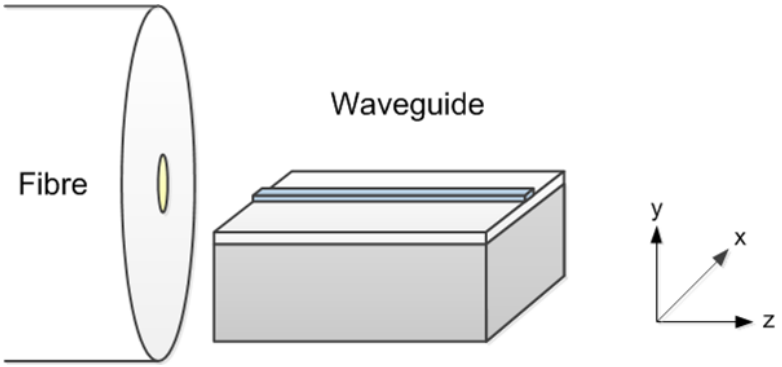

Figure 3.17: Direct coupling from fiber to waveguide

cause of the small size of the optical waveguide core, normally in sub-micron range, the alignment between the fiber and the optical waveguide is rather critical. A small misalignment will lead to a large signal loss (shown in Fig 3.17), which is not desired in a sensing system, especially in a plug-and-play sensing system where relaxing alignment tolerance is needed. Thus the interconnect between the optical fiber and the waveguide that can improve the coupling efficiency and alignment tolerance is of great importance. Hence, couplers will be designed and then added to the system.

Currently used coupling methods contain end-fire couplers, prism couplers, grating couplers, and tapered couplers [18]. The end-fire couplers are limited in the application because of the strict alignment tolerance. In the case of prism couplers, for most waveguides, it is difficult to find prism materials that meet the coupling conditions. Since the incident beam must be highly collimated and the coupling efficiency is sensitive to the separation between the prism and the waveguide, this coupling method is not practical. The grating coupling is achieved by introducing light at a specific angle to the grating part, when the phase match condition is met, so that light is coupled in the waveguide. The grating coupler has a theoretically low coupling efficiency and is therefore not sufficiently robust for commercial devices. Tapered coupling is a type of end-butt coupling where light is first coupled to the thicker and wider taper part, then reflected to the narrower transfer part and gradually into the waveguide film or structure. Due to the wider and higher tapered structure, the alignment tolerance is increased. This type of coupler is also easier to fabricate and works reasonably well [19]. Therefore, the tapered coupler was chosen to be added to the system.

For end-butt coupling, there are some factors which would influence the coupling efficiency, including mode mismatch and misalignment effects in waveguide-fiber junction. However, for the tapered coupler, since there will be a loss in the transfer path (slope or narrowing down part), taper angle will have a great influence on it. Thus the taper angle is another factor to be considered in this design.

When designing a waveguide coupler, the dominant factors to be taken into account are mode match, taper transmittance efficiency, and alignment tolerance

for the application consideration. Those demands can be met by adding tapered couplers, which can increase the coupling efficiency and alignment tolerance simultaneously. Here the coupling efficiency influencing factors are mainly introduced, as the alignment tolerance consideration will be illustrated when comes to the specific design in Chapter 4 and Chapter 5.

1. Mode match

   Mode match or field match, which is the overlap of the excitation field and waveguide field, is an important factor in designing couplers. The large mismatch of modes between the optical fiber and waveguides will result in a large loss, which can be relieved by a large taper size. Moreover, when the taper mode matches the optical fiber mode the most, the coupling efficiency is maximized.

   The overlap integral Γ of the two fields E and ε is given by

$$\Gamma = \frac{\int_{-\infty}^{\infty} \mathrm{d}y \int_{-\infty}^{\infty} E\varepsilon \,\mathrm{d}x}{\left[\int_{-\infty}^{\infty} \mathrm{d}y \int_{-\infty}^{\infty} E^2 \,\mathrm{d}x \cdot \int_{-\infty}^{\infty} \mathrm{d}y \int_{-\infty}^{\infty} \varepsilon^2 \,\mathrm{d}x\right]^{1/2}} \tag{3.23}$$

   for which Γ lies between 0 and 1. A simple way to obtain a reasonable idea of overlap between the excitation field and the waveguide field is to use Gaussian approximation. The power coupling efficiency can then be described by:

$$\Gamma^2 = \frac{\frac{4}{\omega^2}\left[\frac{1}{\omega_x \omega_y}\right]}{\left[\frac{1}{\omega_x^2} + \frac{1}{\omega_0^2}\right]\left[\frac{1}{\omega_y^2} + \frac{1}{\omega_0^2}\right]} \tag{3.24}$$

   where $2\omega_0$ is the mode field diameter of the optical fiber and $2\omega_x$, $2\omega_y$ are mode field widths of $1/e$ of the waveguide field peak value.

2. Taper transmittance efficiency

   There are two directions in tapering, horizontal and vertical, as shown in the 3D images in Fig. 3.18. The side view of the slope is shown in Fig. 3.19, with θ being the slope angle and H being the waveguide height. Together they influence the light transition efficiency from the taper to the waveguide. Generally speaking, the smaller the angle is, the higher the efficiency will be. H also influences the mode match and alignment tolerance mentioned above.

3. Other factors

   There are some other factors that influence the coupling. They are important factors since they affect taper quality and efficiency, but are not dominant in waveguide design. These factors include: (1) Reflection from the waveguide facet caused by the refractive index difference between air and the waveguide.

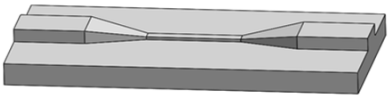

Figure 3.18: Schematic of the 3D taper

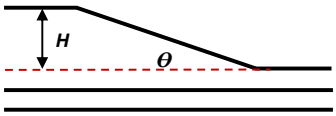

Figure 3.19: Side view of the 3D taper

It can be reduced by adding an anti-reflection coating on the end facet of the waveguide. (2) Quality of the waveguide endface, depending on the fabrication techniques. This can be improved by polishing, cleaving, and etching. (3) Spatial misalignment related to the spatial position between the fiber and the waveguide, in the horizontal and vertical directions, and the gap in between. This is more related to how the setup is handled during the experiment. For the sake of simplicity, it is not further discussed in this thesis.

3.6. Conclusions

In this chapter, we introduced some waveguide structures and summarized commonly used waveguide materials. Simulations were also conducted to compare the performance of these waveguides. To increase the coupling efficiency and alignment tolerance, couplers were introduced. There are more factors that must be considered when it comes to specific waveguide design. In Chapter 4 and Chapter 5, more details will be given.

References

[1] G. T. Reed and A. P. Knight, *Silicon Photonics: an introduction* (John Wiley & Sons Ltd, 2004).

[2] B. T. Cunningham, *Label-free optical biosensors: An introduction,* Label-Free Biosensors: Techniques and Applications , 1 (2009).

[3] F. Dell'Olio and V. M. Passaro, *Optical sensing by optimized silicon slot waveguides.* Optics express **15**, 4977 (2007).

[4] P. M. Sarro, C. R. Deboer, E. Korkmaz, and J. M. W. Laros, *Low-stress PECVD SiC thin films for IC-compatible microstructures,* Sensors and Actuators, A: Physical **67**, 175 (1998).

[5] G. Pandraud, P. J. French, and P. M. Sarro, *Fabrication and characteristics of a PECVD SiC evanescent wave optical sensor,* Sensors and Actuators, A: Physical **142**, 61 (2008).

[6] P. M. Sarro, *Silicon carbide as a new MEMS technology,* Sensors and Actuators, A: Physical **82**, 210 (2000).

[7] A. Purniawan, *Evanescent Waveguide Sensors for Biomedical Applications*, Ph.D. thesis, TU Delft, Delft University of Technology (2014).

[8] L. Eldada and L. W. Shacklette, *Advances in polymer integrated optics,* IEEE Journal on Selected Topics in Quantum Electronics **6**, 54 (2000).

[9] T. C. Sum, A. A. Bettiol, J. A. Van Kan, F. Watt, E. Y. B. Pun, and K. K. Tung, *Proton beam writing of low-loss polymer optical waveguides,* Applied Physics Letters **83**, 1707 (2003).

[10] R. Müller, D. Cristea, M. Kusko, P. Obreja, D. Esinenco, V. Damian, and P. C. Logofatu, *SU8 polymer materials used in integrated optic microsystems,* OPTOELECTRONICS AND ADVANCED MATERIALS-RAPID COMMUNICATIONS **4**, 228 (2010).

[11] N. Chronis and L. P. Lee, *Electrothermally activated su-8 microgripper for single cell manipulation in solution,* Journal of Microelectromechanical systems **14**, 857 (2005).

[12] Microchem, *SU-8 3000 Permanent Epoxy,* Product Datasheet **20** (2000), 10.1146/annurev.matsci.28.1.153.

[13] A. Deepu, V. Sai, and S. Mukherji, *Simple surface modification techniques for immobilization of biomolecules on su-8,* Journal of Materials Science: Materials in Medicine **20**, 25 (2009).

[14] I. Boiragi, R. Makkar, B. D. Choudhury, A. Mallik, K. Chalapathi, and J. Sebastian, *Su-8 Polymer Based Waveguide Biochemical Sensor for Medical Diagnostic Application,* Iccp , 2 (2009).

[15] P. French, P. Sarro, R. Mallée, E. Fakkeldij, and R. Wolffenbuttel, *Optimization of a low-stress silicon nitride process for surface-micromachining applications,* Sensors and Actuators A: Physical **58**, 149 (1997).

[16] M. Henini, *Microelectronics Journal*, Vol. 31 (2000) p. 219.

[17] C. B. Hitz, J. J. Ewing, and J. Hecht, *Introduction to laser technology* (John Wiley & Sons, 2012).

[18] G. T. Reed and A. P. Knights, *Silicon photonics: an introduction* (John Wiley & Sons, 2004).

[19] R. G. Hunsperger, *Integrated Optics,* Springer Science+Business Media, LLC 2009 **DOI 10.100**, 17 (2009), arXiv:arXiv:1502.06504v1 .

4

Design and Fabrication of SiC Waveguide

As discussed in Chapter 3, SiC is a promising material in MEMS field and is widely used to fabricate sensors in many applications. Considering its suitable optical properties, excellent chemical and mechanical properties, and various potential fabrication methods, which satisfy the demands of our waveguide system. So SiC is investigated as the core material of the evanescent waveguide in this chapter. Simulations are conducted to design the structure parameters. LPCVD and PECVD deposition method are combined in fabricating the waveguide. To reduce the coupling loss and misalignment effect, 3D tapered couplers are designed to be added to the input and output of the waveguide. A novel slope transfer method is investigated to fabricate the tapered coupler.

4.1. Introduction

As discussed in Chapter 3, SiC is a very promising material for optical MEMS devices because of its excellent properties in optical, mechanical, electrical, and also good chemical resistance. It is transparent above 0.5μm wavelength, so optical spectrum of visible and near infrared can be guided. SiC is robust and has a high mechanical strength. Furthermore, it is highly stable even in harsh environments and it can be made into sensors for high temperature or changeable environment. It can be deposited by different methods such as LPCVD, PECVD, and APCVD, which can adapt to different layer requirements from thin uniform layer to thick layer faster deposition. Also, by tuning the fabrication process parameters, the optical property can be adjusted. The fact that SiC has a high Young's modulus makes it promising for the development of freestanding waveguide, as can be seen in Fig. 4.1a, which is the schematic of the waveguide sensing system. Fig. 4.1b is the freestanding waveguide sensing area. In this situation, both surfaces can be functionalized with antibodies to be able to detect targets in the solution. In this chapter, SiC is studied as the core material of the waveguide. Considering the development freestanding waveguide system, SiN is chosen as the sub-cladding and supporting layer.

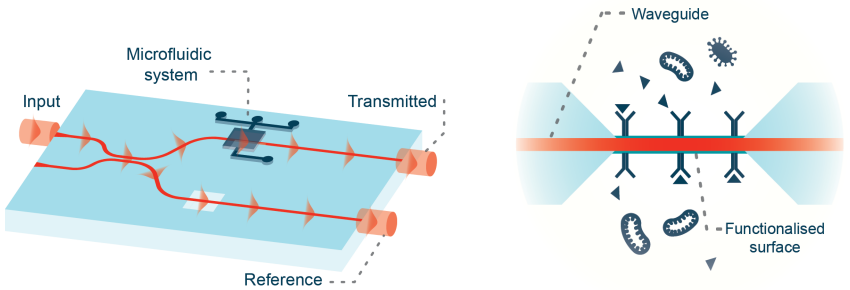

(a) Waveguide sensing system (b) Freestanding structure

Figure 4.1: Waveguide sensing system schematic with freestanding structures

4.2. Waveguide working theory

The basic planar waveguide structure was already analyzed in Chapter 3. The planar waveguide solution is simple and introduced before. For practical application, two dimensional waveguides are more common. In two-dimensional rectangular waveguide, an exact analytical solution is not possible, so an approximate method is proposed to solve the modes of two-dimensional waveguide. This method is known as the effective index method and will be discussed in the following sections.

4.2.1. Two dimensional waveguide model

The schematic of a two dimensional waveguide is shown in Fig. 4.2. Fundamental mode is shown in Fig. 4.3. As can be seen, light is confined in two directions. While in planar waveguide, light is confined only in one direction.

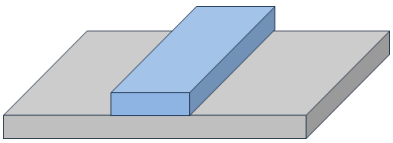

Figure 4.2: Two dimensional waveguide

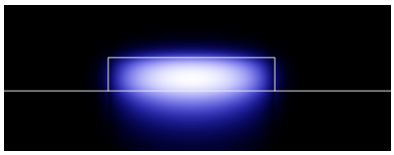

Figure 4.3: Fundamental mode in the two dimensional waveguide

4.2.2. Effective index

To introduce the effective index method, effective index must first be defined. As it is described in Chapter 2, light is confined by total internal reflection. Light propagates along the zig-zag path with wavevector $k = k_0 n_1$. k can be decomposed in the y and z directions into 2 components:

$$k_z = n_1 k_o \sin\theta_1 \tag{4.1}$$

$$k_y = n_1 k_o \cos\theta_1 \tag{4.2}$$

Here N is defined to be the effective index of a mode in the following equation:

$$N = n_1 \sin\theta_1 \tag{4.3}$$

The wave propagation in z direction is of more interest and is often written as β, thus:

$$k_z = \beta = N k_0 \tag{4.4}$$

By this equation, the wave propagation can be considered as a wave propagate along z direction without reflection in a medium with refractive index of N.

$$n_3 \leq N \leq n_1 \tag{4.5}$$

4.2.3. Effective index method

Effective index method [1] is used to find an approximate solution to two-dimensional waveguides, which otherwise will be complicated. The method will consider the two-dimensional waveguide (in Fig. 4.4a) as a combination of two imaginary planar waveguide as shown in Fig. 4.4b. Firstly we solve the planar waveguide eigenvalue equations in one direction, then in the other direction. The effective index of the first waveguide is taken as the core refractive index as the second one.

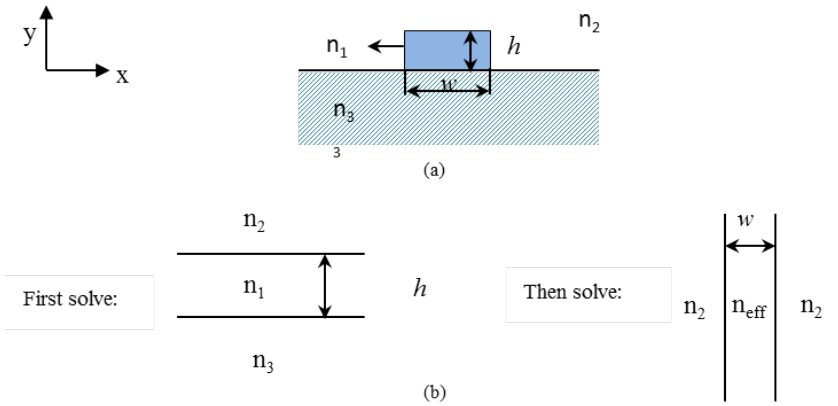

Figure 4.4: (a) two dimensional waveguide structure (b) Decomposition into two planar waveguide

In solving this waveguide, where $w > h$, the first step is to solve the planar waveguide in the vertical direction and then in the horizontal direction. TE eigenvalue function is used for solving the waveguide in the vertical direction in the first imaginary waveguide, and then the obtained eigenvalue is used in TM eigenvalue function in the second imaginary waveguide, for the TE polarized light for the first planar waveguide changes to TM polarized in the second one.

The eigenvalue equation for TE modes in the first planar waveguide is:

$$[k_0 n_1 h \cos\theta_1 - m\pi] = \tan^{-1}\left[\frac{\sqrt{\sin^2\theta_1 - (n_2/n_1)^2}}{\cos\theta_1}\right] + \tan^{-1}\left[\frac{\sqrt{\sin^2\theta_1 - (n_3/n_1)^2}}{\cos\theta_1}\right] \tag{4.6}$$

From Equation (4.4), the effective index of the first planar waveguide is:

$$n_{\text{eff}} = \beta/k_0 = n_1 \sin\theta_1 \tag{4.7}$$

Then the effective index n_{eff} can be used as the core refractive index of the second decomposed planar waveguide. This time the TM eigenvalue equation should be used, which is as following for the symmetrical waveguide:

$$k_0 n_{\text{eff}} w \cos\theta_w = 2\tan^{-1}\left[\frac{\sqrt{(n_{\text{eff}}/n_2)^2 \sin^2\theta_w - 1}}{(n_{\text{eff}}/n_2)\cos\theta_w}\right] \tag{4.8}$$

Then, N_w, θ_w, and propagation constant in z direction β can be deduced.

4.3. Waveguide design and simulations

It has already been introduced in Chapter 3 that the ridge waveguide structure is an advantageous one for our application, thus the SiC waveguide is designed based on ridge waveguide using the previously proposed analytical method.

Parameters of the waveguide should be designed to confine proper optical energy in the waveguide and maintain enough evanescent tails outside for sensing simultaneously. The cross section of the proposed waveguide structure is shown in Fig. 4.5. It comprises of a SiC ridge and SiN sub-cladding with a SiO_2 layer as the isolation layer between the waveguide and the silicon substrate. SiN is added to the waveguide for the aim of making it freestanding in the further development, which can act as a support layer and, at the same time, have a suitable refractive index (1.9) which can match with the SiC waveguide core to fulfill the optical requirement of achieving evanescent wave on the waveguide surface. COMSOL simulations were done to obtain a reasonable evanescent wave for sensing. The cross section of the waveguide is shown in Fig. 4.5. Table 4.1 shows the parameters chosen accordingly to COMSOL simulations.

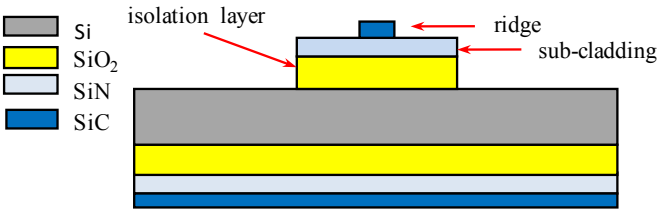

Figure 4.5: Cross section of optical waveguide

Table 4.1: Parameters of the design

Parameter	W_{rib}	W_{ridge}	H_r	H_{ridge}	H_{SiO_2}
Value	5μm	50μm	145nm	200nm	2μm

4.4. Fabrication

SiC can be deposited on wafers using LPCVD and PECVD. By changing processing conditions, such as temperature and gas ratio, a-SiC or poly SiC with adjustable refractive index and mechanical properties can be made, with refractive indices generally ranging from 2.3 to 2.5 [2] or even higher than 2.5 [3]. PECVD SiC has been widely researched in the application of optical waveguides due to its lower deposition temperature (200°C to 400°C). However, LPCVD SiC has a higher Young's modulus comparing to PECVD SiC [4] and shows better uniformity when fabricating very thin layers. It has a deposition rate of around 0.2nm/min while the deposition

rate of PECVD SiC normally ranges from 40nm/min to 100 nm/min [5]. The above points make LPCVD a perfect choice when fabricating thin and uniform film and make PECVD a suitable method to make thicker film. Considering the thickness of the waveguide core to be 145nm, LPCVD SiC deposition was chosen to achieve a uniform thin layer. Because the refractive index of SiC changes with the deposition condition such as gas ratio, pressure, and temperature, so the refractive index and the deposition rate test were first made before fabrication. The deposition condition is set at 760°C at 60Pa, gas ratio of SiH_2Cl_2/C_2H_2 is set to 2. According to former researches, when the conditions are met, the deposition layer quality is optimal [6] and has a uniform surface without hillrocks [7]. The intrinsic stress of the LPCVD SiC layer was tensile around 600MPa. The deposition rate was reported to be 0.2nm/min. The test was conducted for 8.5 hours. The refractive index measurement is shown in Fig. 4.6. The measurement was done using Woollam Ellipsometer. It indicated a value of 2.4 at 1.3μm in Fig. 4.6 and the calculated deposition rate is 0.3nm/min, which is slightly faster than previous reports. Also it showed low absorption at the wavelength that we are using, which meet waveguide material requirements. The refractive index of LPCVD SiN was also measured by a Woollam Ellipsometer and has a value of 1.9 at 1.3μm wavelength. The whole fabrication process was illustrated in the following flowchart (Fig. 4.7).

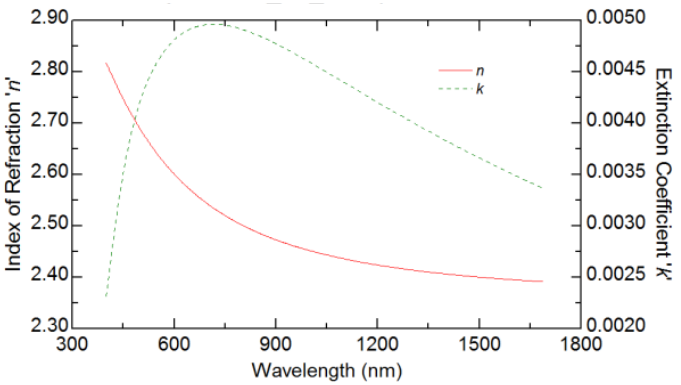

Figure 4.6: SiC refractive index measurement by Woollam Ellipsomete.

SiO_2 was thermally grown on the silicon bare wafer in furnace. Then SiN was LPCVD deposited on the SiO_2 layer at 850°C and SiC was LPCVD deposited consequently under the condition of 760°C with the gas ratio of SiH_2Cl_2/C_2H_2 to 2. The refractive indices of SiN and SiO_2 were measured using a Woollam Ellipsometer and found to be 1.9 and 1.45, respectively. After all layers were formed, photoresist was spin-coated on the wafer and structures were patterned, exposed, and developed. Afterwards, the wafer was etched in Trikon Omega 201 for ICP etching to etch away SiC for the ridge structure. Then the sub-cladding structure was patterned on the wafer and continued with a second plasma etching to form the final structure. Fig. 4.8 shows the fabricated waveguide under the microscope.

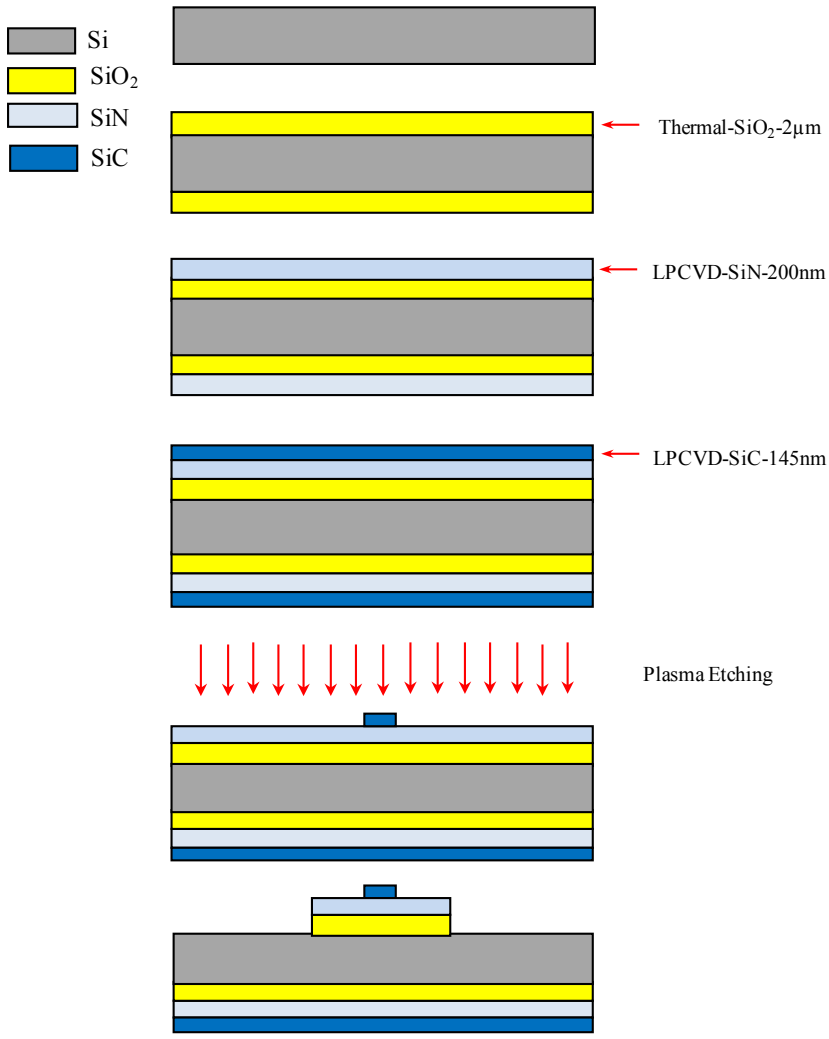

Figure 4.7: Waveguide fabrication process flowchart

4.5. 3D tapered coupler design

Waveguides without couplers usually has a poor coupling efficiency from optical fibre to waveguide and restrict alignment tolerance, which makes coupling operation difficult when conducting the experiments. A small interference would result in a large difference or even the loss of the total signal. So couplers need to be added to the waveguide system. Based on the analysis in Chapter 3, a 3D tapered coupler is designed to improve of the coupling efficiency and also enhance the feasibility of the whole system. The schematic of 3D tapered coupler is shown in Fig. 4.9, with the widened and heightened light entrance. There are several parameters influencing

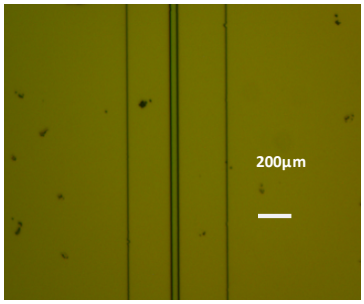

Figure 4.8: Fabricated SiC optical waveguide

the coupling efficiency, taper entrance size which is related to mode match, taper length and taper angle which are related to transmission efficiency of light along taper. Taper entrance size will also influences the alignment tolerance at the same time.

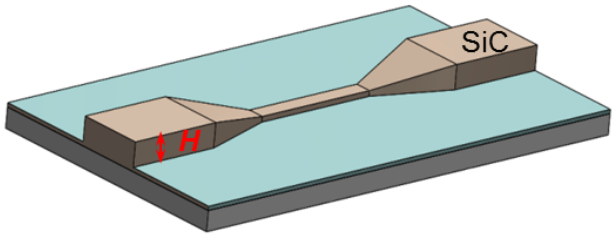

Figure 4.9: Schematic of designed taper

4.5.1. Mode match

In an ideal situation, when mode fields of fibre and waveguide taper match, the coupling efficiency between fibre and taper will be optimal. The waveguide mode in the current waveguide design is shown in Fig. 4.10 with a squeezed flat optical distribution, while the mode in fibre is shown in Fig. 4.11 with a circular optical distribution. It is obvious that there is a big mode mismatch between the waveguide and the optical fibre which will result in a big loss. Considering the mode field in fibre is circular, thus a taper with a square entrance surface is chosen which has a symmetric mode field distribution similar to that in fibre. Simulations about the taper with different sizes (W_r) were done to estimate the mode diameter of the entrance block of the coupler. The mode diameter is defined as the diameter where the near field power falls to $1/e^2$ of its maximum value, which is common for fibre. Here it is also used to estimate the "mode diameter" of the taper by measuring the optical energy along the cutting line in the middle of the taper as shown in Fig. 4.12 and calculating the vertical distance at which the power falls to $1/e^2$ of its maximum value. Fig. 4.12 is the mode field of the taper with the size of 6μm×6μm. Fig. 4.13

is the simulation results of the electric field distribution along the cutting line of the tapers with different entrance sizes. It can be estimated that when the taper size changes from 5μm×5μm to 10μm×10μm, the mode diameter of the taper changes from 3.88μm to 7.67μm as shown in Table 4.2, which is still smaller than that of fibre used in our lab with the mode diameter of (9.2±0.4μm). In the range between 5μm and 10μm, the bigger the size is, the better the mode match will be. However, the mode match is not the only influencing factor, the slope angle and length of the taper are also dominant factors, which are to some extent related to the taper size. These two factors and the relation with taper size will be illustrated in the following subsection.

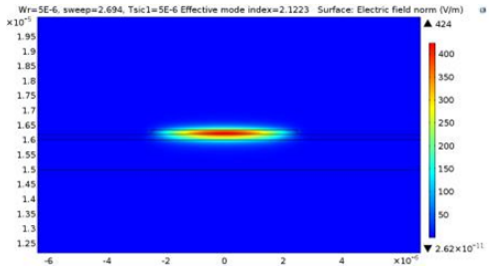

Figure 4.10: Mode in waveguide.

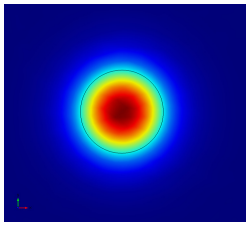

Figure 4.11: Mode in fibre

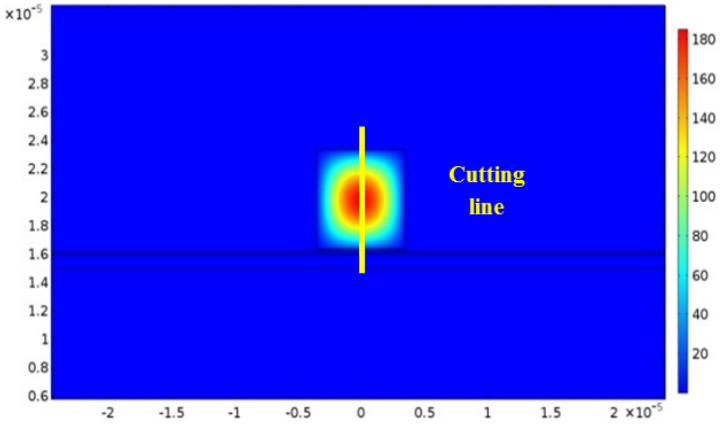

Figure 4.12: Mode on the taper entrance with the size of 6μm×6μm

Table 4.2: Mode diameters of different taper size

taper Size (μm)	5 × 5	6 × 6	7 × 7	8 × 8	9 × 9	10 × 10
Mode diameter (μm)	3.88	4.75	5.51	6.27	6.91	7.67

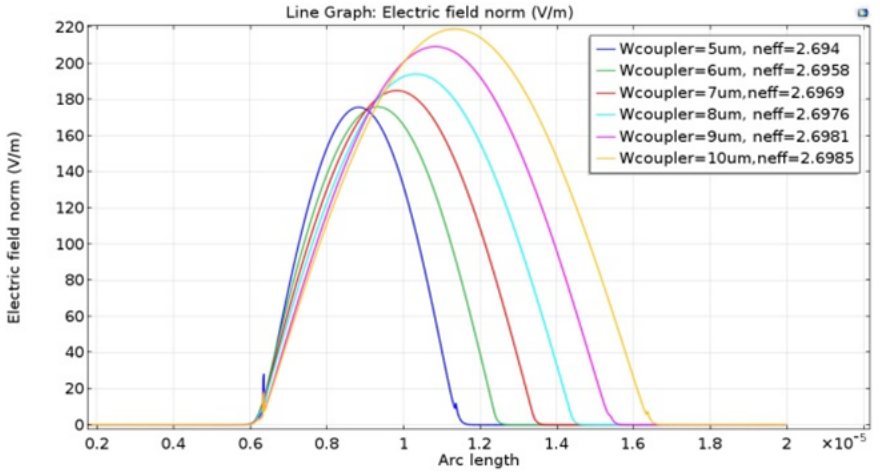

Figure 4.13: The power distributed on the cutting line of tapers with different sizes

4.5.2. Taper angle

The schematic of SiC tapered coupler is already shown in Fig. 4.9. Fig. 4.14 is the side view of the slope. θ is the slope angle of the taper and H is the height of the taper. θ should be small enough to couple light into the waveguide underneath efficiently. If the angle is too large, the scattering will be too much when coupling the light from the taper to the waveguide. However, it cannot be too small since the taper will be too long and the light loss in the taper will be too large. H is the height of the taper, which is closely related to the mode match between the fibre and the taper. For the same taper angle, the higher the taper is, the longer the taper will be and the bigger scattering loss will be caused. There will be a compromise between these factors to get an optimal value. Simulations were done on the coupling efficiency influenced by the height of the taper entrance (h) and also the slope angle (θ) of the taper. Results are shown in Fig. 4.15. When h is fixed, the general trend is that the coupling efficiency drops with the increase of the slope angle. H has a more complex influence on the coupling efficiency as the bigger h not only will contribute to a better mode match but also induce a bigger scattering loss along the taper. A very small angle or very big sizes is not desired. 5° with a taper size around 6μm is considered to be appropriate parameters for the coupler with moderate coupling efficiency and length according to the simulations. Fig. 4.16 shows the light transmission coupled into the waveguide with the optimized coupler (h=6μm, $\theta = 5°$).

4.6. Coupler Fabrication

It is much simpler to fabricate a coupler with only horizontal taper by using a single mask. However, the vertical direction taper is more complex and takes more effort to fabricate. The current fabrication methods to fabricate slopes include greyscale lithography [8], thermal reflow [9], and wet etch in a silicon wafer with a tilted

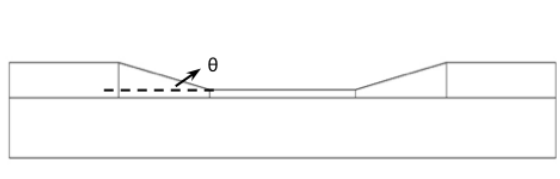

Figure 4.14: Side view of the tapered coupler

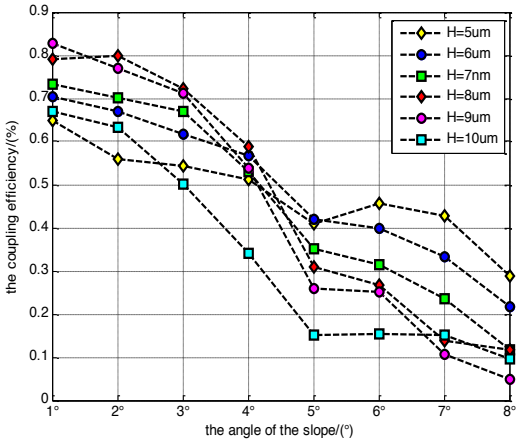

Figure 4.15: Coupling efficiency of tapers with different heights and angles

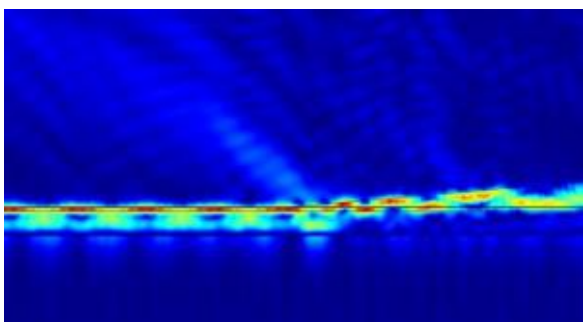

Figure 4.16: The coupling from taper to waveguide at 5° with 6μm×6μm coupler

<1 1 1> crystal orientation [10]. Greyscale lithography is a binary process which will result in a step profile surface. Thermal reflow takes time and has induced edge bead effect [11, 12]. The abruption of the edge bead will influence the optical transmission and hinder the effectiveness of the coupling. The thickness of the photoresist mask depends on the thickness of the etched material and the etching ratio between them. Thus, a more efficient method is needed to fabricate the vertical taper with a slope where the thickness will be several microns and might

be hard to etch. Here, we propose a slope transfer method which takes advantage of the etching ratio between silicon and the etched taper material to transfer slope from silicon into taper.

To channel light into waveguides efficiently, the taper needs to be made from the same material of the waveguide. Simulations were performed with taper of different materials (one with a higher refractive index, one with the same, and another one with a lower) to show the effect. If the taper material has a higher refractive index than the waveguide, light will not be channelled into the waveguide effectively (Fig. 4.17a). The coupling efficiency is only the half of the one with the same refractive index. If the taper material has a lower refractive index than the waveguide core, most of the light is scattered during the transmission in the taper (Fig. 4.17b). When the material is consistent, coupling is the most efficient (Fig. 4.17c). In our research, SiC was chosen for the coupler to be integrated with the SiC waveguide. As SiC is difficult to etch both in wet and dry methods, if photoresist is chosen as a mask layer, a very thick photoresist will be needed to achieve a several micro thick taper. It makes the fabrication methods mentioned above not suitable in this situation. Here, a slope in Si is wet etched in the first step and then the Si slope is used as a mask and transferred into SiC to a certain proportion by dry etching. The etching process is demonstrated in two flows which are illustrated in Fig. 4.17.

4.6.1. Slope transfer with bonding layer

This method and fabrication process are described in [10]. A double side polished <1 0 0> wafer was firstly wet etched to get a slope of 54.74° because of the crystal orientation. And then a photoresist layer was used to bond the double side polished silicon mask wafer with the single side polished wafer with an SiC layer on top. Then the bonded wafer was dry etched and the slope in Si is transferred into SiC. The detailed process is described as following:

Step 1 is the wafer preparation. Two wafers, one single side polished (SSP) and one double side polished (DSP) are needed. Then deposit the DSP wafer with LPCVD SiN on both sides as the etching mask. Thermally grow SiO_2 on SSP wafer in the furnace, and then LPCVD deposit SiN, SiC and SiO2 on both surfaces consequently and PECVD SiC on the polished side in the end. The desired thicknesses are shown in Fig. 4.18a.

Step 2 is etching. Open SiN window on DSP wafer and wet etch it in KOH solution to get a slope with the angle of 54.7°. At the same time, coat SSP wafer with a photoresist layer of 8μm thick as an intermediate transfer layer and also bonding layer.

Step 3 is bonding. Bond two wafers together using photoresist in between in the bonding machine (AML wafer bonder).

Step 4 is slope transfer. Etch the bonded wafer in Trikon Omega 201. The upper Si is functioning as a mask layer here. The slope angle of Si after wet etching is 57.4°. Under dry etching in Omega using the chosen recipe, the etching rate of silicon is bigger than that of photoresist, so the transferred slope angle is smaller than that of silicon. After transferring the slope into the photoresist, it can be used

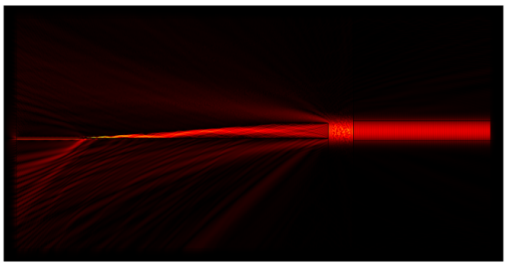

(a) n_{coupler} is the same as $n_{\text{waveguide}}$

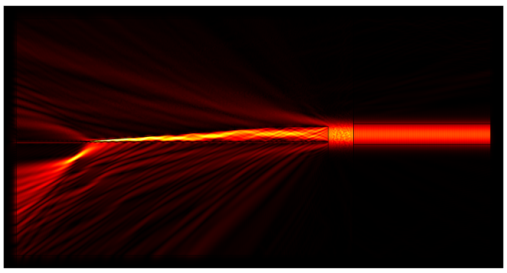

(b) n_{coupler} is lower than $n_{\text{waveguide}}$

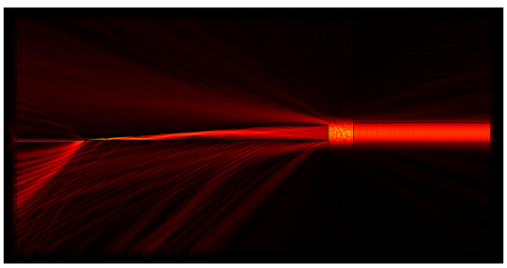

(c) n_{coupler} is higher than $n_{\text{waveguide}}$

Figure 4.17: Coupling effect of taper with different refractive indices

as the mask to etch the SiC to further transfer the slope into SiC.

Step 5 is the final step. The upper wafer is removed after the slope transfer and the following process is continued to fabricate waveguide.

It resulted in 16 degree slope in this flow (Fig. 4.18). The SEM image is shown in Fig. 4.19. The bonding photoresist layer influenced the etching uniformity of the surface and also the slope transfer ratio. When the slope angle is 16 degree, the coupling efficiency is very poor and only around 4% when the taper height is 6μm. The simulation results are shown in Fig. 4.20. So in order to make it efficient enough to be used as the waveguide taper, the transfer process still needs to be improved for better surface quality and slighter slope angle.

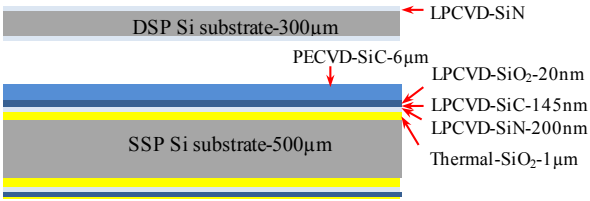

(a) Wafer prepared, one 300μm double polished wafer (DSP) with LPCVD SiN on both sides and another single side polished wafer (SSP) with different layers as shown above

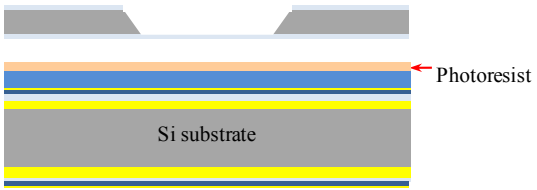

(b) Open SiN window and wet etch through Si in KOH

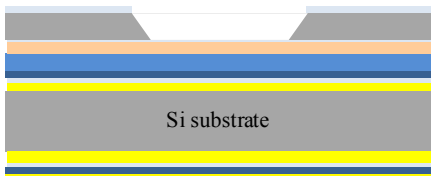

(c) Bonding two wafers in the bonder

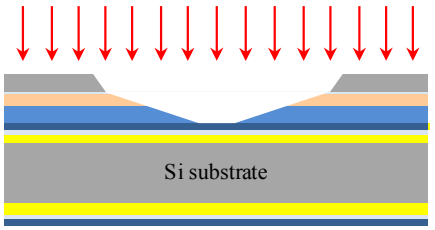

(d) Plasma etching in Omega to transfer slope from Si into SiC

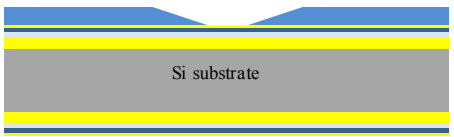

(e) Remove the upper wafer and continue with the following waveguide fabrication process

Figure 4.18: 3D tapered coupler fabrication process

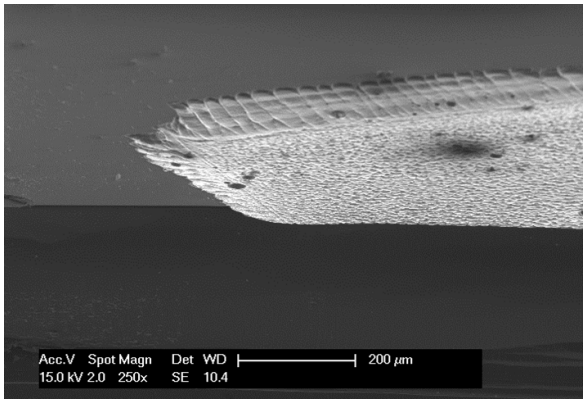

Figure 4.19: SEM image of first transferred slope into SIC

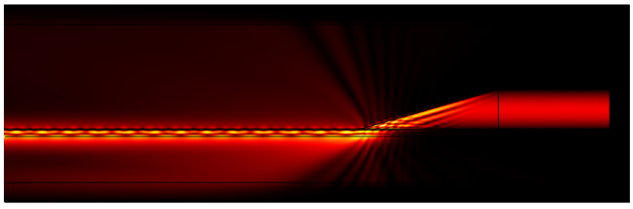

Figure 4.20: Simulation of coupling for coupler with 6μm height and 16 degree slope

4.6.2. Slope transfer without bonding layer

To obtain a lower-angle slope and more uniform surface, we removed the transfer photoresist layer and directly deposit the masking Si layer on top of the SiC taper layer. The fabrication method is still taking advantage of the etching rate difference between Si and SiC for the slope transfer. The fabrication process is shown in Fig. 4.21. A 5μm thick SiC layer was deposited by PECVD under 400°C with a gas mixture of SiH_4 and CH_4 [13]. Then a thick layer of α-Si was sputtering on the SiC layer in Sigma and followed by a layer of PECVD SiO_2 as a mask layer for wet etching. After the layers were prepared, an etch window was opened on the SiO_2, then the whole wafer was dipped into a 25 wt % TMAH solution at 85°C. A short time over etch was conducted to guarantee that the SiC layer underneath was reached. After the wet etch of α-Si in TMAH, a curved slope was formed in silicon. Then the wafer was etched using an SF_6/O_2 gas mixture under 10°C in Omega Trikon RIE etcher. Because of the different etching rates between Si and SiC, the profile in silicon was transferred into SiC with a different (slighter) slope under the dry etch of Omega (shown in Fig. 4.22). After fabrication the slope profile was measured with a Keyence VK-X 3D scanning confocal laser microscope and the slope was found to be lower than 2° (Fig. 4.23). With the coupler of this angle, the coupling efficiency will be greatly improved to around 70% (the simulation result is shown in Fig. 4.24),

which is efficient enough to meet the requirement of the system.

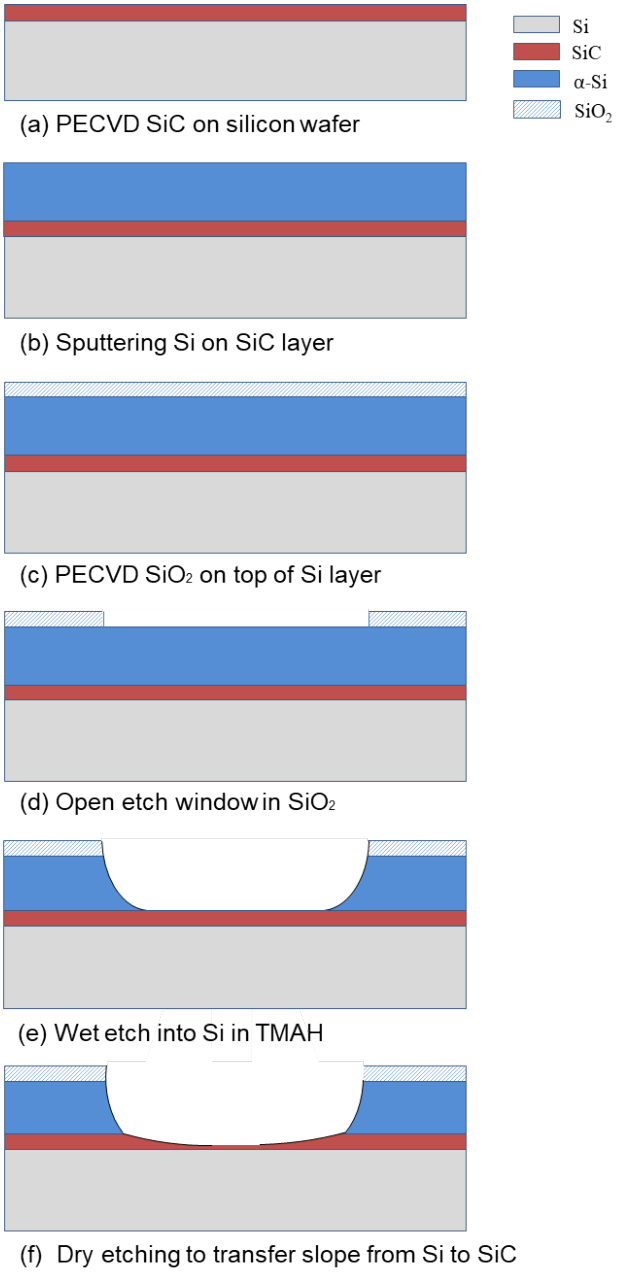

Figure 4.21: The slope transfer method flowchart

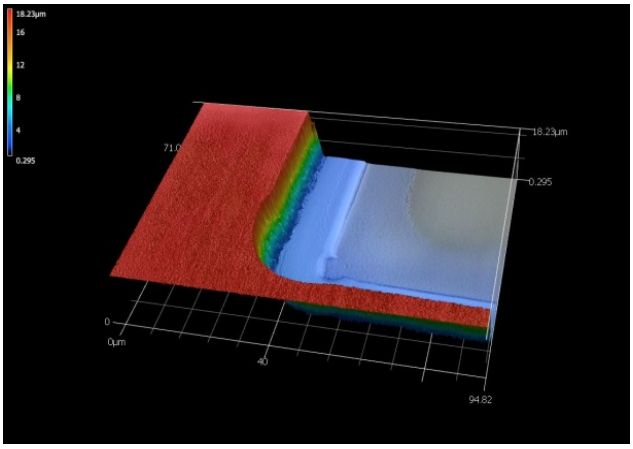

Figure 4.22: The profile of the second slope fabrication

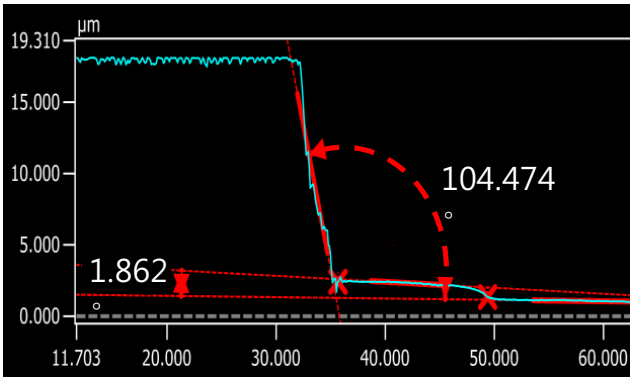

Figure 4.23: The measured angle of the second slope

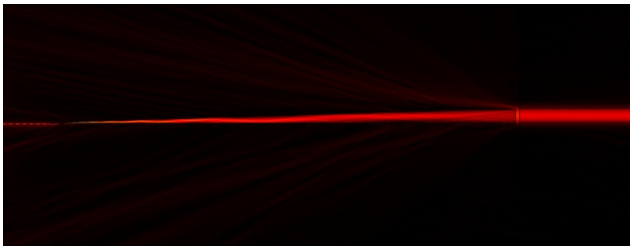

Figure 4.24: Simulation of coupling for coupler with 6μm height and 2 degree slope

4.7. Conclusions

In this chapter, the SiC waveguide design, fabrication, and some tests were performed to demonstrate the waveguide feasibility. To enable the application, a verti-

cal taper was designed. A novel slope transfer method to fabricate vertical waveguide coupler is proposed to achieve the final plug-and-play system. A less than 2° slope was achieved which demonstrated this method and it can be well integrated with SiC waveguides.

References

[1] G. T. Reed and A. P. Knights, *Silicon photonics: an introduction* (John Wiley & Sons, 2004).

[2] P. M. Sarro, C. R. Deboer, E. Korkmaz, and J. M. W. Laros, *Low-stress PECVD SiC thin films for IC-compatible microstructures,* Sensors and Actuators, A: Physical **67**, 175 (1998).

[3] G. Pandraud, P. J. French, and P. M. Sarro, *Fabrication and characteristics of a PECVD SiC evanescent wave optical sensor,* Sensors and Actuators, A: Physical **142**, 61 (2008).

[4] L. Liu, W. Tang, B. Zheng, and H. Zhang, *Fabrication and characterization of SiC thin films,* 2011 6th IEEE International Conference on Nano/Micro Engineered and Molecular Systems , 146 (2011).

[5] P. M. Sarro, *Silicon carbide as a new MEMS technology,* Sensors and Actuators, A: Physical **82**, 210 (2000).

[6] F. Bruno, M. del Guidice, R. Recca, and F. Testa, *Plasma-enhanced chemical vapor deposition of low-loss sion optical waveguides at 1.5-μm wavelength,* Applied optics **30**, 4560 (1991).

[7] B. Morana, G. Pandraud, J. F. Creemer, and P. M. Sarro, *Characterization of LPCVD amorphous silicon carbide (a-SiC) as material for electron transparent windows,* Materials Chemistry and Physics **139**, 654 (2013).

[8] M. Frish, J. Fijol, E. Fike, and Et Al., *Coupling of single mode fibers to planar Si waveguides using vertically tapered mode converters,* Integrated Photonics , 1 (2002).

[9] A. Emadi, H. Wu, S. Grabarnik, G. de Graaf, and R. F. Wolffenbuttel, *Vertically tapered layers for optical applications fabricated using resist reflow,* Journal of Micromechanics and Microengineering **19**, 074014 (2009).

[10] R. Holly and K. Hingerl, *Fabrication of silicon vertical taper structures using KOH anisotropic etching,* Microelectronic Engineering **83**, 1430 (2006).

[11] F. Badar, *Fabrication of microlens in polymers with thermal reflow*, Master's thesis, Universitat Politècnica de Catalunya (2012).

[12] H. Liu, S. Reilly, J. Herrnsdorf, E. Xie, V. G. Savitski, A. J. Kemp, E. Gu, and M. D. Dawson, *Large radius of curvature micro-lenses on single crystal diamond for application in monolithic diamond Raman lasers,* Diamond and Related Materials **65**, 37 (2016).

[13] V. Rajaraman, L. S. Pakula, H. Yang, P. J. French, and P. M. Sarro, *PECVD silicon carbide surface micromachining technology and selected MEMS applications,* International Journal of Advances in Engineering Sciences and Applied Mathematics **2**, 28 (2010).

5

Design and Fabrication of Vertical SU-8 Waveguide

In this chapter, a vertical SU-8 waveguide is proposed for evanescent biomedical sensing. The waveguide structure is designed to be vertical and narrow generating evanescent waves on both sides of the waveguide surface to increase the sensitivity by increasing the sensing areas. Simulations are carried out to monitor the influence of different parameters on the waveguide performance, including waveguide heights and widths. E-beam lithography is chosen to fabricate the waveguide and this one-step process enables easy and high-resolution fabrication. It reduces the sidewall roughness and further decreases the induced scattering loss which is a major loss source of waveguide. Tapers are added to improve the coupling efficiency and alignment tolerance, which will contribute to the feasibility of the plug-and-play optical system.

5.1. Introduction

Polymers are important materials for MEMS applications and are commonly used in integrated optics due to their adjustable refractive indices, good mechanical properties, low cost, compatibility with semi-conductor technology, etc. [1]. The SU-8 is a photon-sensitive material and allows fabrication by photolithography which simplifies the fabrication process. By avoiding the usage of dry etching in the process, sidewall roughness is reduced and scattering loss is lowered. SU-8, as an epoxy photoresist, can be fabricated by UV or E-beam lithography making it stands out with the advantage of being maskless processes, low-cost prototyping, fast and sub-micron fabrication with high precision [2]. At the same time, SU-8 is a suitable material for optical waveguides in mechanical, optical, and bio-chemical perspectives. Mechanically, it is very stable after polymerization and hard baking which is important for optical sensing [3–5]. Optically, it is transparent above 400nm and with a refractive of 1.57 at 1.3μm [2, 3] which meets the demands of waveguide core materials when SiO_2 is used as a substrate. Another important characteristic is that the surface of SU-8 has good biocompatibility and chemical resistance which play important roles in the biomedical application. Furthermore, the surface of SU-8 can be functionalized with antibodies [6], which broadens the application of this material such as biomedical sensor [3], medical diagnostic application [7], etc. Considering the proper characteristics of SU-8, it is chosen in the paper as a waveguide material. Most of the SU-8 waveguides so far researched are designed with traditional waveguide structures (low ratio height-width structures). In this paper, we propose a different waveguide structure for evanescent sensing to increase the sensitivity by enlarging the sensing area.

5.2. Working principal of SU-8 vertical waveguide

The basic waveguide working principal is already shown in Chapter 4, which is a horizontal waveguide. The waveguide structure in this chapter is vertical. The analysis method is still based on effective refractive index method with some modifications.

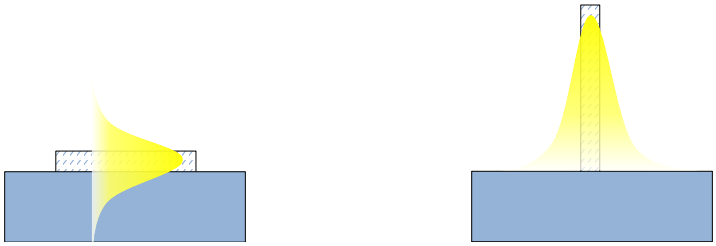

(a) Horizontal waveguide (b) Vertical waveguide

Figure 5.1: The evanescent wave distribution.

Structure analysis

In horizontal waveguides, the higher modes are mainly supported in the horizontal direction, while in waveguides with vertical cross sections, the higher modes are mainly supported in the vertical direction. For the horizontal one, the optical ray is mainly bounced on the upper and lower surfaces and the evanescent wave is distributed on the upper cladding of the waveguide, while the vertical one has the evanescent wave on the left and right sides of the waveguide. The evanescent wave distribution is shown in Fig. 5.1a and 5.1b, which are of horizontal and vertical waveguides, respectively.

The cladding filling factor [8, 9] is a criteria for the energy distribution of evanescent waves that can be utilized for sensing, which also determines how sensitive waveguides could be. To compare the theoretical performance of horizontal and vertical waveguides, simulations were performed to compare the energy distribution of these two structures. Two structures with reverse parameters, where the height of horizontal waveguide is the width of the vertical one and same goes to the other parameter. The parameters and results are shown in Table 5.1. In the horizontal SOI waveguide with parameter of $H = 0.1\mu$m, $W = 2\mu$m, for the fundamental $\mathrm{TE}_{0,0}$ mode, the cladding filling factor in the left and right areas is less than 0.0015%, while that of top is around 20%. In contrast, a vertical SOI waveguide with parameters of $H = 2\mu$m, $W = 0.1\mu$m, the cladding filling factor in the left and right claddings is 46%, while that in the top is only 0.00127% for the fundamental $\mathrm{TM}_{0,0}$ mode. The fundamental mode in waveguides are shown in Fig. 5.2. By comparison, it shows that the vertical waveguide not only has a larger sensing area, but also a higher cladding filling factor, which means a higher sensitivity.

Table 5.1: Comparison of energy distribution of horizontal and vertical structures

	Width	Height	Energy in top cladding	Energy in side cladding
Horizontal	2μm	0.1μm	20%	0.0015%
Vertical	0.1μm	2μm	0.00127%	46%

The effective index analysis method [10] is used to analyze the waveguide. Using this method, the waveguides are considered as a combination of two imaginary planar waveguide as shown in Fig. 5.3. Firstly we solve the planar waveguide eigen-

(a) Horizontal waveguide (b) Vertical waveguide

Figure 5.2: Fundamental modes

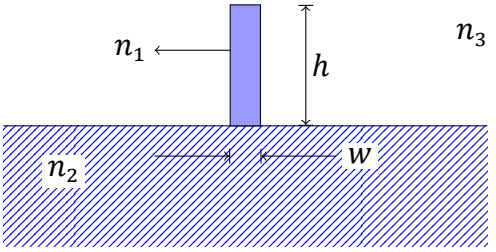

(a) Novel vertical waveguide structure

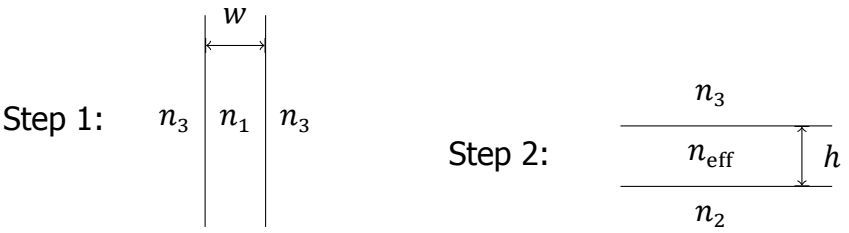

(b) Vertical waveguide structure (c) Solve by splitting into two planar waveguides

Figure 5.3: Effective index analysis method to analyze the vertical waveguide

value equations in one direction, then in the other direction. The effective index of the first waveguide is taken as the core refractive index as the second one. In this way, the cut off condition and single mode condition can be calculated for the design instruction. In this paper, vertical waveguides with different heights ranging from 3μm to 10μm are analyzed to obtain corresponding widths that meet the single mode condition. The results are shown in Fig. 5.4. The green field between two lines is where the parameters meet the single mode condition.

5.2.1. Waveguide design and simulations

To maximize the evanescent wave in the cladding for sensing, simulations were done to get optimal parameters. Waveguide height and width both have an influence on the modes and the cladding filling factor. For different heights, the evanescent

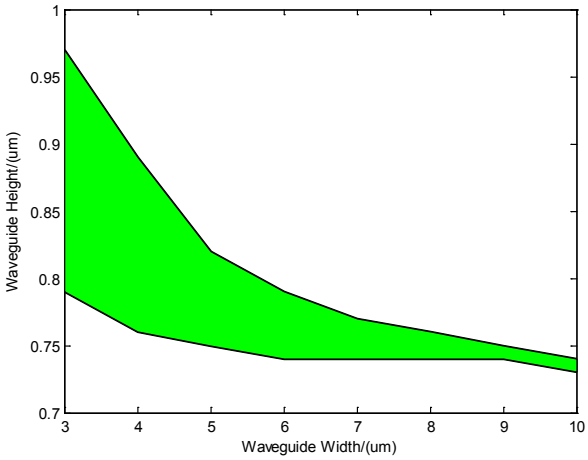

Figure 5.4: The single mode conditions of the waveguide

cladding filling factor is changing with the width. Simulations are shown in Fig 5.5. All the simulations were done based on the waveguides with parameters meeting the single mode conditions. The simulation results indicate that the higher the waveguide the larger the cladding filling factor. However, it also requires stricter tolerances for the waveguide width which translates into tighter fabrication tolerances. Considering both the cladding filling factor and the fabrication tolerance, 5μm would be an optimal height in this design.

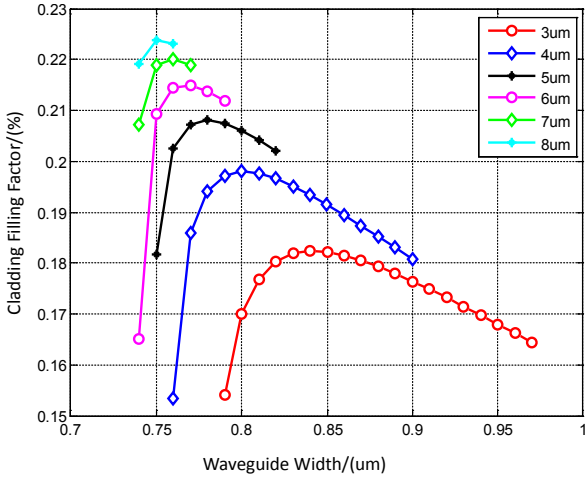

Figure 5.5: Cladding filling factors of waveguides with different heights and widths

5.3. Coupler design and simulations

Coupling light into optical waveguides is very important and also critical because the sizes of optical waveguide cores are small, usually sub-microns for evanescent sensing waveguides. The fact that the induced loss during coupling is large and the alignment tolerance between fibre and waveguide is small makes coupling rather difficult. This means that a coupler in between is needed to increase the coupling efficiency and the alignment tolerance. There are various ways to couple light into waveguides, where the common methods include end-fire coupling, butt coupling, prism coupling, and grating coupling [10]. The first two methods are similar, which are channeling light to the end of the waveguide. The grating coupling is achieved by introducing light at a specific angle to the grating part and has a theoretical low coupling efficiency and thus not sufficiently robust for commercial devices. Considering the fabrication feasibility and operation simplicity, we choose to add a tapered coupler to the waveguides.

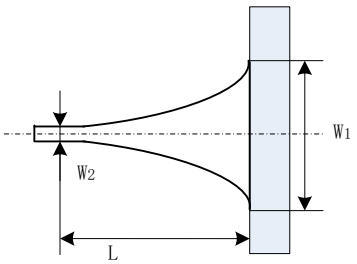

Figure 5.6: Taper model

The taper model was built as shown in Fig. 5.6. The end of the waveguide was tapered horizontally to have a large coupling entrance to increase the coupling efficiency and alignment tolerance. To investigate how the taper profile influences coupling efficiency, exponent functions:

$$w(x) = \alpha(L-x)^m + w_2 \tag{5.1}$$
$$w(0) = w_1 \tag{5.2}$$
$$w(L) = w_2 \tag{5.3}$$
$$\alpha = (w_1 - w_2)/L^m \tag{5.4}$$

are used to define the profile of the taper [11]. $w(0)$ is the taper width at the entrance which is w_1. $w(x)$ is the taper width at x axis and L is the total taper length. $w(L)$ is the taper width of taper end which is defined as w_2 here. m is the parameter of the exponent function which defines the taper profile. To optimize the value of m, a parameter sweep was built up to track the light transmission rate through the waveguide. The simulation results in Fig. 5.7 show that for the exponent function defined taper, the transmission changes quite significantly with m and there exists an optimal parameter that enables the taper with the highest transmission rate. When $m = 1.15$, the coupler is found to be most efficient. The simulation results

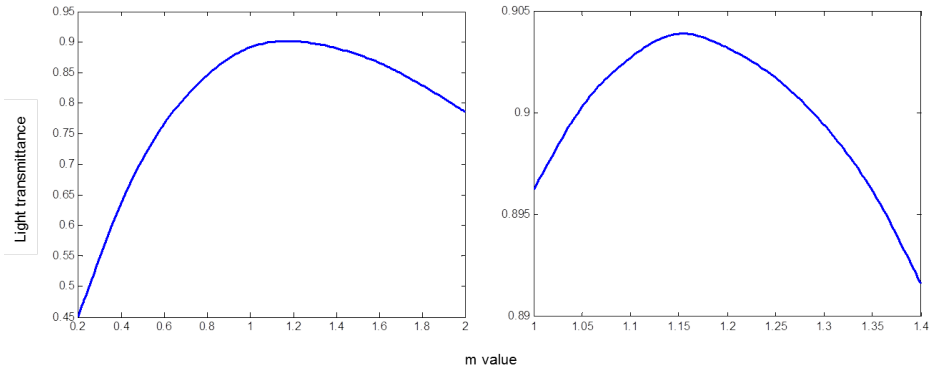

Figure 5.7: Transmission rate with different m

are shown in Fig. 5.8a, 5.8b, 5.8c and depict the light transmission when $m = 0.5$, $m = 1.15$, and $m = 2$. When $m = 1$, the coupling efficiency is just slightly lower than the highest point but this would simplify our design and fabrication, so $m = 1$ was further chosen for the design.

The height of the SU-8 vertical waveguide is already relatively high, so the added taper can increase the coupling efficiency and alignment tolerance in the horizontal direction and guarantee a proper performance in the vertical direction. The schematic of a designed waveguide with taper is shown in Fig. 5.9. Taper width and angle (or length) are two dominant factors for the coupling efficiency and alignment tolerance. Different taper widths and angles were combined in the simulation to obtain an optimal transmittance. The results are shown in Fig. 5.10. From the figure, it can be concluded that there exists an optimal parameter for the tapers. Generally speaking, the coupling efficiency will be higher with a smaller angle. However, the fact that in practical situations, when the angle is too small, the taper length will be very long which will result in a larger loss due to the scattering loss induced by the surface roughness and absorption by material itself. Also, it harms the compactness of the system. Thus, the taper angle should not be too small. Meanwhile, the alignment tolerance is increasing with the width of taper, but at the same time the coupling efficiency is decreasing when the length is fixed. Simulations on how alignment tolerance is influenced by taper width have been done and some results are shown in Fig. 5.11. It illustrates that the taper width has an proportional influence on the alignment tolerance. The alignment tolerance definition can be referred to Chapter 4. It has the same situation with tapers of SiC waveguides. Some compromise needs to be taken to achieve a reasonable coupling efficiency and alignment tolerance.

5.4. Fabrication

Basic MEMS fabrications has already been introduced in Chapter 2. As stated before, the waveguide structure profile defining step-dry etch will deteriorate the surface

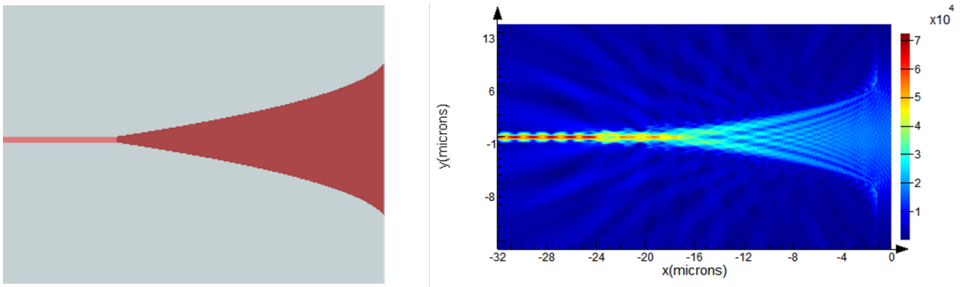

(a) $m = 0.5$

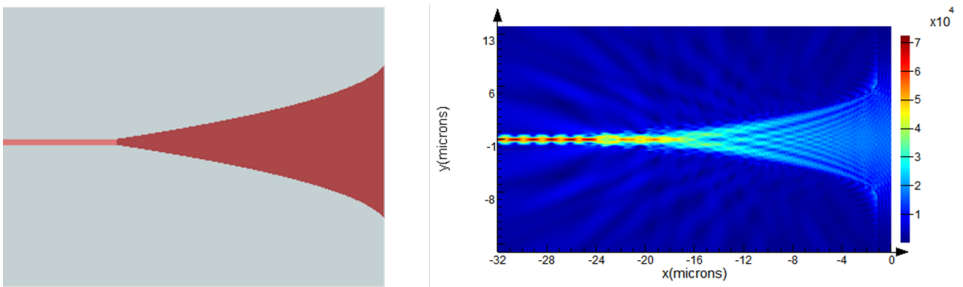

(b) $m = 1.15$

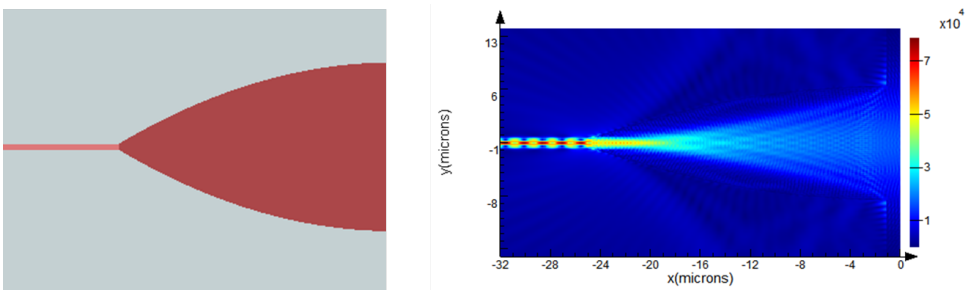

(c) $m = 2$

Figure 5.8: Transmission simulations of taper with different m

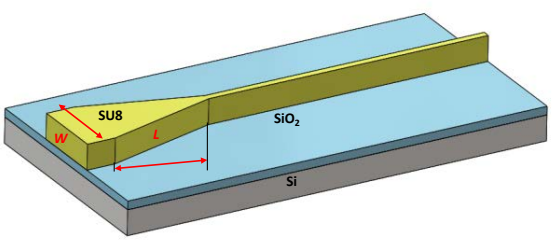

Figure 5.9: Schematic of SU-8 waveguide with taper

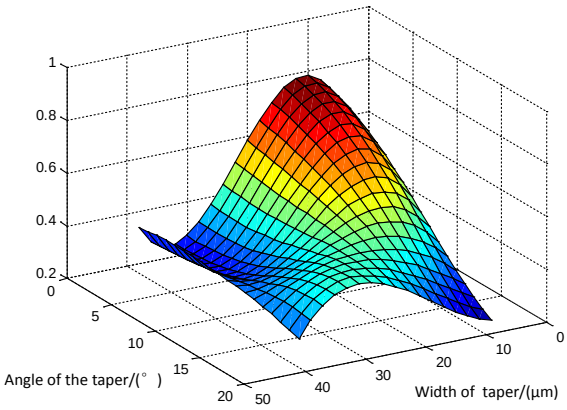

Figure 5.10: Coupling efficiency of SU-8 taper coupler with different parameters

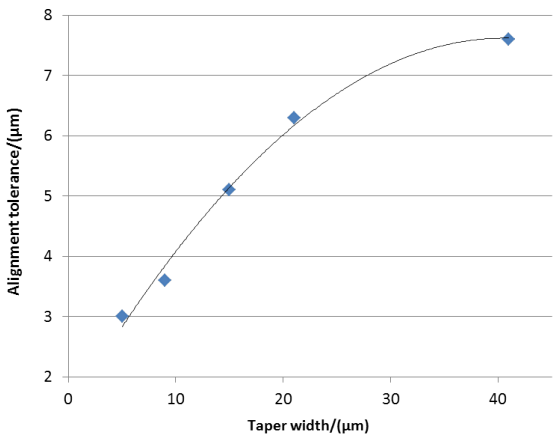

Figure 5.11: SU-8 waveguide alignment tolerance with 1dB excess loss

quality of the waveguide which will further increase the propagating loss of the waveguide. In this design, SU-8 is the waveguide material. It has the advantage of photosensitive and can be fabricated by lithography with no more further steps, which is simple, fast, and high surface quality. Among these techniques, there are direct writing techniques such as E-beam lithography, proton beam lithography, and direct laser writing. Compared with traditional photolithography, these techniques are maskless which allow rapid prototyping. Thus, we used Electron-beam lithography for the waveguide fabrication.

5.4.1. Electron-beam lithography

E-beam lithography is a maskless direct writing technique. It exposes pattern using a highly focused electron beam which is possible to make nanostructures with the resolution of 10nm or even smaller. It shows how Electron-beam lithography works in Fig. 5.12.

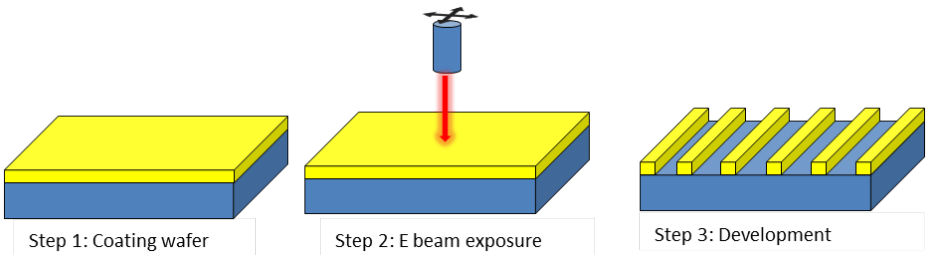

Figure 5.12: Working steps of E-beam lithography

5.4.2. Fabrication flows and techniques

First fabrication with standard flow

The fabrication of the waveguide was conducted by standard MEMS processes in the cleanrooms of Kavli and EKL of TU Delft. A 2μm thick SiO_2 was first deposited on the wafer by PECVD as an isolation layer to prevent optical leakage to the substrate. A 5μm thick SU-8 2005 photoresist was then spin-coated on the SiO_2 layer. Then the wafer underwent 4min @ 65°C + 10min @ 95°C soft bake. Then E-beam lithography was continued to fabricate the waveguide structure. After that, the wafer was post-baked for 4min @ 65°C + 10min @ 95°C and developed and then the wafer was hard baked at 200°C to stabilize the property of SU-8. Fig. 5.13 shows the microscopic image of the SU-8 waveguide with tapers, where the inset pictures are the taper and waveguide sensing part. The taper profile was measured under Dektak (in Fig. 5.14) and the height of the taper turned out to be 4.5μm because of the hard bake. The vertical angle is measured to be 89.91°. The whole fabrication process for the vertical waveguide structure was completed in only one step since SU-8 is photosensitive, making the proposed fabrication process simple and cost efficient. In this fabrication process, some adhesion problems were observed where some of the tiny structures detached from the substrate, which deteriorated the intactness

of the waveguide. Some tests were performed to improve the adhesion of SU-8 to the substrate, which will be explained in the following paragraph.

Figure 5.13: Microscopic image of SU-8 waveguide with tapers

Optimized fabrication with adhesion improvement

To improve the adhesion problem, several steps were taken for this purpose. First, SU-8 3005 was used to replace the former SU-8 2005 which has been reported to have a better adhesion to silicon dioxide substrate [5]. Secondly, a thermal oxide layer was used to replace the PECVD SiO_2 layer. According to [12], a long time and low temperature baking with a slow heating up and cooling down process will increase the adhesion, so this step was also introduced to prebake and post-bake. The process will be introduced later. After fabrication, the protecting layer was removed and the structures adhere well on the substrate even with the most delicate waveguide.

The second fabrication were conducted with the improvement of adhesion. The process steps is described as following.

- A 3μm thick SiO_2 was firstly thermal oxidized at 1100°C on a silicon wafer, acting as an isolation layer to prevent light leakage into the silicon substrate.

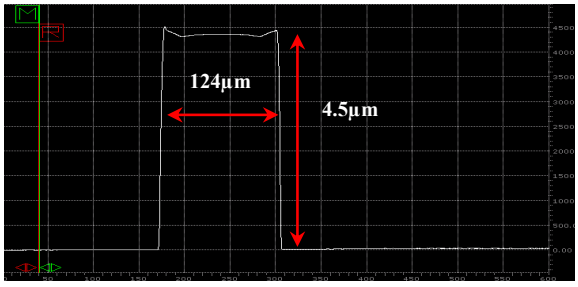

Figure 5.14: Profile measurement of the taper

- Then plasma treatment was conducted in Tepla to improve the adhesion of SU-8 photoresist to the substrate.
- A 5μm thick SU8-3005 photoresist was then spin-coated on the SiO_2 layer with the recipe of (1) spin at 500rpm for 10 seconds with the acceleration of 100rpm/sec and (2) spin at 3000rpm for 30 seconds with acceleration of 300rpm/sec [5].
- Prebake the wafer with slow temperature ramping up to 65°C @ 10°C/min and keep for 10min, then ramping up to 95°C @ 10°C/min and keep for 10min. Cool down the wafer to 50°C @ 2°C/min and keep at 50°C for 10min, then cool down to room temperature. Ramping up and cooling down slowly to prevent any potential induced stress to guarantee good adhesion [12].
- Then the whole wafer was processed by E-beam lithography by machine Raith EBPG-5200.
- Post bake was also conducted by slow temperature ramping up and cooling down with the same procedure.
- The wafer was developed for 1min to 5min and rinsed in IPA for 10s. If there are residuals, repeat rinsing.
- Hard bake at 120°C was done to stabilize the structure.
- Then whole wafer was diced with a protection layer on top. The fabricated waveguides with tapers are shown in Fig. 5.15. The structures are attached well and intact on the substrate.

The fabricated waveguides with tapers are shown in Fig. 5.15. The structures attached well and intact on the substrate after dicing. Measurements were conducted under Keyence VK-X 3D scanning confocal laser microscope. The cross section was shown in Fig. 5.16, with 1.38μm width and 4.849μm height. The 3D image in Fig. 5.17 shows the waveguide sensing part has a relatively vertical sidewall and reasonably good surface in the upper part. Nevertheless, the structures were overexposed and the sidewall roughness are slightly higher near the substrate and also with some residues, where the lithography parameters (expose dose, expose energy, and development time) can be optimized to improve the fabrication accuracy. The residue around the taper on the substrate can be better removed by increasing the developing time. But in the perspective of sensing, because the light is weak in the contact surface between SU-8 and substrate, with most light distributed in the middle area of the core, the residues will only have a limited influence on the sensor performance. And the fact that our sensor monitors bacteria by comparing light changes also makes the residue influence negligible.

5.5. Conclusions

In this chapter, we designed and fabricated a waveguide with a vertical structure. With this design, the sensing area and applicable evanescent waves are both improved, which can further improve the waveguide sensitivity. The use of SU-8 as

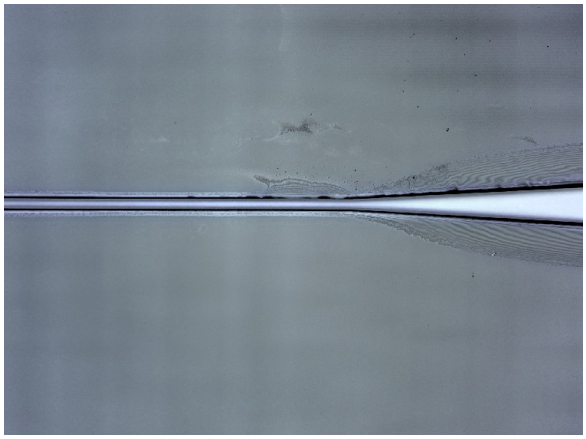

Figure 5.15: Fabricated SU-8 optical waveguide with taper

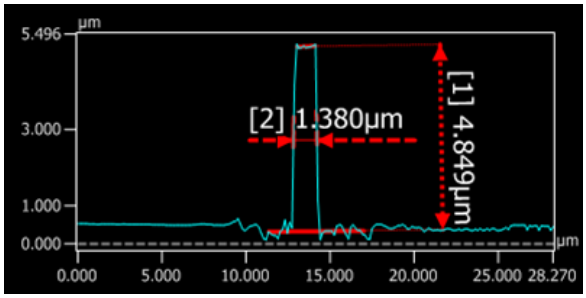

Figure 5.16: Measurement of waveguide height and width

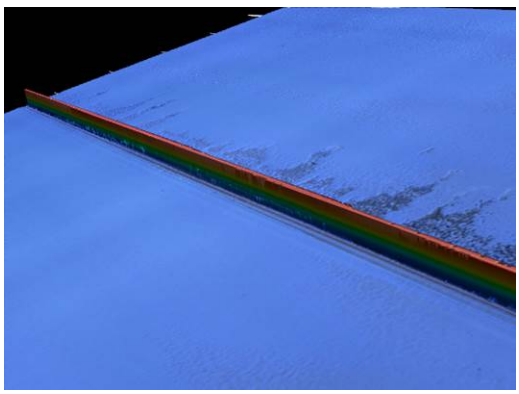

(a) Waveguide line

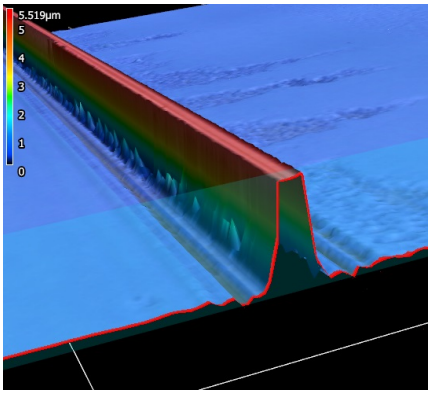

(b) Cross section

Figure 5.17: 3D image by Keyence

waveguide material simplified the fabrication process greatly by finishing the structure fabrication through one-step lithography. This is very efficient to cut down the design, fabrication time and in the meantime improve the quality of the waveguide sensing surface compared with dry etching. Horizontal tapers were added to increase coupling efficiency and also alignment tolerance. The fabrication results showed a good surface quality. Further measurements will be conducted and illustrated in the next chapter.

References

[1] L. Eldada and L. W. Shacklette, *Advances in polymer integrated optics,* IEEE Journal on Selected Topics in Quantum Electronics **6**, 54 (2000).

[2] T. C. Sum, A. A. Bettiol, J. A. Van Kan, F. Watt, E. Y. B. Pun, and K. K. Tung, *Proton beam writing of low-loss polymer optical waveguides,* Applied Physics Letters **83**, 1707 (2003).

[3] R. Müller, D. Cristea, M. Kusko, P. Obreja, D. Esinenco, V. Damian, and P. C. Logofatu, *SU8 polymer materials used in integrated optic microsystems,* OPTOELECTRONICS AND ADVANCED MATERIALS-RAPID COMMUNICATIONS **4**, 228 (2010).

[4] N. Chronis and L. P. Lee, *Electrothermally activated su-8 microgripper for single cell manipulation in solution,* Journal of Microelectromechanical systems **14**, 857 (2005).

[5] Microchem, *SU-8 3000 Permanent Epoxy,* Product Datasheet **20** (2000), 10.1146/annurev.matsci.28.1.153.

[6] A. Deepu, V. Sai, and S. Mukherji, *Simple surface modification techniques for immobilization of biomolecules on su-8,* Journal of Materials Science: Materials in Medicine **20**, 25 (2009).

[7] I. Boiragi, R. Makkar, B. D. Choudhury, A. Mallik, K. Chalapathi, and J. Sebastian, *Su-8 Polymer Based Waveguide Biochemical Sensor for Medical Diagnostic Application,* Iccp , 2 (2009).

[8] F. Dell'Olio and V. M. Passaro, *Optical sensing by optimized silicon slot waveguides.* Optics express **15**, 4977 (2007).

[9] H. Zengzhi, Y. Zhang, C. Zeng, D. Li, M. S. Nisar, J. Yu, and J. Xia, *High Confinement Factor Ridge Slot Waveguide for Optical Sensing,* IEEE Photonics Technology Letters **27**, 2395 (2015).

[10] G. T. Reed and A. P. Knight, *Silicon Photonics: an introduction* (John Wiley & Sons Ltd, 2004).

[11] O. Mitomi, K. Kasaya, and H. Miyazawa, *Design of a single-mode tapered waveguide for low-loss chip-to-fiber coupling,* IEEE Journal of Quantum Electronics **30**, 1787 (1994).

[12] T. M. Verhaar, J. Wei, and P. M. Sarro, *Pattern transfer on a vertical cavity sidewall using SU8,* Journal of Micromechanics and Microengineering **19**, 074018 (2009).

6

Waveguide Sensing Measurements

The previous chapters have introduced the design and fabrication of SiC and SU-8 waveguide systems. In this chapter, some experiments will be carried out to demonstrate these waveguides, including optical measurements, alignment tolerance tests, sensitivity tests, followed by a look at the reusability of the systems. In addition, applications in the biomedical field will be introduced and proved theoretically and experimentally.

6.1. Introduction

After fabrication, a series of tests were performed with an optical setup, shown in Fig. 6.1. It consists of:

1. A waveguide with an adjustable platform, see Fig. 6.2a.
2. A light source: SLEDs (EXS1320-2111, EXALOS), the SLEDs board driver, and fibers (P3-SMF28-FC-2, Thorlabs), see Fig. 6.2b.
3. Photodiode Power Sensors (Seri S122C, Thorlabs) and a power meter (PM100D, Thorlab), see Fig. 6.2c.

The optical source is connected by the FC connector with single mode fibers, which are mounted on the three-direction adjustable platform in the slots. The transmitted optical energy is detected by the photodiode and displayed on the power meter. The microscope and related software in PC is to assist alignment and observation.

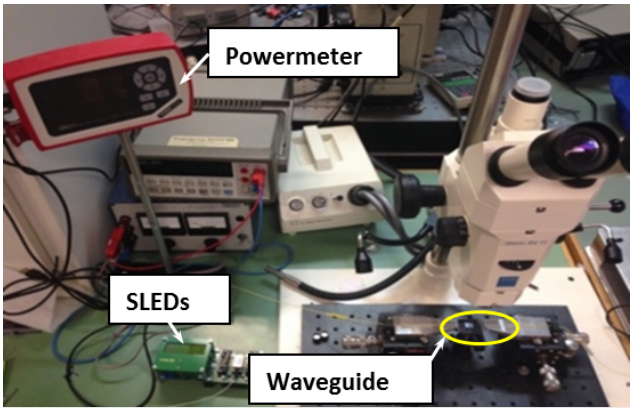

Figure 6.1: Optical measurement setup

6.2. Optical property measurements

The loss in the optical waveguide has already been discussed before in Chapter 2. Propagation loss is an important parameter in the optical waveguide performance. Although it is not very critical in our application, it should not be too large so that it

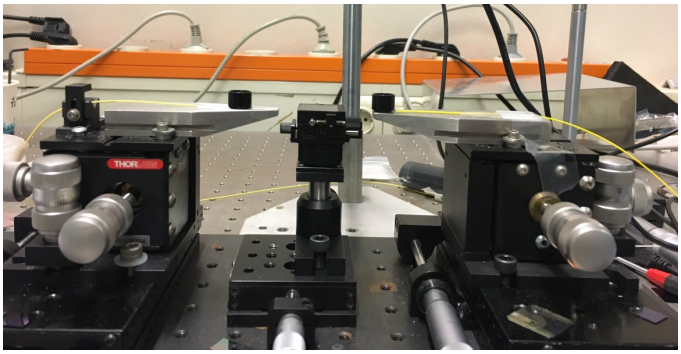

(a) Waveguide with an adjustable platform

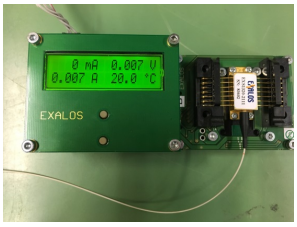

(b) Light source

(c) Photodiode power sensors

Figure 6.2: Compositions of the optical setup

influences optical energy applied for detection. To measure the optical waveguide propagation loss, the most common and simple approach is the cut-back method.

6.2.1. The cut-back method

It is assumed that light is transmitted in a waveguide with a length of L_1 and output power of I_1. Then the light is coupled into an identical waveguide with a length of L_2 and transmitted power measured to be I_2. L_1 is assumed larger than L_2. The input power is I_0. Then the propagation loss of the waveguide length $(L_1 - L_2)$ is related to the transmit power difference. This can be expressed as [1]:

$$\frac{I_1}{I_2} = \exp[-\alpha(L_1 - L_2)] \tag{6.1}$$

Thus:

$$\alpha = (\frac{1}{L_1 - L_2}) \ln(\frac{I_1}{I_2}) \tag{6.2}$$

The accuracy of the measurement can be improved with multiple measurements and plotting the optical loss against the waveguide length in a figure. Then the loss can be calculated.

6.2.2. Measurements

SU-8 waveguides with different lengths (0.5cm, 1cm, and 1.5cm) were fabricated. Optical measurements were taken to obtain the transmission loss of the SU-8

waveguide. Light is generated by SLEDs at 1.3μm and channeled by a single mode fiber (SMF) into SU-8 waveguides. The cut-back method mentioned above is used to calculate the transmission loss [2]. The optical transmittance in waveguides with different lengths was measured each time. The transmission loss of the waveguide was calculated afterwards. The results are shown in Fig. 6.3. The propagation loss is calculated to be 1.03$\pm$0.19dB/cm for this SU-8 waveguide according to Equation (6.1) and (6.2). The insertion loss is as large as 14dB/facet. This is because the samples were diced, the mechanical process of which caused high roughness at the cross-section. Loss can be reduced by cleaving the samples instead of dicing them.

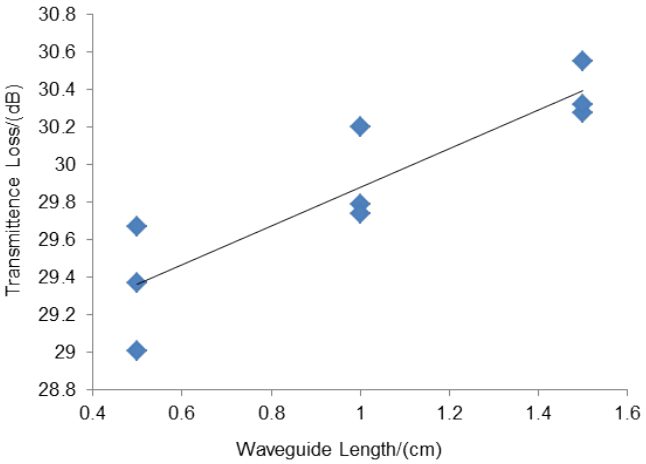

Figure 6.3: Cut-back method to calculate the propagation loss in the SU-8 waveguide

6.3. Sensitivity measurements

Sensitivity is a defining criterion in optical sensing systems besides the optical properties shown above. The waveguide system needs to be sensitive enough to meet certain demands, such as the ability to detect a minimum change in the refractive index or solution concentration.

Sensitivity measurements were conducted first using saline solution of different concentrations on both the SiC waveguide and SU-8 waveguide. The schematic of the sensing experiments is shown in Fig. 6.4. This figure also gives a general idea of how the experiments were conducted. During the experiments, the same amount of the detected solution was dropped on the optical sensing area with the absorption being measured each time.

6.3.1. Theoretical sensitivity comparison

Simulations on the waveguides were carried out beforehand to compare the sensitivity of the SU-8 and SiC waveguides. 3D models (vertical SU-8 waveguide and horizontal SiC waveguide) were first built in COMSOL. The cladding of waveguides in the model was set as saline solutions with different concentrations. The absorption

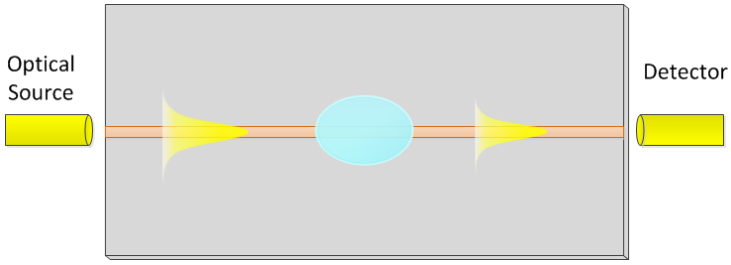

Figure 6.4: Schematic of experimental operation

of the saline solution is dominated by water at 1.3μm [3], where k is 0.000013759 [4]. Therefore, the change in concentrations are reflected by the change of refractive index n. The absorption rate will be mainly influenced by a refractive index change. In this way, the simulations show the situation of saline solution sensing. The sensing length is set to be 1cm. The sensitivity here is defined as the ratio of absorption difference to the refractive index change with different saline concentrations as shown in Equation (6.3). Simulation results are shown in Fig. 6.5a and 6.5b:

$$S = \frac{\Delta A}{\Delta n_c} \tag{6.3}$$

From Fig. 6.5, it can be calculated that the sensitivity of the vertical SU-8 waveguide is 5.15dB per RI unit while that of the horizontal SiC waveguide is 3.32dB per RI unit. This demonstrates that the sensitivity of the SU-8 waveguide is expected to be larger than that of the SiC waveguide.

6.3.2. Experimental sensitivity comparison

Experiments were performed with saline solutions of different concentrations using 1.3μm wavelength light. Different concentrations have a different refractive index, which is shown in [3]. As mentioned before, the absorption rate is dominated by water, thus the change in the refractive index will influence the cladding filling factor and further influence the absorption of the waveguide. Test results on the SiC waveguide and SU-8 waveguide are shown in Fig. 6.6 and Fig. 6.7, respectively. Both results show that the absorption rates increase with the increase in concentration of the saline concentration (refractive index). The absorption rate was plotted against refractive index. The sensitivity was calculated to be 3.8dB per RI unit of the SiC waveguide system and 4.8dB per RI unit of the SU-8 waveguide system. They demonstrate the feasibility of both evanescent waveguide systems, with the SU-8 waveguide having a 25% higher sensitivity than the current SiC waveguide system.

Furthermore, SU-8 waveguide sensitivity measurements were continued using solutions of isopropyl alcohol (IPA) and water mixture. IPA has a different absorption rate (α=0.19937cm^{-1}) from water (α=1.33cm^{-1}) at 1.3μm. The absorption coefficient of water is much higher than IPA which means with the increasing proportion of IPA in the mixture, the absorption rate of the mixture will decrease.

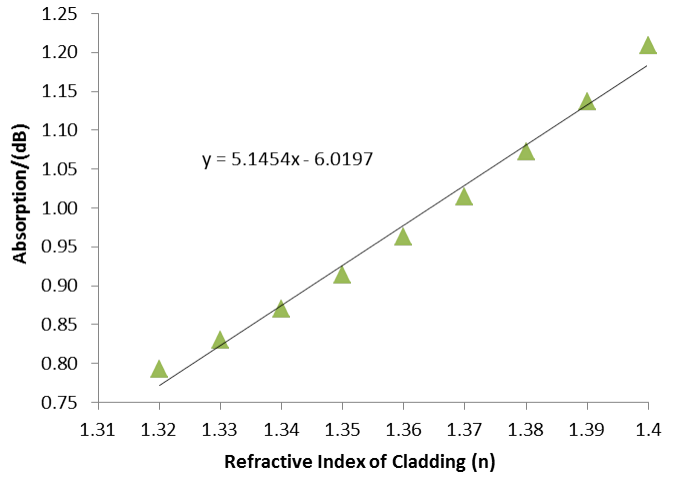

(a) SU-8 waveguide

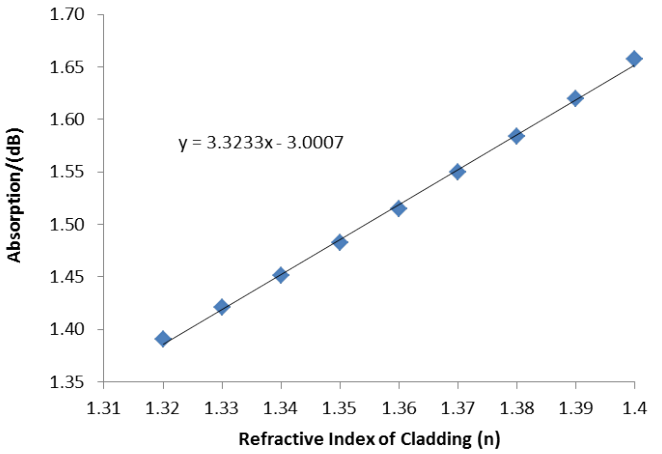

(b) SiC waveguide

Figure 6.5: Simulations on the sensitivity of two waveguides

On the other hand, the refractive index of IPA is higher than water. When the IPA concentration increases, the refractive index of the mixture (cladding) will also increase which has a reverse influence on the absorbance of the waveguide. Simulations of waveguide absorbance with different IPA-water mixtures were performed to investigate the influence of the IPA ratio on waveguide absorbance. The results, illustrated in Fig. 6.8, show that the absorption rate of the waveguide system decreases with an increase in the proportion of IPA. Next, tests were conducted with an IPA solution. The sensitivity of the waveguide was calculated by measuring the different light transmissions with different IPA concentrations. The sensitivity in this

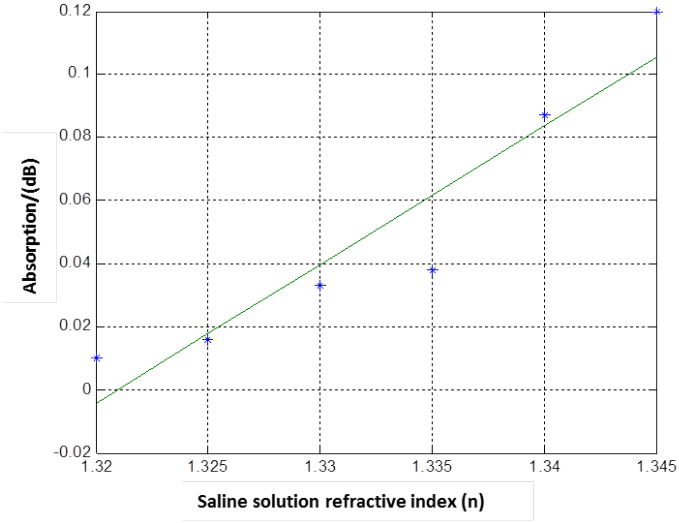

Figure 6.6: SiC waveguide sensitivity measurement with different saline concentration

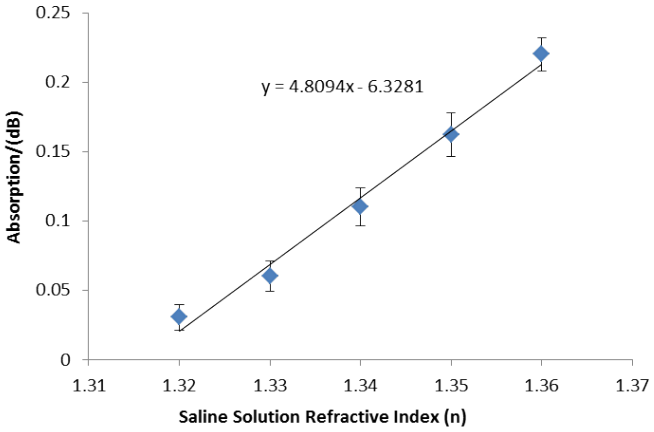

Figure 6.7: SU-8 waveguide sensitivity measurement with different saline concentration

situation is the absorption-to-volume percentage (%v/v) of IPA which is the input signal here. This is defined in the following equation [5]:

$$S = \frac{\Delta A}{\Delta \%\mathrm{v/v}} \tag{6.4}$$

The mixtures used here were 0% (pure water), 25% IPA, 50% IPA, 75% IPA, and 100% IPA by volume percentage. The transmitted light was measured 10 seconds after applying the mixture to the waveguide sensing area every time, waiting for

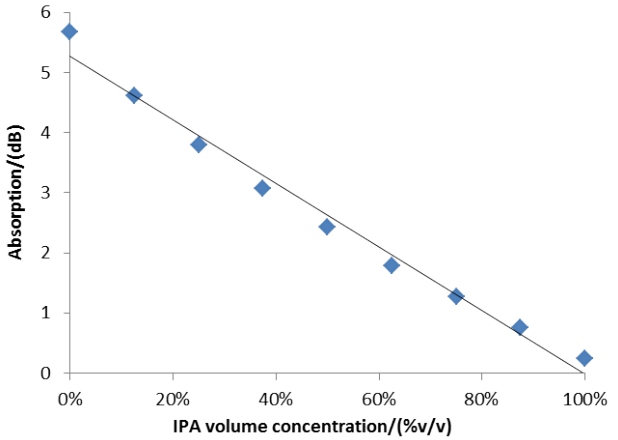

Figure 6.8: Simulations of the sensitivity of the SU-8 waveguide in the IPA-water mixture environment

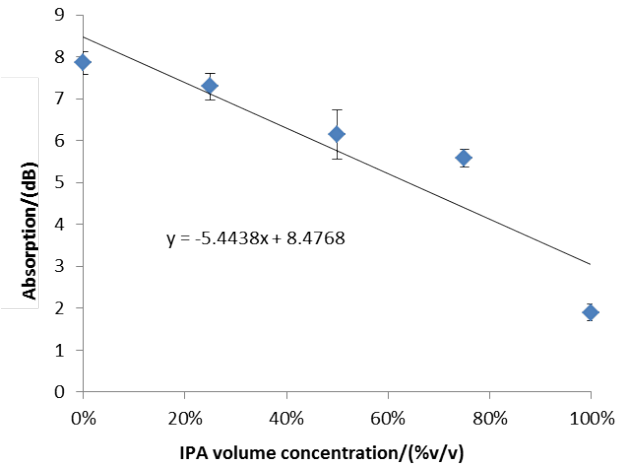

Figure 6.9: Absorption rates when applying solutions with different IPA concentrations

the signal to be stable. The results are plotted in Fig. 6.9. The experimental data were not absolutely linear in this test. The reasons mainly lie in the drift of the setup and evaporation of IPA solution. The drift of the setup had an impact on the alignment between the fiber and optical source, which influenced the input and output signals. The IPA solution with a higher concentration evaporated faster than lower one, which also had a non-linear effect on the measurement results. The measurements were taken after only 10 seconds to keep the influence minimal. The measurement error each time is also influencing the results. Considering all these deviations, the results are still valid enough to show the waveguide sensitivity based on multiple measurements. The waveguide was measured with a sensitivity

of 5.4dB/(%v/v), which shows a great improvement compared with the previously researched horizontal waveguides [5].

6.4. Alignment tolerance measurements

Alignment tolerance is very important in waveguide sensing systems, especially in a plug-and-play system. A large alignment tolerance can benefit both the stability of the system and operational ease. The alignment tolerance criterion is defined as the misalignment range that causes 1dB excess loss in the horizontal direction.

The alignment tolerance test was conducted by changing the position of the input fiber and output fiber, respectively, in the horizontal direction and recording the power received at the same time. The results are shown in Fig. 6.10. The 1dB alignment tolerance for the waveguide with a 125μm taper at the entrance is around 39.4μm for a moving input fiber and 30.4μm when the output fiber moves. For tapers with a 20μm taper width, alignment tolerance tests were also conducted, which was measured to be 7.2$\pm$0.93μm.

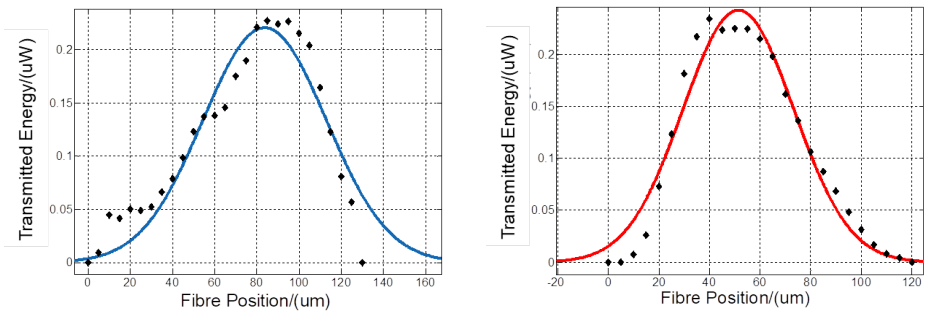

(a) Moving input fiber and fixed output fiber (b) Moving output fiber and fixed input fiber

Figure 6.10: Alignment tolerance for 1dB extra loss. Solid line is the Gaussian data fit curve.

6.5. Reusability

Reusability is another important property in optical waveguide sensing systems. It can decrease the cost and reduce the sensing chip replacement frequency, which also saves time. However, reusability also depends on the application field and situation. In some situations, a disposable device is more preferable, such as in a hospital.

To test the reusability of the waveguide, after repeating the measurement 10 times, the propagation loss and sensitivity were tested again. The results of propagation loss are shown in Fig. 6.11 and the sensitivity results are shown in Fig. 6.12. The results showed an increase in loss and a decrease in sensitivity. These were mainly caused by residues from the previous tests not completely flushed away. However, the waveguide was still stable enough to be used repeatedly. The results also demonstrate the stability of the SU-8 waveguide system.

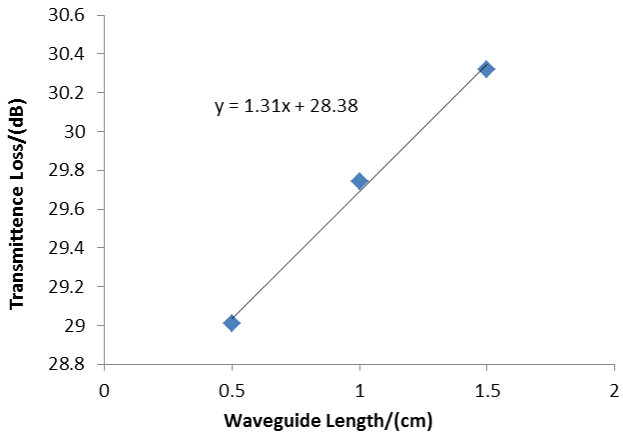

Figure 6.11: Propagation loss in the SU-8 waveguide measurement

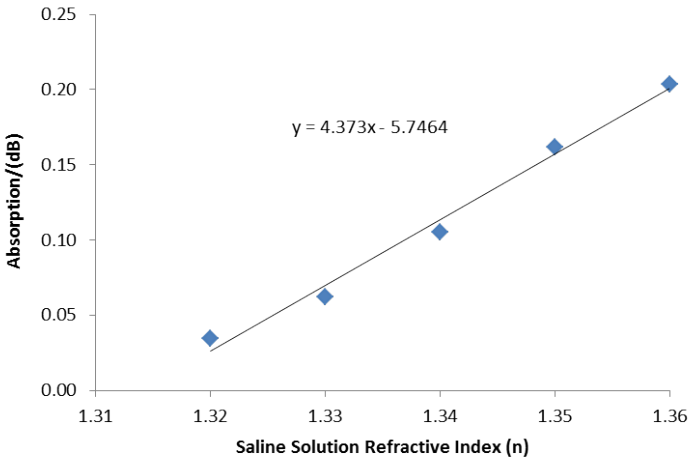

Figure 6.12: The SU-8 waveguide sensitivity measurements with different saline concentrations

6.6. Biomedical application

The sensing system has been demonstrated effectively in the optical and chemical field. Additionally, since SU-8 is stable after fabrication and has the ability to be biomedically treated, it also has potential in the biomedical field. This section will introduce the tests of the SU-8 waveguide system for biomedical application. It has already been demonstrated in many studies that the surface of SU-8 can be functionalized efficiently [6–10].

6.6.1. Surface functionalization

Surface functionalization is the process of attaching antigen/antibody to the surface of a waveguide. This includes surface modification and antibody/antigen immobilization [11]. Surface modification is aimed at creating a surface with the property that can react with the antibody afterwards.

The general procedure starts with creating –OH groups on the surface and then creating amine groups on the underlying layer. After that, by applying glutaraldehyde on the chip, the amine groups and antibodies can be bridged. After the antibodies are immobilized on the surface, the wafer is successfully functionalized and is ready for antigen immobilization. The procedure is illustrated in Fig. 6.13.

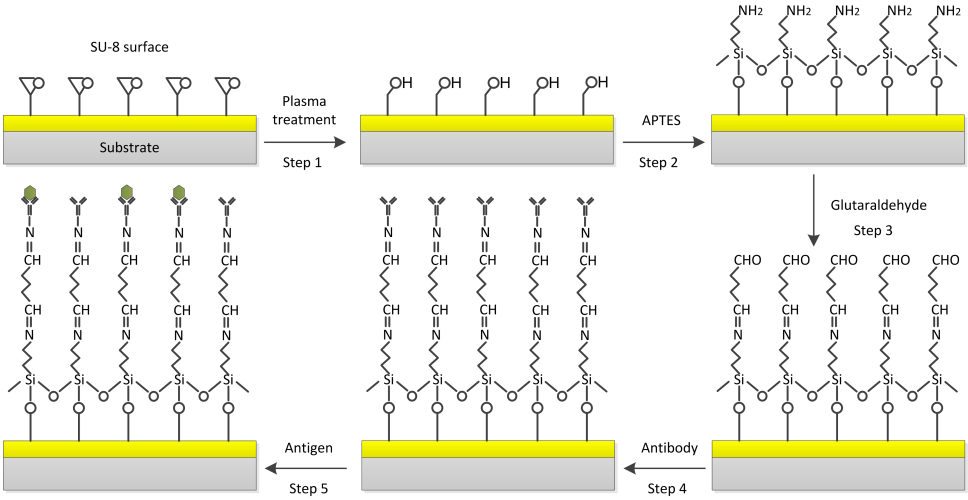

Figure 6.13: SU-8 surface functionalization process

The detailed functionalization steps are:

1. Step 1: Plasma treatment

   The SU-8 surface is activated by oxygen plasma for 5min at a pressure of 200mTorr and a power of 30W [12, 13]. By plasma treatment, the epoxy group is opened and –OH groups are created on the SU-8 surface.

2. Step 2: APTES Treatment

   This step creates amine groups on the surface. APTES is diluted in 75% ethanol and 25% water with a 1:100 ratio. Then the chips are incubated overnight at room temperature.

3. Step 3: Glutaraldehyde treatment

   The wafer is activated using a 1.2%(v/v) glutaraldehyde solution in 1× phosphate buffer saline (1× PBS) at room temperature for 2h. Then it is washed excessively with DI water and 1× PBS. Glutaraldehyde is a di-aldehyde, which

contains 2 active aldehyde moieties (= CHO). These aldehydes react with amine groups which are present on the APTES and on the antibody. In this way, glutaraldehyde bridges the APTES with the antibody.

4. Step 4: Antibody immobilization

   (a) The original antibody solution is diluted in 1×PBS to make an antibody solution of 10μg/mL.

   (b) The solution is dropped on the surface and incubated for one hour at room temperature.

   After the reaction, the antibody will be immobilized on the surface and the chips can be used for the reaction with *Escherichia coli(E. coli)*.

5. Step 5: Antigen reaction

   This step is to create an *E. coli*/antibody association, through the process of:

   (a) Applying *E. coli* on the functionalized specimens and incubating the bacteria for a defined time period (2 hours)

   (b) Washing the incubated specimens with DI water.

   After the steps designated above, the chips are functionalized with *E. coli* and ready for the following optical measurements.

6.6.2. *E. coli* culture

E. coli K12 is the analysis target in this thesis. Before measurements, the bacteria needed to be cultured and counted . These procedures were conducted in the Biocatalysis group, Department of Biotechnology, TU Delft.

Culturing

First, *E. coli* K12 was streaked onto a solid LB-agar plate from a frozen glycerol stock. A single colony was picked to inoculate a pre-culture in a 10mL LB medium. Then, the solution was incubated by shaking it at 37°C overnight. The cultured solution is called "original *E. coli* culture".

The amount of bacteria in a culture can be defined by optical density (OD value) at 600nm (OD_{600}). First, the absorption of the original culture needed to be defined. This was done by measuring the OD_{600} value of the original culture by Spectrophotometer (Bio-chrom Libra S12 UV/Visible spectrophotometer, λ=600nm). The OD_{600} value of the LB medium was used as a reference, for which the OD value was set to zero. The measured value showed a OD_{600} value of 0.505, so with a correction of 10 for the reference, the absolute OD value of the original culture was 5.05.

Table 6.1: Calibration and calculation of *E. coli* concentration in different cultures. $10^{-2}\times$, $10^{-4}\times$, $10^{-6}\times$ is the dilutions from the original solutions

	Calibration	Original	$10^{-2}\times$	$10^{-4}\times$	$10^{-6}\times$
OD_{600}value	1	5.05			
Concentration (CFU/mL)	3×10^7	1.5×10^8	1.5×10^6	1.5×10^4	1.5×10^2

Counting

In order to know how many living bacteria existed in the culture and were used in the experiments, the OD_{600} value had to be correlated to the amount of colony forming units (CFUs). Because the concentration of *E. coli* K12 was too high in the original culture, the original culture was diluted to obtain countable single colonies after plating. Solid LB agar was prepared and used as the medium. 100μL of the dilution was dropped onto the agar plate surface and spread with a plastic stick. The plates were incubated in an incubator at 37°C overnight, during which colonies formed on the LB agar plates. By counting the colonies, the original culture concentration could be calculated. The OD value was calibrated to be 3×10^7 CFU/mL (colony-forming units per milliliter) for OD_{600}=1. Table 6.1 shows the calibration and calculations of the colonies in different cultures.

6.6.3. Surface functionalization test

To confirm the surface functionalization method, the functionalization method was first demonstrated on chips coated with a SU-8 layer on top. All the chemical and biomedical treatments were applied as designed previously. After the surface was functionalized with antibodies (*E. coli* K99 (6911): sc-57716 from Santa Cruz), the chips were incubated in *E. coli* cultures of different concentrations, which are 10^2 CFU/mL, 10^4 CFU/mL, and 10^6 CFU/mL. As a negative control, chips without antibody treatment, but still have gone through all the chemical treatments, were incubated with *E. coli* cultures and set as a separate group.

After surface functionalization, the waveguide is able to capture bacteria on the surface which is specific to the immobilized antibodies (*E. coli* K99). When the *E. coli* culture was applied to the surface, the bacteria were captured by antibodies on the surface. After incubation with *E. coli* K12 cultures for 2 hours, the chips were rinsed with PBS for three times to flush away the excess *E. coli* that was not bound to antibodies on the SU-8 surface. Then *E. coli* were fixed with a fixation solution, which contained 4% formaldehyde and 1% glutaraldehyde in a 10mM phosphate buffer, at a pH of 7.4 for 2 hours. Through this procedure, the *E. coli* on the chips were killed and fixed on the SU-8 surface. Then the chips were washed in MilliQ water for 10 min.

The *E. coli* cultures that reacted to the functionalized chips were plated the same way to check the *E. coli* concentration change in the culture. Fig. 6.14 shows the colonies formed on the LB agar plate (a) incubated with the original culture, (b) incubated for 30min with the functionalized chips, and (c) incubated 2 hours with the functionalized chips. The figure shows that the cultures which were incubated with functionalized chips formed fewer *E. coli* colonies than the original one and

longer incubation culture resulted in fewer colonies formed. This demonstrates the effectiveness of attaching *E. coli* to the treated surface.

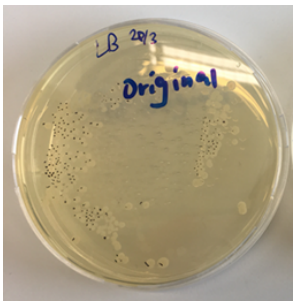

(a) Original culture incubation

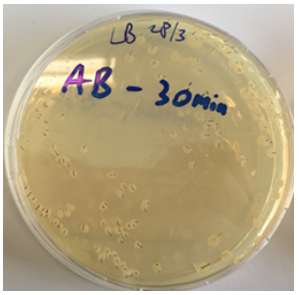

(b) Culture incubated for 30min with functionalized chips

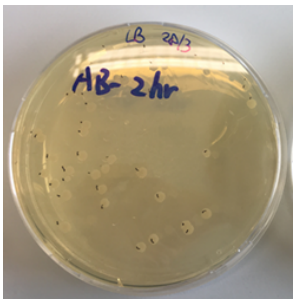

(c) Culture incubated 2 hours with functionalized chips

Figure 6.14: Colonies formed on LB agar plate after incubated with different cultures

To confirm the results of surface functionalization on the SU-8, Syto 9 dye was used. This dye can bind with the DNA of captured *E. coli* on the surface and emits fluorescence at 498nm when excited at a 485nm wavelength. After incubating the dye with the treated chips, they were measured with a confocal microscope. The confocal microscope was set at the right parameters which were in accordance with Syto 9 dye. The observed fluorescence confirms the existence of *E. coli*. The results are shown in Fig. 6.15 with images taken under the confocal microscope. The chips in Fig. 6.15a, 6.15b, 6.15c were treated with different *E. coli* concentrations, which were 10^6CFU/mL, 10^4CFU/mL, 10^2CFU/mL respectively, while Fig. 6.15d is the negative control which went through all the functionalization treatment without antibodies and was incubated with 10^6CFU/mL cultures as a negative control. The cultures with a higher *E. coli* concentrations result in a higher density of *E. coli* captured on the SU-8 surface and the one without antibody treatment showed no capture.

To obtain a wider scope of the immobilization, the chips were studied using a Keyence Laser Microscope to further check the effect of the proposed functionalization method. The observed surface with different *E. coli* solution treatments are shown in the following table.

Table 6.2 shows the *E. coli* treatment on the SU-8 surface with different concentrations. The first row contains the chips with surface functionalization (chemical treatment + antibody treatment) and incubated with *E. coli* cultures with different concentrations for 2 hours, and the second row presents the ones without antibody treatment that were incubated with the identical *E. coli* cultures for 2 hours, acting as a negative control. There is a big difference between chips with the chemical treatment + antibody treatment and with only the chemical treatment. For the chips going through whole surface treatment procedure, the results indicate that the chip surfaces which incubated with higher concentrations captured more *E. coli*. By contrast, the chips without antibody treatment rarely captured any *E. coli* on the surface. This confirms the effectiveness of surface functionalization and different

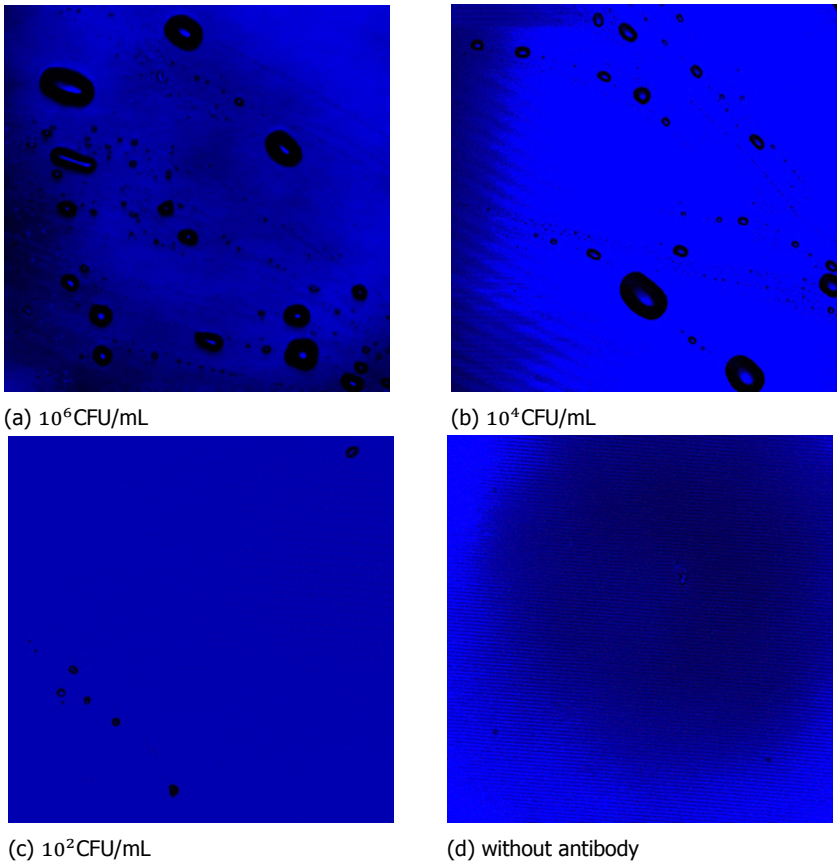

(a) 10^6CFU/mL (b) 10^4CFU/mL

(c) 10^2CFU/mL (d) without antibody

Figure 6.15: Measurement of Syto 9 dyed *E. coli* on functionalized chips under a confocal microscope; the chips were treated with different *E. coli* concentrations

concentrations of *E. coli* in solutions that can be reflected on the different numbers of *E. coli* captured on the surface.

6.6.4. *E. coli* measurements

After the former functionalization method demonstration with SU-8 test wafers, the same process was performed on chips with SU-8 waveguide structures. All the chips were incubated with *E. coli* cultures with concentrations of 10^2CFU/mL, 10^3CFU/mL, 10^4CFU/mL, 10^5CFU/mL, 10^6CFU/mL for 2 hours. A negative group was also set up with the same chemical treatment but without antibody treatment. When fluid was applied to the sensing area, the target bacteria were captured on the surface by antibodies. The more targets present in the fluid, the more that were fixed. After flush away, the waveguide with captured bacteria on the surface absorbed more optical energy than the reference waveguide without antibody treatment. In this way, a relative bacteria (*E. coli*) concentration can be obtained. The real

Table 6.2: Observation of *E. coli* on chips under Keyence Laser Microscope with different *E. coli* culture treatments

	10^6CFU/mL	10^4CFU/mL	10^2CFU/mL
2hrs	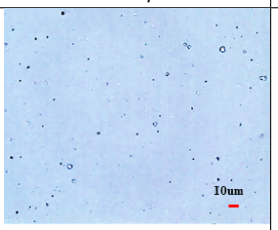	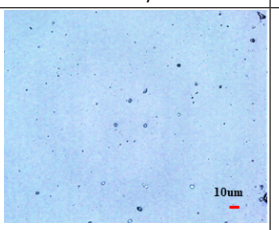	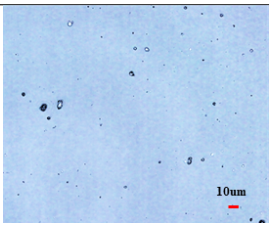
Negative control	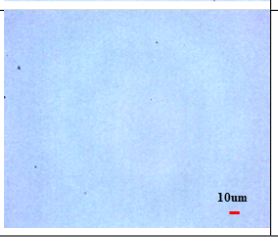	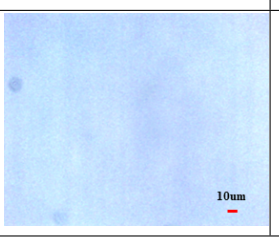	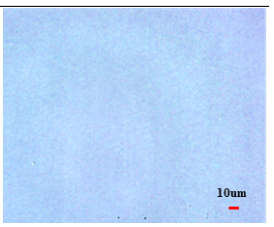

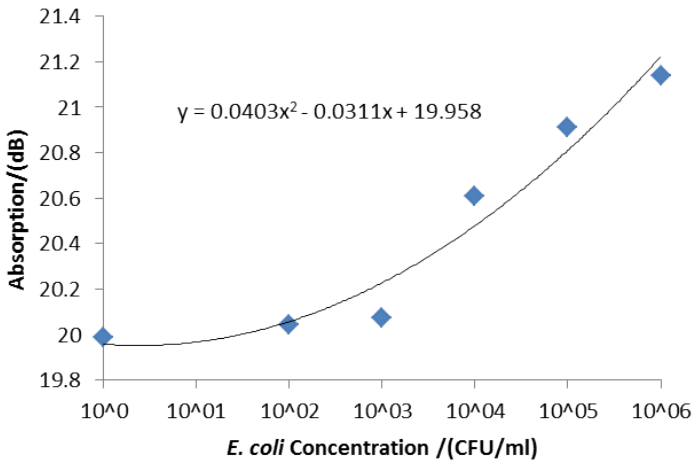

Figure 6.16: Absorption of the waveguide with *E. coli* solution incubation of different concentrations

value was calculated after calibration. After incubation, the chips were fixed and then measured on the optical setup as shown above in Fig. 6.1. The absorption of waveguides with different *E. coli* treatments was measured. The results are shown in Fig. 6.16. This figure shows an increasing trend with the increase in *E. coli* concentration, which demonstrates its sensitivity to *E. coli*. The waveguide is able to detect bacteria when the concentration is 10^2CFU/mL. Moreover, it becomes more significant when the concentration reaches 10^4CFU/mL. To monitor leakage of patients, the sign of leakage in patients is normally when *E. coli* concentration quickly

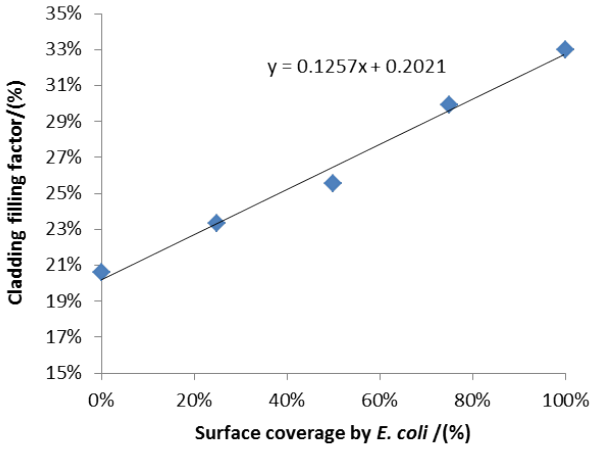

Figure 6.17: Cladding filling factor simulation of the waveguide with different *E. coli* surface coverage

ramps up to 10^5CFU/mL in the drain fluid after surgery [14]. Therefore, the designed waveguide system meets the medical requirements. Compared to previous research results in [15], the system also shows an improvement in sensitivity.

6.6.5. Theoretical analysis

E. coli have a refractive index of around 1.37 at a wavelength of 1.3μm [16]. For absorption-based evanescent waveguide sensing, the absorbance can be expressed in terms of an evanescent power ratio, evanescent bulk coefficient and interaction length. The first two parts are directly related to the species concentration. This can be expressed:

$$P(z) = P_0 \exp(-\gamma z) \tag{6.5}$$

where z is the distance light is transmitted along the waveguide, P_0 is the transmitted power without detecting the species, and γ is the evanescent absorption coefficient, which is related to the bulk absorption coefficient (α) when the detected species is present and power distribution ratio in cladding (Γ) [17].

$$\alpha = \frac{\alpha_d C \lambda}{4\pi} \tag{6.6}$$

Here, C is the concentration of the absorbed molecule coverage on the surface or chemical species concentration. α_d is the target absorption coefficient, and λ is the wavelength.

$$\Gamma_c = \frac{\iint_c |E(x,y)|^2 \, \mathrm{d}x \, \mathrm{d}y}{\iint_\infty |E(x,y)|^2 \, \mathrm{d}x \, \mathrm{d}y} \tag{6.7}$$

Here, $E(x,y)$ is the electric field vector and C is the medium area in the cladding.

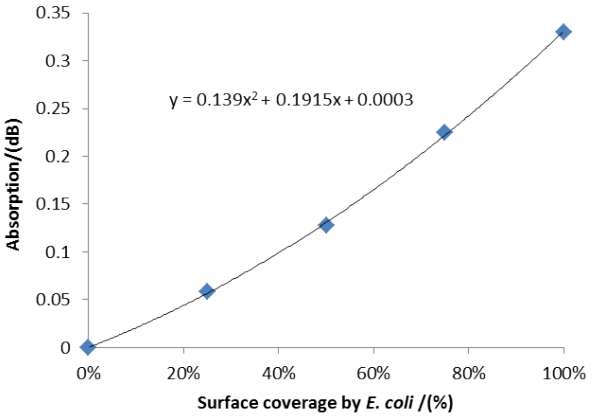

Figure 6.18: Absorption simulation of the waveguide with different *E. coli* surface coverage

Therefore, the evanescent absorption by the targets on a waveguide with a sensing length of L is defined as:

$$A = 4.343\alpha L\Gamma_c \tag{6.8}$$

Simulations of the cladding filling factor (Γ) and the absorption (A) with different *E. coli* surface coverages deduced from equation are shown in Fig. 6.17 and Fig. 6.18. The cladding filling factor is proportional to the surface coverage, and absorption has a polynomial relationship with the surface coverage. The theoretical analysis and simulation curve trends agree well with the measurement results, which further substantiate the capability of the waveguide system.

6.7. Conclusions

In this chapter, the optical, sensitivity and alignment tolerance of the fabricated waveguide were measured and compared, with the SU-8 waveguide system demonstrating higher sensitivity in chemical sensing. The capability of implementing the SU-8 waveguide system in the biomedical field has also been demonstrated with respect to detecting *E. coli* solutions/cultures of different concentrations.

References

[1] G. T. Reed and A. P. Knights, *Silicon photonics: an introduction* (John Wiley & Sons, 2004).

[2] G. Pandraud, E. Margallo-Balbas, C. K. Yang, and P. J. French, *Experimental characterization of roughness induced scattering losses in PECVD SiC waveguides,* Journal of Lightwave Technology **29**, 744 (2011).

[3] X. Li, L. Liu, J. Zhao, and J. Tan, *Optical Properties of Sodium Chloride Solution*

Within the Spectral Range from 300 to 2500 nm at Room Temperature, Applied Spectroscopy **69**, 635 (2015).

[4] S. Kedenburg, M. Vieweg, T. Gissibl, and H. Giessen, *Linear refractive index and absorption measurements of nonlinear optical liquids in the visible and near-infrared spectral region,* Optical Materials Express **2**, 1588 (2012).

[5] A. Purniawan, G. Pandraud, K. Vakalopoulos, P. French, and P. Sarro, *Surface functionalisation of tio 2 evanescent waveguide sensor for e. coli monitoring,* in *Optical Sensing and Detection II*, Vol. 8439 (International Society for Optics and Photonics, 2012) p. 843926.

[6] A. Deepu, V. V. R. Sai, and S. Mukherji, *Simple surface modification techniques for immobilization of biomolecules on SU-8,* Journal of Materials Science: Materials in Medicine **20**, 25 (2009).

[7] B. Y. Shew, Y. C. Cheng, and Y. H. Tsai, *Monolithic SU-8 micro-interferometer for biochemical detections,* Sensors and Actuators, A: Physical **141**, 299 (2008).

[8] S. L. Tao, K. C. Popat, J. J. Norman, and T. A. Desai, *Surface modification of SU-8 for enhanced biofunctionality and nonfouling properties,* Langmuir **24**, 2631 (2008).

[9] L. Jiang, K. P. Gerhardt, B. Myer, Y. Zohar, and S. Pau, *Evanescent-wave spectroscopy using an SU-8 waveguide for rapid quantitative detection of biomolecules,* Journal of Microelectromechanical Systems **17**, 1495 (2008).

[10] M. Joshi, R. Pinto, V. R. Rao, and S. Mukherji, *Silanization and antibody immobilization on SU-8,* Applied Surface Science **253**, 3127 (2007).

[11] I. Boiragi, R. Makkar, B. D. Choudhury, A. Mallik, K. Chalapathi, and J. Sebastian, *Su-8 Polymer Based Waveguide Biochemical Sensor for Medical Diagnostic Application,* Iccp , 2 (2009).

[12] I. A. Grimaldi, G. Testa, G. Persichetti, F. Loffredo, F. Villani, and R. Bernini, *Plasma functionalization procedure for antibody immobilization for su-8 based sensor,* Biosensors and Bioelectronics **86**, 827 (2016).

[13] F. S. Hamdi, M. Woytasik, M. Couty, O. Francais, B. Le Pioufle, and E. Dufour-Gergam, *Low temperature irreversible poly (dimethyl) siloxane packaging of silanized su8 microchannels: Characterization and lab-on-chip application,* Journal of Microelectromechanical Systems **23**, 1015 (2014).

[14] N. Komen, J. Slieker, P. Willemsen, G. Mannaerts, P. Pattyn, T. Karsten, H. De Wilt, E. Van Der Harst, W. Van Leeuwen, C. Decaestecker, H. Jeekel, and J. F. Lange, *Polymerase chain reaction for Enterococcus faecalis in drain fluid: The first screening test for symptomatic colorectal anastomotic leakage. The Appeal-study: Analysis of Parameters Predictive for Evident Anastomotic Leakage,* International Journal of Colorectal Disease **29**, 15 (2014).

[15] A. Purniawan, *Evanescent Waveguide Sensors for Biomedical Applications*, Ph.D. thesis, TU Delft, Delft University of Technology (2014).

[16] A. E. Balaev, K. N. Dvoretski, and V. a. Doubrovski, *Refractive index of escherichia coli cells,* Proceedings of SPIE (Saratov Fall Meeting 2001: Optical Technologies in Biophysics and Medicine III) **4707**, 253 (2002).

[17] V. Ruddy, B. D. MacCraith, and J. A. Murphy, *Evanescent wave absorption spectroscopy using multimode fibers,* Journal of Applied Physics **67**, 6070 (1990).

7

Conclusions and Future Work

7.1. Conclusions

In this thesis, plug-and-play optical waveguide sensing systems are proposed for chemical and biomedical detection. The thesis consists of the development and optimization of optical systems in terms of structures and the materials. The design and fabrication of two types of waveguide sensing systems have been investigated and optimized. Sensing measurements were conducted for the two waveguide sensing systems, both showing good potential in sensing applications.

In Chapter 2, an overall review of micromachined optical waveguides is summarized, starting with MOEMS and gradually going deep into optical waveguide structures, materials, MEMS fabrication, and applications. This comprehensive overview benefits the design and fabrication of optical devices. This chapter also discusses commonly used structures, materials, and fabrication techniques with important details. The applications and development trend are also illustrated.

In Chapter 3, some commonly used waveguides for sensing are introduced and analyzed in detail. Simulations have been carried out to compare the performance of three waveguides: the rib waveguide, ridge waveguide, and slot waveguide. They give an idea of how the parameters influence the performance of waveguides and lay the foundation for subsequent design specifications. Tapers of different types are introduced to increase the coupling efficiency and alignment tolerance, which facilitates the realization of the desired plug-and-play sensing systems.

In Chapter 4, SiC is researched as the core material of evanescent waveguides because of its suitable optical, chemical, and mechanical properties. LPCVD and PECVD depositions are combined when fabricating the waveguide. To reduce the coupling loss and misalignment effect, and to achieve the final plug-and-play system, 3D tapered couplers have been designed to be added to the input and output of the waveguide. In order to fabricate the coupler, a novel slope transfer method

was proposed. A less than 2° slope is achieved by the proposed method. This method can be well integrated into SiC waveguides and enables the further development of the plug-and-play system. It also gives an alternative for the slope fabrication in other materials.

In Chapter 5, a novel vertical SU-8 waveguide is proposed for evanescent biomedical sensing. The waveguide is designed to have a narrow and vertical cross section to generate evanescent waves on both sides of the waveguide surfaces. With this waveguide design, the sensing area and applicable evanescent waves were both improved, allowing for further improvement in the waveguide sensitivity. Simulations have been performed to monitor the influence of different parameters on the waveguide performance including waveguide height and width. The use of SU-8 as the waveguide material simplified the fabrication process greatly with one-step lithography. E-beam lithography was utilized, enabling simple yet high-resolution fabrication. It reduced the sidewall roughness and decreased the induced scattering loss, which is a major source of loss in waveguides. This method was also effective for reducing the design and fabrication time. Furthermore, the quality of the waveguide sensing surface was also improved compared with a dry etching method. Horizontal tapers were added to the system to improve the coupling efficiency and alignment tolerance for a plug-and-play optical system.

In Chapter 6, experiments and demonstrations have been carried out with the SiC and SU-8 waveguides, including optical measurements and tests on alignment tolerance, sensitivity, and the reusability of the sensors. A comparison between SiC waveguides and SU-8 waveguides show that both systems are sensitive to changes in cladding, with the sensitivity of SU-8 waveguides being higher than SiC waveguides. The results are in accord with the theoretical analysis. In addition, potential applications in the biomedical field is also proposed and demonstrated, with a reasonable level of sensitivity obtained which meets the clinical requirements for detecting anostomosis leakage in patients after colorectal surgery.

7.2. Future Work

The waveguide systems proposed in this thesis have demonstrated improved performance in both the optical and chemical fields. Nevertheless, they can be further optimized and developed for the following aspects:

1. The systems could be developed into a compact system containing a light source, waveguide sensors, and optical detectors. Furthermore, waveguide arrays could be developed on a chip containing different coating layers. This would enable a number of different types of bacteria to be detected in a single unit.

2. SiC waveguides show great potential to be designed as freestanding structures to increase sensitivity. Simulations of the mechanical properties already carried out demonstrate that the structure has enough mechanical stability. The next step is to demonstrate the sensitivity and stability of the freestanding system by conducting fabrication and sensing tests.

3. The fabrication parameters of the waveguide system can be further optimized, such as the E-beam fabrication parameters for SU-8 waveguides. More fabrication and testing are needed to stabilize the process. The proposed SU-8 waveguide system has the potential to be widely used because of its good performance, easy operation, and low cost fabrication. It can easily be made into a disposable sensing element.

Acknowledgements

Finally, I arrive at this point to recall my Ph.D. journey and get the chance to show my sincere gratitude to all the people I luckily met and played an important role. It is because of you, my families, my friends, and my colleagues, who help me go through all the darkness and share the joy, that makes this journey meaningful.

First, I would like to express my deep gratitude to my promoter, Prof. Paddy French. You encouraged me a lot since the first time we met. At that time, I was a little nervous with all the new surroundings. Since then, we had many meetings and I learned a lot from you, about research and also about life. With your patient supervision and support from many aspects, I finally went through the tough moments. You always say something funny but wise, which influenced me a lot. Maybe in the future, I can write a book named "Paddy says". It will definitely be popular.

I also want to express my sincere appreciation to my daily supervisor Dr. Pandraud Gregory. You gave me a lot of instructions and help during my Ph.D. research. Thank you for sparing your time discussing with me, especially when you are busy. You always inspired me with some insightful ideas. What's more, your patience and passion encouraged me really a lot. You call everyone "big boss", but you are a real "da lao ban".

I would also like to thank all my committee members for sparing your time to attend my defense. Special thanks to Prof. Ernst Sudhölter for your help and instructions in the chemical area.

Of course, I want to say thanks to you all, the big EI family. Prof. Kofi Makinwa, thank you for making the EI lab a great place to work. Joyce, many thanks for dealing with all the arrangement staff for me and all the support during the last period of my stay here. Your help makes everything go on well. Lukasz, my great polish friend/colleague, thanks for all the technical help you gave me. You also shared my desperate moments and shed a light on my doomy sky. Those supported me a lot and will always be remembered. Zuyao, thanks for helping me a lot with the COMSOL and some stupid softwares. You always know what happened. Thanks for Jeroen, Ron, Ger for helping manage the devices. Special thanks to Prof. Gerard Meijer, Prof. Johan Huijsing, Dr. ir. Andre Bossche for the solid and rich courses. I also want to show respect to Prof. Albert Theuwissen, Dr. Stoyan Nihtianov, Dr. ir. Michiel Pertijs, Dr. ir. Reinoud Wolffenbuttel, and Dr. Fabio Sebastiano.

Many thanks to my former and current officemates from 15.070: Zeyu (The first and longest officemate, I still remember you gave me a banana cake when I first came here. During the following years, you gave me many advices in different aspects. It is always a lot of fun with you.), Yang Xu (We had so many good time together, running, outing, drawing your wedding...I still remembered the time we rode into a wild, sitting and talking aside a river, then we got lost in the darkness.

You also gave me many good advices as a senior researcher which helped a lot.), Junfeng (a person who has so many hidden skills. You know more when you spent longer time with him. Please don't hate Pisces anymore.), Yang Liu (a considerate girl and we shared some good moments). Then, to my current roommates, Douwe (how to define you: smart? happy? helpful? No, maybe as my best dutch friend. Thank you for all the happiness you bring to to our office. I enjoy talking with you about all the random things, art, music, food, and...(Paddy)...As you said on the new year card, I have managed to make my first half of 2018 colorful, with the presence of you. Thanks for the translation, suggestions and being my photographer. See you in China!), Jing (As a reliable and calm friend, thank you a lot for listening to me during my messy days and the advice you offered, it relieved me a lot. It is a pity that we didn't share some hotpots together, maybe in the future.), Javad (Thank you for saving me from "Paddy Silence", which I will remember for a long time. It is interesting to talk with you, new things, different ideas...). My dear officemates, you make Room 15.070 a great place, thanks a lot.

Then I would also like to thank Long (maybe later?), Hui (You are a thoughtful person, thanks for the goodbye gift that you and Yan prepared for me, and all the nice chats we had), Miss Wang (we had so many coincidences in life that make me feel very close to you when I came here. Thank you for the cakes, dinners and talks which make me feel that I am not far away from home.), Xiaoliang, Chao (thanks for liking my drawings and some interesting things you shared), Zhao, Fei , Weihan (for sharing some nice wines together), Sining (for always being there for some urgent help), Mingliang (it took me a long time to think of your real name), Mengying (a little sister, you will make it), Qinwen, Shuang (Thanks for the carings and the unique birthday cake), Lorenzo, Amir (of course, thank you for the discussion we had together, about optics, COMSOL and other random staff. That helped me a lot), Johan, Denis(for tell me acting as skull when "somebody" keeps talking. It works!!!), Pelin, Eunchul, and Bahman...and also the former colleagues Ruimin (a thoughful "哥" who always stood on the cutting edge of fashion), Qilong, Rui, Yuming, we had orgnised a dumplings party on the 2014 Spring Festival, there was a lot of fun. Also, Yixuan and Weichen for sharing many tasty dinners outside.

My sincere gratitude should also be expressed to all the working staff in EKL. Tom, Mario, Salvana, Henk, Johannes, Alex, Wim, Koos, Luke, Stephen... Thanks for all the help and instructions in the Cleanroom, which is very important. Paolo, Sten, Bruno, thanks for training me for some equipments. You are always friendly to me and ready to help. Xueming (for the drawing together and the encouragement), Dianel Yi (for all the help and sharings), Jian (for the strong and kind help every time, and interesting talks), Boyao, Jia, Yue Zhang (for help dice my chips), Ziqiao, Aleksandar (thanks for lending me the optical device and the discussions we had), Willam, Juan, Niko, Violeta, I enjoy working with you all.

Also special thanks to Kai Zhang, Yiming, who helped me a lot in the final step of my research, really appreciate that, especially when you were super busy. Linda, the experiment will be much harder without your help, thanks for spending the whole days with me in the lab. I learned a lot of new things in biomedical area from you. Anja, thanks for all the suppport, suggestion and help with the E-beam

fabrication, and all your patience.

I also want to show my respect to people from Micro-nano System Lab in NUDT, who had supported me a lot in my research. Prof. Xuezhong Wu, you became my mentor and supervisor since my first year of bachelor in NUDT, both in academic and in life, and you still are. When I need to make important decisions, you always gave me suggestions that would be good for me in the long run. I really appreciate all your guidance and patience for all these years. Prof. Dingbang Xiao, thank you for support me in my Ph.D. research and it is your help that encouraged me to carry on. Dr. Yongmeng Zhang, as a former colleague and also a good, trustworthy friend, I want to thank you officially here for all the selfless help you gave me during my Ph.D. and the big dinner (小龙虾) you treated me when I was in Changsha. We need to plan the next one now.

I would like to show my gratitude to all the NUDTers. Shanshan (We know each other long before. Thank you for offering me the first few nights' stay when I came. I will always remember the fun we had together, the help and warmth you gave me.), Xu Huang and Xu Xie, thanks for always fighting together and all the support. Ke Tao (a reliable and helpful friend, thank you for quitting the band "MengMengDa" which gave me a chance to be famous, and all the other strong help), Yunlong Li (encourage me a lot during my struggling), Jun Zhang (you are always nice and helped a lot to help me get used to the life here), Chang; Jianjian&Tiantian, Yueyue, Xiang&Kunkun(my brilliant "nephew" and gifted "niece"), you are the special exists here that always make me feel at home. All the wolf nights and fun time we had together is shining in my memory and never fade. I think the most brightest star will be that one night we played the build room cards, hush... Laobing&Xingxing, Jiapeng&Yuan, Yazhou you are always warm-hearted and helpful. Jinfeng Mu (for the support and discussion in optical field and the warm host in Twente). Thanks for Liang Liu, Shilong, Guangming and all the other NUDTers, it is a great thing to have you here. We are families.

Many many thanks to my dear friends here and in China. Peiyao (the first time we met, we knew everything. Thanks for always being my side and offering me the strong support. The thing I regrets most is we should have travelled together), Longlong (e...my dear Tsundere friend, you, Jie, and me, we spent a great time together that summer pretending to be football fans. It will never fades. I like talking with you, though sometimes your words made me crazy), Jie (Why you are always so calm about everything? Problems seem to be nothing when I ask for your suggestions. We started the basketball group but you were more persistent. The time you were in NL are happy and meaningful), Yueting (You are always nice, helpful and know a lot. Thanks for trusting me in lending me many important things), Anqi (for all the selfless help), Fei, Yixiao, Daijie&Sixin (there is no arguments about your cooking), Yihao, Yifeng (Uncle Shao, for all the drinks and talks), Boling (the discussions related and unrelated opitics), Tianzi (We met because of basketball. Thanks for the art gifts. We had some nice meals and spent lovely time together), Qian, Yuanyuan, for some pleasant nights. Lingling, my girl, I am so glad to have you here. I like all time we spent together doing nothing but drinking, talking... Your fabulous baking and cooking always make my stomach full. You make my life

so sweet. Zixuan, of course the great moments always have you together, movies, games. Don't hurt your feet any more...

Time goes to "MengMengDa" Band and its fans. Zhijie (left guitarist), Momo (our keyboard), Yongjia (it is strange to write your real name, 大师 or 右吉胖, right guitarist), Xinyuan (excellent dancer!), and me as the bass, we had a lot of great time together rehearsing, chatting and drinking together. Although our band broke up after the performance, but the story continue. Long Xu (now you are here), as a colleague and friend, there are so many intersections in our life and we shared many happy memories together with Mengting. Mengting, you are so considerate and being or talking with you is always comfortable. Your attitude towards life and work is very inspiring. Feifei (女王大人), we always had a lot of fun together, sharing different ideas and I enjoyed that. Xiaoyu (the Nature Guy, looks not but indeed considerate). The time with you guys was really great and nearly impossible to describe with words (不可描述). You know it!

I would like also show my gratitude to Clare, as my language teacher and friend, you and Ian influenced me a lot in my study here. I enjoyed the homemade British dinner a lot and thanks for introducing me to the wine world. Janice and Bill, thank you a lot for your help and encouragement to help me get through the tough time. Janice, you are always with passion which inspired me a lot. Thanks for the gifts (your CD, books...), I like them a lot. Also, my gratitude to Prof. Haixiang Lin, for the support you gave. Jos Weber, for the cares every time. Ruud and Durk, thanks for the COMSOL support on site and on line, you helped me solve many problems. I would also like to thank my friends who appear in my life in different ways. Kai Li, Shulan, Li Zhu, thanks for the care you provided me when we were roommates. Regardless the food, talks...the worries for me when I got home late always touched me and made me feel warm. Zhuoling, Wenjie, Xiangrong, Hai Gong, Yiyu, Chenjie, Jintao, Jin Chang, Xiaoming, Wei Shi&Lili Jiang, Bo, Qin Lin, Diyu, Zejun, Qujiang, Zhouqiao Wu, Xin Guo (all the sweet things), Yunlong Yu, Xiawei, Qile, Dong Li, Qu Lei, Qing Ding&Yana. We had good memories together and those mean a lot to me. Furthermore, I need and must say thank you to my dear friends in China, who are always there being my backbone: 磊神 (Lei Xi), 大嘴 (Zhaomin), 鸟 (Zhimiao), Yanbo, Junyao, Yuyin, Qiao, 杜桑 & 龙妹妹, Qingsong, Wenzi, Yiming... thanks for the companion, care, and support, which I will cherish forever.

For all my dear friends, who have come, chose to stay, or have left, thanks for appearing in my life. Life will be incomplete without you.

I would like to show my sincere gratitude to Zhijie's parents, for your concerns and support from all aspects.

Of course, I owe a big thank to my parents, who always love me more than everything else and always stand behind me no matter what happens. You give me the strength to carry on when I feel tired. Especially my mom, I must tell you that I feel so lucky to be your daughter, although I never said that to you. I love you two.

Last but the most important, my deepest gratitude goes to my beloved, Zhijie. Your support, encouragement, patience, and everything you have done, is the reason for me to be here. I like the me when I am with you, but I like the us more

when we are together. Thanks for coming into my life.

Yu
May, 2018
Delft, the Netherlands

Curriculum Vitæ

Yu XIN

17-03-1990 Born in Henan, China.

Education

2007–2011 BS in Mechanical Engineering
National University of Defense Technology, Changsha, China

2011–2013 MSc in Mechanical and Elctronic Engineering
National University of Defense Technology, Changsha, China

2013–2018 Ph.D. in Electronic Instrumentation Laboratory, Microelectronics Department
Delft University of Technology, Delft, The Netherlands
Promotor: Prof. dr. P.J. French

List of Publications

1. **Y. Xin**, A. Purniawan, L.S. Pakula, G. Pandraud, P. J. French, *Simulation of Bio-medical Waveguide in Mechanical and Optical Fields*, COMSOL Conference, Cambridge, UK, September, 2014.
2. **Y. Xin**, A. Purniawan, G. Pandraud, L.S. Pakula, P. J. French, *Optical Waveguide with Freestanding Grating Couplers*, IEEE Photonics Conference, Twente, the Netherlands, November, 2014.
3. **Y. Xin**, A. Purniawan, G. Pandraud, L.S. Pakula, P.J. French, *Optimisation of Bio-medical Optical Waveguide*, International Smart System Integration, Copenhagen, Denmark, March, 2015.
4. **Y. Xin**, G. Pandraud, L. S. Pakula, B. Morana, P. J. French, *Combination of LPCVD and PECVD SiC in Fabricating Evanescent Waveguides*, IEEE NEMS, Japan, April, 2016.
5. **Y. Xin**, Y.M. Zhang, G. Pandraud, P.J. French, *Design and fabrication of two types of tapered waveguides for evanescent sensing*, International Smart System Integration, Cork, Ireland, March, 2017.
6. **Y. Xin**, G.Pandraud, A. van Langen-Suurling, P.J. French, *Tapered SU8 Waveguide for Evanescent Sensing by Single–Step Fabrication*, IEEE Sensors, Glasgow, UK, November, 2017.
7. **Y. Xin**, G.Pandraud, L. Otten, Y.M. Zhang, P.J. French, *Surface functionalization of SU-8 vertical waveguide for biomedical sensing: bacteria diagnosis*, Eurosensors, Graz, Austria, 2018.
8. **Y. Xin**, G. Pandraud, P.J. French, *Small Angle Vertical Coupler in SiC and its Transfer Fabrication Method*, Photonic Technology Letters. (under review)
9. **Y. Xin**, G. Pandraud, A. van Langen-Suurling, Y.M. Zhang, P.J. French, *Tapered Vertical SU8 Waveguide Fabricated by E-Beam Lithography for Biomedical Sensing*, Sensors and Actuators A: Physical. (under review)
10. **Y. Xin**, Y.M. Zhang, G. Pandraud, P.J. French, *Micro-machined optical waveguide review*, to be submitted to Journal of Micromechanics and Microengineering.